

國立臺灣大學電機資訊學院電信工程學研究所

碩士論文

Graduate Institute of Communication Engineering  
College of Electrical Engineering and Computer Science

National Taiwan University

Master Thesis



廣義分頻多工系統之矩陣式參數化與其低複雜度收發  
機與最佳原型濾波器設計之應用

Matrix Characterization for Generalized Frequency  
Division Multiplexing Systems and its Applications in  
Low-Complexity Transceivers and Optimal Prototype  
Filter Designs

陳柏志

Po-Chih Chen

指導教授：蘇柏青 博士

Advisor: Borching Su, Ph.D.

中華民國 106 年 6 月

June, 2017

國立臺灣大學碩士學位論文  
口試委員會審定書

廣義分頻多工系統之矩陣式參數化與其低複雜度收發  
機與最佳原型濾波器設計之應用

Matrix Characterization for Generalized Frequency  
Division Multiplexing Systems and its Applications in  
Low-Complexity Transceivers and Optimal Prototype Filter  
Designs

本論文係陳柏志君 (R04942037) 在國立臺灣大學電信工程學研  
究所完成之碩士學位論文，於民國 106 年 6 月 14 日承下列考試委員審  
查通過及口試及格，特此證明

口試委員：

陳柏志 (簽名)  
(指導教授)

馮地

王奕翔

林澤

所 長

吳宗霖 (簽名)



## 誌謝

我能夠順利完成這篇論文，需要感謝許多人的幫助。

首先，謝謝我的指導教授蘇柏青老師在我開始接觸研究初期，帶我認識許多文獻中被提出的次世代通訊系統之候選波形。在此之前，我少有文獻搜索的經驗，蘇老師的教導讓我了解最新通訊系統可能的研究方向。我也是在這過程中，認識了作為我論文題目基礎的廣義分頻多工系統。

其次，感謝黃彥銘學長發現文獻中認為廣義分頻多工系統具有的一個不適用於偶數參數設定的缺陷。這個發現成為我整篇論文的最初動機，後續帶出豐碩的研究成果。

同時，感謝黃彥銘學長與唐明甫學長在我的研究過程中，提供許多寶貴的看法與建議。也謝謝實驗室同學許晉維、陳漢翔、陳啟祐在兩年同窗期間的相互砥礪與協助。

再者，感謝我的家人的包容與支持，讓我能專心在我的研究上，順利完成這篇論文。

最後，再次感謝蘇柏青老師從大四專題研究以來，給我的無數建議與鼓勵。尤其謝謝蘇老師非常用心地和我一同修改我投稿的論文，讓我成功在碩士期間發表一篇期刊論文與一篇會議論文。我從蘇老師身上學到許多專業知識與做研究的方法，在此表達我深深的謝意。





## 摘要

廣義分頻多工為一極富可能性之調變方式，藉由使用原型濾波器，其具有低頻帶外輻射之特性。然而，當使用文獻中常見的一些原型濾波器時，廣義分頻多工系統通常是非正交的，因而招致相較於正交分頻多工，在接收機均方誤差與符元錯誤率上的頻帶內效能退化。

本論文提出一種新的基於矩陣來將廣義分頻多工傳送機矩陣參數化之方式，而非如傳統上利用原型濾波器之基於向量的參數化方式。此新的參數化方式使我們很容易推導廣義分頻多工（傳送機）矩陣的性質，包括使廣義分頻多工矩陣為非奇異與么正各自的條件。

藉由使用此新的參數化方式，我們推導出使最小均方誤差接收機之一種低複雜度實現方式存在的充分且必要條件。若選用么正的廣義分頻多工傳送機矩陣，此實現方式在多路徑通道的情況下存在。在此實現方式不存在的情況下，我們提出一種低複雜度次最佳最小均方誤差接收機，其效能近似最小均方誤差接收機之效能。

此新的參數化方式也使我們能推導出可最小化接收機均方誤差的最佳原型濾波器。在許多情況下，這些最佳原型濾波器對應於使用么正的廣義分頻多工矩陣。在廣義分頻多工系統使用這些最佳原型濾波器不會導致雜訊增強的問題，使得系統展現與正交分頻多工相同的均方誤差效能。

此外，基於提出的矩陣式參數化方式，我們為廣義分頻多工發展出一個能最小化頻帶外輻射並保持優良頻帶內效能的原型濾波器最佳化演算法。透過將特徵矩陣作為最佳化變數，該濾波器設計問題被表示為一個非凸問題。在一些轉換之後，我們提出一個迭代解決兩個凸問

題的演算法來處理原問題。模擬結果顯示在相同頻譜效率的情況下，相較於正交分頻多工與文獻中的原型濾波器，最佳化所得的濾波器在頻帶外輻射與符元錯誤率上皆表現最好。

關鍵詞：廣義分頻多工；特徵矩陣；么正矩陣；低複雜度實現方式；最佳原型濾波器；頻帶外輻射；符元錯誤率效能。





# Abstract

Generalized frequency division multiplexing (GFDM) is a promising modulation scheme featuring low out-of-band (OOB) radiation, which is achieved through the use of prototype filters. However, GFDM systems are usually non-orthogonal with prototype filters commonly used in the literature, incurring in-band performance degradation in receiver mean square error (MSE) and symbol error rate (SER) compared to that achieved through orthogonal frequency division multiplexing (OFDM).

In this thesis, a new matrix-based characterization of GFDM transmitter matrices is proposed, as opposed to traditional vector-based characterization with prototype filters. The new characterization facilitates deriving properties of GFDM (transmitter) matrices, including conditions for GFDM matrices being nonsingular and unitary, respectively.

Using the new characterization, the necessary and sufficient conditions for the existence of a form of low-complexity implementation for a minimum mean square error (MMSE) receiver are derived. Such an implementation exists under multipath channels if the GFDM transmitter matrix is selected to be unitary. For cases where this implementation does not exist, a low-complexity suboptimal MMSE receiver is proposed, with its performance approximating that of an MMSE receiver.

The new characterization also enables derivations of optimal prototype filters in terms of minimizing receiver MSE. They are found to correspond to the use of unitary GFDM matrices under many scenarios. The use of such

optimal filters in GFDM systems does not cause the problem of noise enhancement, thereby demonstrating the same MSE performance as OFDM.

In addition, based on the proposed matrix characterization, a filter optimization algorithm that minimizes OOB radiation while maintaining good in-band performance is developed for GFDM. Through the characteristic matrix as the optimizing variable, the filter design problem is formulated as a non-convex problem. After some transformations, an algorithm in which two convex problems are solved iteratively is proposed to tackle the original problem. Simulation results show that under the same spectral efficiency, optimized filters perform the best in terms of both OOB radiation and SER performance, compared to OFDM and prototype filters existing in the literature.

*Keywords:* Generalized frequency division multiplexing (GFDM); characteristic matrix; unitary matrix; low-complexity implementation; optimal prototype filters; out-of-band (OOB) radiation; symbol-error-rate (SER) performance.





# Contents

誌謝	i
摘要	iii
<b>Abstract</b>	<b>v</b>
<b>Contents</b>	<b>vii</b>
<b>List of Figures</b>	<b>xi</b>
<b>List of Tables</b>	<b>xv</b>
<b>1 Introduction</b>	<b>1</b>
<b>2 Characterization of GFDM Systems</b>	<b>5</b>
2.1 Characterization of GFDM Matrices: Basic Definitions . . . . .	6
2.2 GFDM Transmitter Implementations . . . . .	8
2.2.1 Direct implementation . . . . .	9
2.2.2 Frequency-domain implementation . . . . .	9
2.2.3 Characteristic-matrix-domain implementation . . . . .	9
2.3 Unitary and Invertible GFDM Matrices . . . . .	11
<b>3 GFDM Receiver Implementations</b>	<b>13</b>
3.1 Low-Complexity ZF Receivers . . . . .	14
3.2 Low-Complexity MMSE Receivers . . . . .	15
3.3 Low-Complexity Approximated MMSE Receivers . . . . .	19

3.3.1	Simulation Results . . . . .	19
3.4	Remarks on Soft-Output Demodulation . . . . .	21
<b>4</b>	<b>Complexity Analysis</b>	<b>25</b>
4.1	Additional Complexity Comparison Results . . . . .	30
<b>5</b>	<b>Power Spectral Density and OOB Leakage</b>	<b>33</b>
<b>6</b>	<b>Optimal Prototype Filters that Minimize MSE</b>	<b>37</b>
6.1	Optimization Results for ZF Receivers . . . . .	38
6.2	Optimization Results for MMSE Receivers . . . . .	40
6.3	Comparison of Prototype Filter Candidates . . . . .	42
6.4	Simulation Results . . . . .	45
6.4.1	MSE and SER Performance . . . . .	45
6.4.2	PAPR . . . . .	51
6.4.3	OOB Leakage . . . . .	52
6.4.4	Additional Simulation Results for SER Performance . . . . .	53
<b>7</b>	<b>Optimal Prototype Filters that Minimize MSE and OOB Radiation</b>	<b>57</b>
7.1	Problem Formulation . . . . .	57
7.2	Proposed Algorithm . . . . .	58
7.3	Simulation Results . . . . .	61
7.3.1	Parameter Settings . . . . .	61
7.3.2	Simulation Results for the Case of $\eta = 1$ . . . . .	62
7.3.3	Influence of the Weight $w$ . . . . .	65
7.3.4	Simulation Results for the Case of $\eta > 1$ . . . . .	66
7.4	Future Work . . . . .	67
<b>8</b>	<b>Multiple Access with Optimized Prototype Filters</b>	<b>69</b>
<b>9</b>	<b>Conclusions</b>	<b>73</b>
	<b>Bibliography</b>	<b>74</b>



**A Proof of Theorem 5**

**81**

**B Proof of Theorem 6**

**83**

**C Proof of Corollaries 1 and 2**

**85**





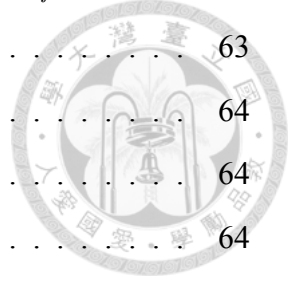


# List of Figures

2.1	Block diagram of the transceiver. ("r/m" stands for "remove".)	6
2.2	Characteristic-matrix-domain Form-1 transmitter implementation.	10
2.3	Characteristic-matrix-domain Form-2 transmitter implementation.	10
3.1	Characteristic-matrix-domain Form-2 receiver implementation.	14
3.2	MSE for GFDM approximated MMSE (AMMSE) receiver over the Rayleigh fading channel (compared to the corresponding ZF and MMSE receivers).	21
3.3	SER for GFDM approximated MMSE (AMMSE) receiver over the Rayleigh fading channel (compared to the corresponding ZF and MMSE receivers).	22
3.4	SER for GFDM approximated MMSE (AMMSE) receiver over the Rayleigh fading channel (compared to the corresponding ZF and MMSE receivers).	22
4.1	Computational complexity of GFDM transmitter implementations. $K = 64$ .	27
4.2	Computational complexity of GFDM ZF receiver implementations. $K = 64$ .	28
4.3	Computational complexity of GFDM MMSE receiver implementations. $K = 64$ .	29
4.4	Computational complexity of GFDM transmitter implementations. $M = 31$ .	30
4.5	Computational complexity of GFDM ZF receiver implementations. $M = 31$ .	31
4.6	Computational complexity of GFDM MMSE receiver implementations. $M = 31$ .	31

6.1	Magnitudes of entries in characteristics matrices $\mathbf{G}$ for several GFDM prototype filters when $K = 8, M = 4$ . . . . .	44
6.2	MSE for GFDM ZF receiver over a deep-fade-excluded Rayleigh fading (DFERF) channel and the corresponding OFDM receiver. $K = 8, M = 5$ . . . . .	47
6.3	MSE for GFDM ZF receiver over a deep-fade-excluded Rayleigh fading (DFERF) channel and the corresponding OFDM receiver. $K = 8, M = 4$ . . . . .	48
6.4	MSE for GFDM MMSE receiver over the Rayleigh fading (RF) channel and the corresponding OFDM receiver. $K = 32, M = 16$ . . . . .	48
6.5	MSE for GFDM ZF receiver over the AWGN channel and the corresponding OFDM receiver. $K = 8, M = 4$ . . . . .	49
6.6	MSE for GFDM MMSE receiver over the AWGN channel and the corresponding OFDM receiver. $K = 8, M = 4$ . . . . .	49
6.7	MSE for GFDM ZF receiver over a (static) multipath (MP) channel and the corresponding OFDM receivers. $K = 8, M = 4$ . . . . .	50
6.8	Magnitude response of the frequency-domain prototype filter $\mathbf{g}_f$ . . . . .	51
6.9	CCDF of PAPR for MMSE-RF. $K = 32, M = 16$ . . . . .	51
6.10	PSD for GFDM and OFDM. . . . .	52
6.11	SER for GFDM ZF receiver over a deep-fade-excluded Rayleigh fading (DFERF) channel and the corresponding OFDM receiver. $K = 8, M = 5$ . . . . .	53
6.12	SER for GFDM ZF receiver over a deep-fade-excluded Rayleigh fading (DFERF) channel and the corresponding OFDM receiver. $K = 8, M = 4$ . . . . .	54
6.13	SER for GFDM MMSE receiver over the Rayleigh fading (RF) channel and the corresponding OFDM receiver. $K = 32, M = 16$ . . . . .	54
6.14	SER for GFDM ZF receiver over the AWGN channel and the corresponding OFDM receiver. $K = 8, M = 4$ . . . . .	55
6.15	SER for GFDM MMSE receiver over the AWGN channel and the corresponding OFDM receiver. $K = 8, M = 4$ . . . . .	55
6.16	SER for GFDM ZF receiver over a (static) multipath (MP) channel and the corresponding OFDM receivers. $K = 8, M = 4$ . . . . .	56

7.1	Magnitude response of the frequency-domain prototype filter $\mathbf{g}_f$ for Case 1.	63
7.2	PSD for Case 1. . . . .	63
7.3	SER for Case 1. . . . .	64
7.4	PSD for Case 2. . . . .	64
7.5	PSD for Case 3. . . . .	64
7.6	Maximum OOB PSD $\max_{f \in \mathcal{B}_O} S_a(f)$ and $\text{rank}(\mathbf{S})$ obtained at convergence, and number of iterations $N_I$ versus weight $w$ for Case 3. . . . .	65
7.7	Magnitude response of the frequency-domain prototype filter $\mathbf{g}_f$ for Case 1. $\eta = 1.1$ . . . . .	66
7.8	PSD for Case 1. $\eta = 1.1$ . . . . .	66
8.1	MSE for GFDMA ZF receiver over a deep-fade-excluded Rayleigh fading channel and the corresponding OFDMA receiver. $K = 32, M = 15$ . . . .	70
8.2	SER for GFDMA ZF receiver over a deep-fade-excluded Rayleigh fading channel and the corresponding OFDMA receiver. $K = 32, M = 15$ . . . .	70









# List of Tables

4.1	Computational complexity of GFDM transmitter and ZF receiver implementations under multipath channels . . . . .	26
4.2	Computational complexity of GFDM MMSE receiver implementations under multipath channels . . . . .	26
6.1	OOB leakage in dB of the simulation in Fig. 6.10 . . . . .	53
7.1	Parameter settings . . . . .	62
7.2	Maximum OOB PSD $\max_{f \in \mathcal{B}_O} S_a(f)$ in dB and energy $\xi_H$ . . . . .	63
7.3	Maximum OOB PSD $\max_{f \in \mathcal{B}_O} S_a(f)$ in dB and energy $\xi_H$ for Case 1 . . . . .	67





# Chapter 1

## Introduction

Generalized frequency division multiplexing (GFDM) [1], extensively studied in recent years, is a potential modulation scheme for future wireless communication systems because it features good properties including low out-of-band (OOB) radiation and flexible time-frequency structures to adapt to various application scenarios, such as cognitive radios and low latency applications [2]. However, some drawbacks for GFDM arise from the non-orthogonality [3] of the system as a result of using prototype transmit filters [2]. In this study, we address two specific drawbacks: the difficulty in designing low-complexity transceivers, and performance degradation in receiver mean square error (MSE) and symbol error rate (SER) compared to that achieved through orthogonal frequency division multiplexing (OFDM) [4]. The severity of the performance degradation depends heavily on the prototype transmit filter that is selected [3].

For GFDM systems with a matched filter (MF) receiver [2, 5], inter-carrier interference (ICI) and inter-symbol interference (ISI) exist. To cancel ICI and ISI, successive interference cancellation (SIC) receivers are employed [2, 6, 7]. However, long delays are incurred in the process of interference cancellation. In this thesis, we focus on zero-forcing (ZF) and linear minimum mean square error (MMSE) receivers [2, 5], which eliminate ICI and ISI. Although the ZF receiver is known for its low-complexity implementation under either additive white Gaussian noise (AWGN) or multipath channels, MMSE receiver implementations with linearithmic complexity, to the best of our knowledge, is known only for the AWGN channels (see recent references [8, 9]). In [10, 11], MMSE receivers for

multipath channels with reduced complexity were proposed, but they still have at least a quadratic complexity (in terms of numbers of GFDM subsymbols or subcarriers). In this thesis, we study the feasibility of low-complexity MMSE receivers in presence of multipath channels and propose the first implementation with linearithmic complexity thereof.

In addition, we study the impact of GFDM prototype transmit filters on MSE and SER performance. In the literature [1–3, 5, 8, 9, 12–28], many prototype filters, including the raised-cosine (RC), root-raised-cosine (RRC), Xia [29], Dirichlet [3], and Gaussian pulses, have been proposed and used for GFDM systems. These prototype filters are mostly designed to reduce OOB radiation of transmitted signals except that the Dirichlet pulse is claimed to be rate-optimal under the ZF or MMSE receiver over the AWGN channel [23]. However, GFDM systems using all these filters are mostly non-orthogonal (except the Dirichlet pulse) [3]. In other words, the corresponding GFDM transmitter matrices [2] generally have a greater-than-unity condition number. This creates the noise enhancement effect [5, 13, 23], and GFDM systems using these filters suffer from MSE and SER performance degradation compared to OFDM systems.

This study offers three main contributions:

1) *New matrix characterization of GFDM transceivers*: The modulation process in a GFDM transmitter can be performed by multiplying the data vector by a matrix with a special structure, called a GFDM matrix. A GFDM matrix is commonly characterized by its first column, usually referred to as the *prototype filter* [2]. In some other references [8, 12], a GFDM matrix is characterized by the *frequency-domain prototype filter*, i.e., the discrete Fourier transform (DFT) of the prototype filter, which leads to some advanced implementations of GFDM transceivers. In this thesis, we propose an alternative means for characterizing GFDM matrices, in which a *characteristic matrix* is used. On the basis of this new characterization, we investigated several properties of GFDM matrices and found that the conditions for some properties of a GFDM matrix (e.g., non-singularity, unitary property) can be expressed very clearly with the new characterization parameters. This characterization also leads to low-complexity transmitter implementations and provides a foundation for the other two contributions, described as follows.

2) *Low-complexity MMSE receivers under multipath channels*: In this thesis, we propose a form of low-complexity implementation for an MMSE receiver. The necessary and sufficient conditions for the existence of such an implementation are derived and clearly expressed in terms of the new matrix characterization parameters. Particularly, the use of a *unitary* GFDM transmitter matrix is a sufficient condition. Moreover, for cases where the necessary condition is not satisfied, we also propose a low-complexity suboptimal MMSE receiver whose performance approximates that of an MMSE receiver. This makes GFDM transceivers very practicable even in multipath channels. The complexity of our proposed implementation is analyzed in detail and compared to existing solutions. We show that significant complexity reduction can be obtained through the use of our implementation.

3) *Optimal prototype transmit filters in receiver MSE*: In this study, we investigate optimal prototype transmit filters that minimize in-band MSE or SER performance and OOB radiation. We first identify the optimal prototype transmit filters in terms of minimizing receiver MSEs with both ZF and MMSE receivers under the AWGN channel as well as static and statistical linear time-invariant channels. We find that the optimal GFDM transmitter matrices under most scenarios are unitary GFDM matrices and do not suffer from the noise enhancement effect. Then, a filter optimization algorithm that minimizes OOB radiation while maintaining good in-band performance is proposed. Simulation results show that under the same spectral efficiency, our optimized filters perform the best in terms of both OOB radiation and SER performance, compared to RC filters, Dirichlet pulses, and OFDM.

The remainder of this thesis is structured as follows. In Chapter 2, we present the GFDM system model and the new matrix characterization. We also derive some properties of GFDM matrices and present low-complexity transmitter implementations. In Chapter 3, we propose low-complexity ZF and MMSE receiver implementations. In Chapter 4, we present a thorough complexity analysis for GFDM implementations. In Chapter 5, we derive the analytical expression of power spectral density (PSD) and define the OOB leakage as a performance measure for the OOB radiation. In Chapter 6, optimal prototype transmit filters in terms of minimizing receiver MSEs are derived, and the optimality is

verified by simulation results. In Chapter 7, optimal prototype transmit filters in terms of minimizing OOB radiation under MSE performance constraints are derived, and the optimality is verified by simulation results. In Chapter 8, a multiple-access scenario is presented. Finally, the study conclusion is provided in Chapter 9.

Some parts (e.g., Chapters 2 to 6) of the thesis have been accepted to and will appear in *IEEE Transactions on Signal Processing* [30]. The materials in Chapter 7 will also be presented in the 18th IEEE International Workshop on Signal Processing Advances in Wireless Communications (SPAWC), 2017 [31].

*Notations:* Boldfaced capital letters denote matrices, and boldfaced lowercase letters are reserved for column vectors. We use  $\langle \cdot \rangle_D$ ,  $(\cdot)^*$ ,  $(\cdot)^T$ , and  $(\cdot)^H$  to denote modulo  $D$ , complex conjugate, transpose, and Hermitian transpose, respectively. We also use  $(\cdot)^{-H}$  to denote  $((\cdot)^{-1})^H$ . Given a matrix  $\mathbf{A}$ , we denote by  $[\mathbf{A}]_{m,n}$ ,  $[\mathbf{A}]_{:,r}$ ,  $\|\mathbf{A}\|_F$ ,  $\text{vec}(\mathbf{A})$ ,  $\text{tr}(\mathbf{A})$ ,  $\text{rank}(\mathbf{A})$ , and  $\mathbf{A}^{\circ-1}$  its  $(m, n)$ th entry (zero-based indexing),  $r$ th column, Frobenius norm, column-wise vectorization, trace, rank, and Hadamard inverse (defined by  $[\mathbf{A}^{\circ-1}]_{m,n} = [\mathbf{A}]_{m,n}^{-1}$ ,  $\forall m, n$ ), respectively. For any diagonal matrix  $\mathbf{A}$ ,  $[\mathbf{A}]_n$  denotes  $[\mathbf{A}]_{n,n}$ . For any matrices  $\mathbf{A}$  and  $\mathbf{B}$ ,  $\mathbf{A} \otimes \mathbf{B}$  denotes their Kronecker product, and  $\mathbf{A} \circ \mathbf{B}$  their Hadamard product. Given a vector  $\mathbf{u}$ , we use  $[\mathbf{u}]_n$  to denote the  $n$ th component of  $\mathbf{u}$ ,  $\|\mathbf{u}\|$  the L2-norm of  $\mathbf{u}$ ,  $\text{diag}(\mathbf{u})$  the diagonal matrix containing  $\mathbf{u}$  on its diagonal, and  $\Psi(\mathbf{u})$  the circulant matrix whose first column is  $\mathbf{u}$ . Given square matrices  $\mathbf{A}_m$ ,  $\forall 0 \leq m < p$  for any positive integer  $p$ , we use  $\text{blkdiag}(\{\mathbf{A}_m\}_{m=0}^{p-1})$  to denote a block diagonal matrix whose  $m$ th diagonal block is  $\mathbf{A}_m$ . We define  $\mathbf{I}_p$  to be the  $p \times p$  identity matrix,  $\mathbf{1}_p$  the  $p \times 1$  vector of ones,  $\mathbf{W}_p$  the normalized  $p$ -point DFT matrix with  $[\mathbf{W}_p]_{m,n} = e^{-j2\pi mn/p} / \sqrt{p}$  for any positive integer  $p$ , and  $\delta_{kl}$  the Kronecker delta. We use  $\angle C$  to denote the phase  $\phi \in (-\pi, \pi]$  of a nonzero complex number  $C$ , and  $\angle \mathbf{A}$  the matrix such that  $[\angle \mathbf{A}]_{m,n} = \angle [\mathbf{A}]_{m,n}$  for each entry. We use  $\mathbb{H}_+^D$  to denote the set of Hermitian positive semidefinite  $D \times D$  matrices, and  $\preceq$  to denote the matrix inequality. For any set  $\mathcal{A}$ , we denote its cardinality by  $|\mathcal{A}|$ . Finally, we use  $\text{E}\{\cdot\}$  to denote the expectation operator.



## Chapter 2

# Characterization of GFDM Systems

GFDM is a block-based communication scheme as shown in Fig. 2.1 [2]. In a GFDM block,  $M$  complex-valued subsymbols are transmitted on each of the  $K$  subcarriers, so a total of  $D = KM$  data symbols are transmitted. The data symbol vector  $\mathbf{d}[l]$  is decomposed as  $\mathbf{d}[l] = [d_{0,0}[l] \cdots d_{K-1,0}[l] \ d_{0,1}[l] \cdots d_{K-1,1}[l] \cdots d_{K-1,M-1}[l]]^T$ , where  $d_{k,m}[l]$  is the data symbol on the  $k$ th subcarrier and  $m$ th subsymbol in the  $l$ th block, taken from a complex constellation. Assume the data symbols are zero-mean and independent and identically distributed (i.i.d.) with symbol energy  $E_S$ , i.e.,  $E\{\mathbf{d}[l]\mathbf{d}^H[n]\} = E_S \mathbf{I}_D \delta_{ln}$ . Each data symbol  $d_{k,m}[l]$  is pulse-shaped by the vector  $\mathbf{g}_{k,m}$  whose  $n$ th entry is

$$[\mathbf{g}_{k,m}]_n = [\mathbf{g}]_{\langle n-mK \rangle_D} e^{j2\pi kn/K}, n = 0, 1, \dots, D-1, \quad (2.1)$$

where  $\mathbf{g}$  is a  $D \times 1$  vector, referred to as the *prototype transmit filter* [2]. Let  $\mathbf{x}[l] = [x_0[l] \ x_1[l] \cdots x_{D-1}[l]]^T$  be the vector containing the transmit samples. Then, the GFDM modulator can be formulated as the transmitter matrix [2]

$$\mathbf{A} = [\mathbf{g}_{0,0} \cdots \mathbf{g}_{K-1,0} \ \mathbf{g}_{0,1} \cdots \mathbf{g}_{K-1,1} \cdots \mathbf{g}_{K-1,M-1}] \quad (2.2)$$

such that  $\mathbf{x}[l] = \mathbf{A}\mathbf{d}[l]$ . The matrix  $\mathbf{A}$  as defined in (2.2) is called hereafter a *GFDM matrix* with a *prototype filter*  $\mathbf{g}$ . The vector  $\mathbf{x}[l]$  is further added a cyclic prefix (CP) before sending to the receiver through a linear time-invariant (LTI) channel. Details on the channel effects

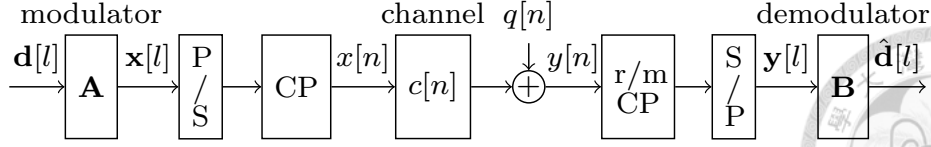


Figure 2.1: Block diagram of the transceiver. ("r/m" stands for "remove".)

and the receiver are elaborated in Chapter 3.

## 2.1 Characterization of GFDM Matrices: Basic Definitions

In the literature, GFDM transmitter matrices are often characterized by the prototype transmit filter  $\mathbf{g}$ . Alternatively, in [8, 12, 23], GFDM matrices have been parametrized by the frequency-domain prototype transmit filter  $\mathbf{g}_f = \sqrt{D}\mathbf{W}_D\mathbf{g}$ , i.e., the  $D$ -point DFT of  $\mathbf{g}$ .

In this thesis, we propose an alternative means for characterizing a GFDM transmitter matrix, namely, the *characteristic matrix*  $\mathbf{G}$  of size  $K \times M$ . We show that the proposed characterization is useful for understanding some important properties of GFDM transmitter matrices not easily derived in terms of the characterization of traditional time-domain or frequency-domain prototype filters. The proposed characterization is essentially equivalent to the discrete Zak transform (DZT) [5, 32], but all derivations in the thesis do not require knowledge of the DZT. A formal definition of this characterization of a GFDM transmitter matrix is given as follows.

**Definition 1 (Characteristic matrix)** Consider a  $KM \times KM$  GFDM matrix  $\mathbf{A}$  in (2.2) with a prototype filter  $\mathbf{g}$ . We define the characteristic matrix  $\mathbf{G}$  of the GFDM matrix  $\mathbf{A}$  as

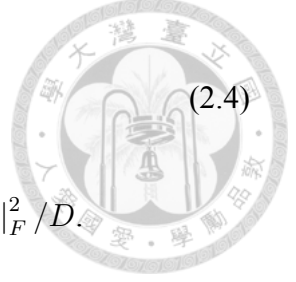
$$\mathbf{G} = \sqrt{D} \text{reshape}(\mathbf{g}, K, M)\mathbf{W}_M, \quad (2.3)$$

where  $\text{reshape}(\mathbf{g}, K, M)$  is a  $K \times M$  matrix whose  $(k, m)$ -entry is  $[\mathbf{g}]_{k+mK}$ ,  $\forall 0 \leq k < K$ ,  $0 \leq m < M$ . Moreover, the phase-shifted characteristic matrix  $\bar{\mathbf{G}}$  of the GFDM matrix



$\mathbf{A}$  is defined as the  $K \times M$  matrix whose  $(k, m)$ -entry is

$$[\bar{\mathbf{G}}]_{k,m} = [\mathbf{G}]_{k,m} e^{-j2\pi km/D}. \quad (2.4)$$



Finally, the *energy*  $\xi_G$  of the GFDM matrix  $\mathbf{A}$  is defined by  $\xi_G = \|\mathbf{G}\|_F^2 / D$ .

The following lemma would be useful for derivations of low-complexity transceiver implementations and optimal prototype filters later.

**Lemma 1** *Let  $\mathbf{A}$  be a GFDM matrix with a  $K \times M$  characteristic matrix  $\mathbf{G}$ , a  $K \times M$  phase-shifted characteristic matrix  $\bar{\mathbf{G}}$ , a  $D \times 1$  prototype filter  $\mathbf{g}$ , and energy  $\xi_G$ , where  $D = KM$ . Then,*

- (a) *The prototype filter  $\mathbf{g}$  can be expressed as  $\mathbf{g} = \text{vec}(\mathbf{G}\mathbf{W}_M^H) / \sqrt{D}$ .*
- (b) *The frequency-domain prototype filter  $\mathbf{g}_f \triangleq \sqrt{D}\mathbf{W}_D\mathbf{g}$  can be expressed as  $\mathbf{g}_f = \text{vec}(\bar{\mathbf{G}}^T\mathbf{W}_K)$ .*
- (c) *The matrix  $\mathbf{A}$  satisfies*

$$\mathbf{A} = (\mathbf{W}_M^H \otimes \mathbf{I}_K) \text{diag}(\text{vec}(\mathbf{G}))(\mathbf{W}_M \otimes \mathbf{W}_K^H). \quad (2.5)$$

- (d) *The energy  $\xi_G$  satisfies  $\xi_G = \|\mathbf{g}\|^2$ .*

*Proof:* (a) The statement follows from the inverse operation of (2.3).

(b) According to (a), the prototype filter  $\mathbf{g}$  satisfies  $[\mathbf{g}]_{mK+k} = [\mathbf{G}\mathbf{W}_M^H]_{k,m} / \sqrt{D}$ . Thus,  $\mathbf{g}_f$  satisfies

$$\begin{aligned} [\mathbf{g}_f]_{k'M+m'} &= \sum_{k=0}^{K-1} \sum_{m=0}^{M-1} [\mathbf{g}]_{mK+k} e^{-j2\pi(mK+k)(k'M+m')/D} \\ &= \frac{1}{\sqrt{K}} \sum_{k=0}^{K-1} [\mathbf{G}]_{k,m'} e^{-j2\pi k(k'M+m')/D}, \end{aligned} \quad (2.6)$$

$\forall 0 \leq k' < K, 0 \leq m' < M$ , i.e.,  $\mathbf{g}_f = \text{vec}(\bar{\mathbf{G}}^T\mathbf{W}_K)$ .

(c) Using the famous matrix identity  $\text{vec}(\mathbf{ABC}) = (\mathbf{C}^T \otimes \mathbf{A}) \text{vec}(\mathbf{B})$  [33], we first obtain that  $(\mathbf{W}_M^H \otimes \mathbf{I}_K) \text{vec}(\mathbf{G}) = \text{vec}(\mathbf{I}_K\mathbf{G}(\mathbf{W}_M^H)^T) = \text{vec}(\mathbf{G}\mathbf{W}_M^H) = \sqrt{D}\mathbf{g}$ . Then, the zeroth

column of the right-hand side of (2.5) is  $(\mathbf{W}_M^H \otimes \mathbf{I}_K) \text{diag}(\text{vec}(\mathbf{G})) \cdot \frac{1}{\sqrt{D}} \mathbf{1}_D = (\mathbf{W}_M^H \otimes \mathbf{I}_K) \text{vec}(\mathbf{G})/\sqrt{D} = \mathbf{g}$ , i.e., the prototype filter of  $\mathbf{A}$ . The equality of the other columns of both sides in (2.5) can be verified similarly, by noting that the  $(k + mK)$ th column of  $\mathbf{W}_M \otimes \mathbf{W}_K^H$  is  $[\mathbf{W}_M]_{:,m} \otimes [\mathbf{W}_K]_{:,k}$ .

(d) The proof is trivial in view of Lemma 1(a) and Parseval's theorem. ■

Lemmas 1(a) and 1(b) indicate the one-to-one correspondence among  $\mathbf{G}$ ,  $\mathbf{g}$ , and  $\mathbf{g}_f$  and are useful in developments later in this thesis. It is noted that a mathematically equivalent form of them can also be derived from the definition and frequency-domain expression of the DZT [32]. The statements and proofs provided here, however, do not require knowledge of the DZT. Lemma 1(c) is a simplified form of the decomposition proposed in [34], and we give a simple alternative proof above. We will use (2.5) to develop transceiver implementations. Finally, Lemma 1(d) shows that the energy of  $\mathbf{A}$  is simply the energy of the prototype filter  $\mathbf{g}$ , which can also be proved by unitarity of the DZT [32].

## 2.2 GFDM Transmitter Implementations

As presented earlier in this thesis, the transmitter simply modulates the data symbol vector by

$$\mathbf{x}[l] = \mathbf{A}\mathbf{d}[l]. \quad (2.7)$$

Then,  $\mathbf{x}[l]$  is passed through a parallel-to-serial (P/S) converter, and a CP of length  $L$  is added, as shown in Fig. 2.1. Denote  $\mathcal{K} \subseteq \{0, 1, \dots, K-1\}$  and  $\mathcal{M} \subseteq \{0, 1, \dots, M-1\}$  as the set of subcarrier indices and set of subsymbol indices, respectively, that are actually used. The digital baseband transmit signal of GFDM can then be expressed as

$$x[n] = \sum_{l=-\infty}^{\infty} \sum_{k \in \mathcal{K}} \sum_{m \in \mathcal{M}} d_{k,m}[l] g_m[n - lD'] e^{j2\pi \frac{k(n-lD')}{K}}, \quad (2.8)$$

where  $D' = D + L$  and

$$g_m[n] = \begin{cases} [\mathbf{g}]_{\langle n-mK-L \rangle_D}, & n = 0, 1, \dots, D' - 1 \\ 0, & \text{otherwise} \end{cases} \quad (2.9)$$



In most instances of this thesis, we omit the block index "[ $l$ ]" for notational brevity.

For the implementation of the transmitter matrix  $\mathbf{A}$ , two types pertaining to the conventional time [2] and frequency [8] domains, respectively, are found in the literature. In this thesis, we propose another implementation based on the characteristic matrix. These implementations are described as follows:

### 2.2.1 Direct implementation

The matrix multiplication in (2.7) is directly implemented, which can be considered a time-domain implementation that deals with the prototype filter  $\mathbf{g}$  directly [2].

### 2.2.2 Frequency-domain implementation

Previous frequency-domain implementations [8, 12] have been proposed for complexity reduction. The transmit signal is produced with

$$\mathbf{x} = \frac{1}{\sqrt{K}} \mathbf{W}_D^H \sum_{k \in \mathcal{K}} \mathbf{P}^{(k)} \text{diag}(\mathbf{g}_f) \mathbf{R} \mathbf{W}_M \mathbf{d}_k, \quad (2.10)$$

where  $\mathbf{d}_k = [d_{k,0} \ d_{k,1} \ \dots \ d_{k,M-1}]^T$ ,  $\mathbf{R} = \mathbf{1}_K \otimes \mathbf{I}_M$ , and  $\mathbf{P}^{(k)} = \Psi(\mathbf{p}^{(k)}) \otimes \mathbf{I}_M$ , with  $\mathbf{p}^{(k)}$  being the  $K \times 1$  vector equal to the  $k$ th column of  $\mathbf{I}_K$ .

### 2.2.3 Characteristic-matrix-domain implementation

We propose two forms of *characteristic-matrix-domain implementation*. Using Lemma 1(c), we obtain a transmitter implementation based on (2.5), which we call Form-1 implementation, as shown in Fig. 2.2. An alternative form of decomposition of the transmitter

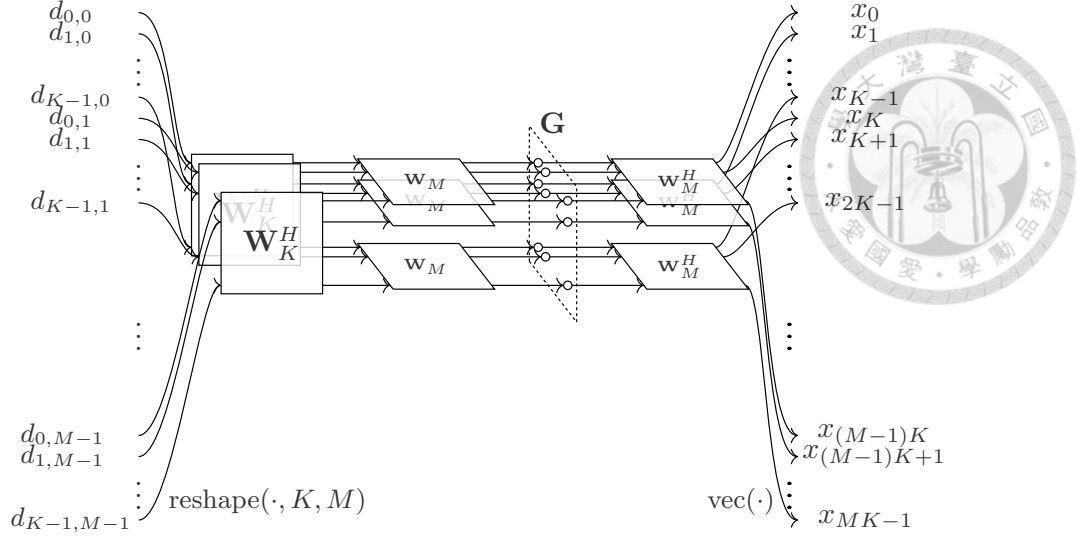


Figure 2.2: Characteristic-matrix-domain Form-1 transmitter implementation.

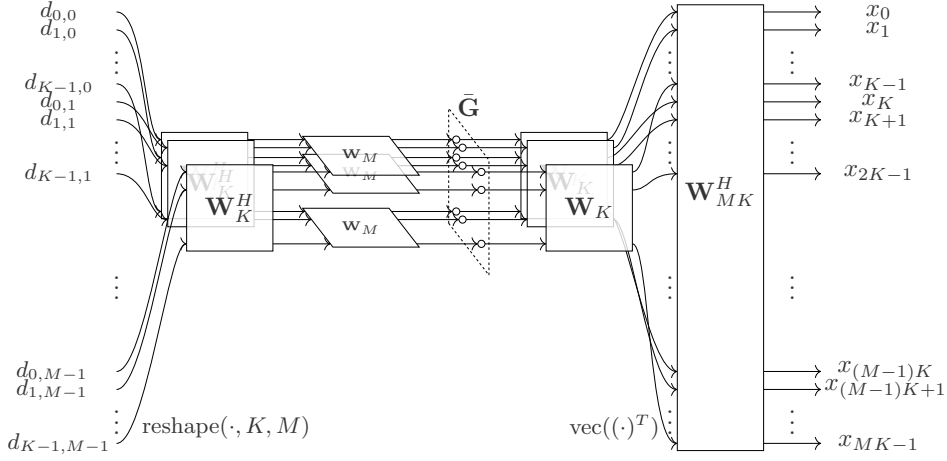


Figure 2.3: Characteristic-matrix-domain Form-2 transmitter implementation.

matrix that exploits the phase-shifted characteristic matrix  $\bar{\mathbf{G}}$  is formulated as

$$\mathbf{A} = \mathbf{W}_D^H \mathbf{\Pi} (\mathbf{I}_M \otimes \mathbf{W}_K) \text{diag}(\text{vec}(\bar{\mathbf{G}})) (\mathbf{W}_M \otimes \mathbf{W}_K^H), \quad (2.11)$$

where  $\mathbf{\Pi}$  is the  $D \times D$  permutation matrix defined by

$$[\mathbf{\Pi}]_{kM+m, nK+l} = \delta_{kl} \delta_{mn}, \quad (2.12)$$

$\forall 0 \leq k, l < K, 0 \leq m, n < M$ . The matrix  $\mathbf{\Pi}$  can be understood through the identity  $\text{vec}(\mathbf{M}^T) = \mathbf{\Pi} \text{vec}(\mathbf{M})$ , where  $\mathbf{M}$  is any  $K \times M$  matrix. We obtain (2.11) by using

(2.5) and the fact that a  $KM$ -point DFT can be decomposed into a  $K$ -point DFT, an  $M$ -point DFT, and twiddle factors of the form  $e^{-j2\pi km/D}$ , which are incorporated into  $\bar{\mathbf{G}}$ . Eq. (2.11) corresponds to the implementation shown in Fig. 2.3, which we call Form-2 implementation. The complexity of both forms are in  $O(KM \log KM)$ . Yet, as will be seen in Chapter 4, the complexity of Form-1 transmitter is slightly lower than that of Form-2 transmitter, while the Form-2 structure based on the decomposition in (2.11) is advantageous for receiver implementation.

## 2.3 Unitary and Invertible GFDM Matrices

With the characteristic-matrix-domain implementation, we can also easily identify the class of unitary GFDM matrices as follows.

**Theorem 1 (Unitary GFDM matrices)** *Let  $\mathbf{A}$  be a GFDM matrix with a  $K \times M$  characteristic matrix  $\mathbf{G}$ . Then,  $\mathbf{A}$  is unitary if and only if  $\mathbf{G}$  contains unit-magnitude entries:  $|\mathbf{G}_{k,l}| = 1 \forall 0 \leq k < K, 0 \leq l < M$ . An equivalent condition is that its phase-shifted characteristic matrix  $\bar{\mathbf{G}}$ , as defined in (2.4), contains unit-magnitude entries:  $|\bar{\mathbf{G}}_{k,l}| = 1 \forall 0 \leq k < K, 0 \leq l < M$ .*

*Proof:* Since  $\mathbf{W}_M^H \otimes \mathbf{I}_K$  and  $\mathbf{W}_M \otimes \mathbf{W}_K^H$  in (2.5) are both unitary,  $\mathbf{A}$  is unitary if and only if the diagonal matrix  $\text{diag}(\text{vec}(\mathbf{G}))$  is unitary. This is the case if and only if  $|\mathbf{G}_{k,l}| = 1 \forall 0 \leq k < K, 0 \leq l < M$ . Finally, we have the equivalent condition since  $|\mathbf{G}_{k,l}| = |\bar{\mathbf{G}}_{k,l}|, \forall k, l$ . ■

Observing the result in Theorem 1, we call a prototype filter  $\mathbf{g}$  a *constant-magnitude-characteristic-matrix (CMCM)* filter if the corresponding characteristic matrix contains constant-magnitude entries, i.e., corresponding to a scalar multiple of a unitary GFDM matrix. We will show that CMCM filters are solutions to several of our problems in minimizing the receiver MSE, and are an important class of filters for GFDM.

The following theorem expresses the conditions for the non-singularity of a GFDM matrix in terms of its characteristic matrix and related properties. Later in this thesis, the theorem is shown to be very useful in our study on a GFDM receiver.

**Theorem 2 (Properties of  $\mathbf{A}^{-1}$ )** Let  $\mathbf{A}$  be a GFDM matrix with a  $K \times M$  characteristic matrix  $\mathbf{G}$ . Then,

(a)  $\mathbf{A}$  is invertible if and only if  $\mathbf{G}$  has no zero entries.

(b) If  $\mathbf{A}$  is invertible, then  $\mathbf{A}^{-H}$  is also a GFDM matrix whose characteristic matrix  $\mathbf{H}$  satisfies  $[\mathbf{H}]_{k,l} = 1/[\mathbf{G}]_{k,l}^*, \forall k, l$ , i.e.,

$$\mathbf{H} = (\mathbf{G}^*)^{\circ-1}. \quad (2.13)$$

(c) If  $\mathbf{A}$  is invertible, the squared norm of each row of  $\mathbf{A}^{-1}$  equals the energy of  $\mathbf{A}^{-H}$ ,  $\xi_H = \|\mathbf{H}\|_F^2 / D$ .

*Proof:* (a) According to (2.5),  $\mathbf{A}$  is invertible if and only if  $\mathbf{G}$  has no zero entries since  $\mathbf{W}_M^H \otimes \mathbf{I}_K$  and  $\mathbf{W}_M \otimes \mathbf{W}_K^H$  are both unitary matrices.

(b) According to (2.5), if  $\mathbf{A}$  is invertible,

$$\mathbf{A}^{-H} = (\mathbf{W}_M^H \otimes \mathbf{I}_K)(\text{diag}(\text{vec}(\mathbf{G}))^{-H}(\mathbf{W}_M \otimes \mathbf{W}_K^H)). \quad (2.14)$$

In other words,  $\mathbf{A}^{-H}$  is a GFDM matrix whose characteristic matrix  $\mathbf{H}$  satisfies (2.13).

(c) According to (b),  $\mathbf{A}^{-H}$  is a GFDM matrix. Since the norm of each column of a GFDM matrix equals the norm of its prototype filter, the result follows from Lemma 1(d). ■

The condition for the singularity of  $\mathbf{A}$  is also found in [34]. In [5], Gabor analysis results [32, 35] and DZT [32] were applied to obtain a similar statement in Theorem 2(b). Our derivations, however, involve only basic linear algebra and DFT, making the properties more accessible to general readers.



## Chapter 3

# GFDM Receiver Implementations

In this section, we complete our description of the GFDM system model as illustrated in Fig. 2.1, and propose a new form of low-complexity implementation of ZF and MMSE receivers: the characteristic-matrix-domain implementation.

As shown in Fig. 2.1, the received signal after transmission through a wireless channel is modeled as an LTI system  $y[n] = c[n] * x[n] + q[n]$ , where  $c[n]$  is the channel impulse response, and  $q[n]$  is the complex AWGN with variance  $N_0$ . When  $c[n] = \delta_{n0}$ , the channel reduces to an AWGN channel. More generally, we consider a multipath channel with arbitrary coefficients  $c[n]$ . The channel order is assumed not to exceed the CP length; that is,  $c[n] = 0$  for all  $n$  such that  $n < 0$  or  $n > L$ . The received samples after CP removal and serial-to-parallel (S/P) conversion are collected as  $\mathbf{y}[l] = [y_0[l]y_1[l] \cdots y_{D-1}[l]]^T$ . The transfer function from the transmitted block  $\mathbf{x}[l]$  to the received block  $\mathbf{y}[l]$  is

$$\mathbf{y}[l] = \mathbf{C}\mathbf{x}[l] + \mathbf{q}[l], \quad (3.1)$$

where  $\mathbf{C}$ , the channel circular convolution matrix [2], equals the circulant matrix  $\Psi([c[0] c[1] \cdots c[D-1]]^T)$  [36]. As there is no inter-block interference, the index “[ $l$ ]” is omitted in most parts of the following developments. Since a circulant matrix can be diagonalized by the DFT matrix, we have

$$\mathbf{C} = \mathbf{W}_D^H \mathbf{D}_C \mathbf{W}_D, \quad (3.2)$$

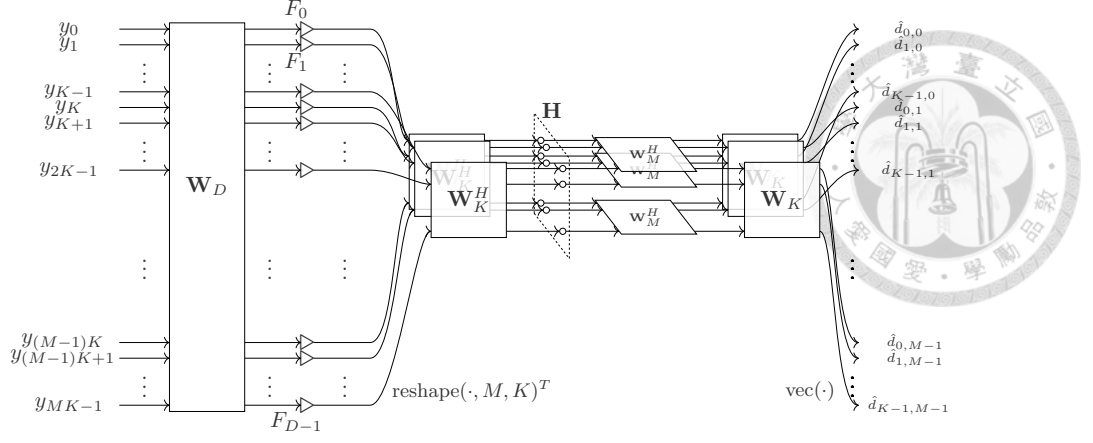


Figure 3.1: Characteristic-matrix-domain Form-2 receiver implementation.

where  $\mathbf{D}_C = \text{diag}([C_0 C_1 \cdots C_{D-1}]^T)$  with  $C_l = \sum_{n=0}^{D-1} c[n] e^{-j2\pi nl/D}$  being the  $D$ -point DFT of  $c[n]$ .

From (2.7) and (3.1), we can express the received block in terms of the source data symbol vector as

$$\mathbf{y} = \mathbf{C}\mathbf{A}\mathbf{d} + \mathbf{q}. \quad (3.3)$$

The receiver is responsible for obtaining the estimated data symbol vector  $\hat{\mathbf{d}}$  given the received block  $\mathbf{y}$ . In the literature, several standard types of receivers have been discussed [2, 5], including MF, ZF, and linear MMSE receivers. Note that when unitary GFDM transmitter matrices are used, an MF receiver is equivalent to a ZF receiver because  $\mathbf{A}^{-1} = \mathbf{A}^H$  if  $\mathbf{A}$  is unitary. We study ZF and MMSE receivers in this thesis.

### 3.1 Low-Complexity ZF Receivers

In the ZF receiver, the demodulator  $\mathbf{B}_{\text{ZF}}$  is formulated as a GFDM receiver matrix  $\mathbf{A}^{-1}$  multiplied by an equalizer  $\mathbf{C}^{-1}$ . The estimated data symbol vector is

$$\hat{\mathbf{d}} = \mathbf{B}_{\text{ZF}}\mathbf{y} = \mathbf{A}^{-1}\mathbf{C}^{-1}\mathbf{y} = \mathbf{d} + \mathbf{A}^{-1}\mathbf{C}^{-1}\mathbf{q}. \quad (3.4)$$

Note that the ZF receiver exists when both  $\mathbf{A}$  and  $\mathbf{C}$  are invertible. Theorem 2(b) implies that  $\mathbf{A}^{-1}$  is just a Hermitian transpose of another GFDM matrix. Combined with the



fact that  $\mathbf{C}$  is diagonalizable by  $\mathbf{W}_D$ , low-complexity implementations for the ZF receiver based on the forms in (2.5) and (2.11) are readily available. Particularly, we obtain the ZF receiver Form-1 implementation

$$\mathbf{B}_{\text{ZF}} = (\mathbf{W}_M^H \otimes \mathbf{W}_K) \mathbf{D}_G^{-1} (\mathbf{W}_M \otimes \mathbf{I}_K) \mathbf{W}_D^H \mathbf{D}_C^{-1} \mathbf{W}_D, \quad (3.5)$$

where  $\mathbf{D}_G = \text{diag}(\text{vec}(\mathbf{G}))$ , and the ZF receiver Form-2 implementation

$$\mathbf{B}_{\text{ZF}} = (\mathbf{W}_M^H \otimes \mathbf{W}_K) \bar{\mathbf{D}}_G^{-1} (\mathbf{I}_M \otimes \mathbf{W}_K^H) \mathbf{\Pi}^T \mathbf{D}_C^{-1} \mathbf{W}_D, \quad (3.6)$$

where  $\bar{\mathbf{D}}_G = \text{diag}(\text{vec}(\bar{\mathbf{G}}))$ . The block diagram of a Form-2 receiver is shown in Fig. 3.1, with  $F_l = 1/C_l, \forall 0 \leq l < D$  and  $\mathbf{H} = \bar{\mathbf{G}}^{\circ-1}$  therein. Although the complexity of both forms is in  $O(KM \log KM)$ , we show in Chapter 4 that Form 2 is generally of lower complexity. Yet, under the special case of the AWGN channel, Form-1 implementation is advantageous since it is simplified to

$$\mathbf{A}^{-1} = (\mathbf{W}_M^H \otimes \mathbf{W}_K) \mathbf{D}_G^{-1} (\mathbf{W}_M \otimes \mathbf{I}_K), \quad (3.7)$$

which does the reverse operation of Fig. 2.2.

The frequency-domain implementation can be used for ZF receivers. It is proposed that the estimated data symbols for the  $k$ th subcarrier in the ZF receiver are given by [8, 12]

$$\hat{\mathbf{d}}_k = \frac{1}{\sqrt{K}} \mathbf{W}_M^H \mathbf{R}^T \text{diag}(\mathbf{h}_f) (\mathbf{P}^{(k)})^T \mathbf{D}_C^{-1} \mathbf{W}_D \mathbf{y}, \quad (3.8)$$

where  $\mathbf{h}_f$  is the ZF frequency-domain prototype receive filter.

## 3.2 Low-Complexity MMSE Receivers

For an MMSE receiver, the existence of a low-complexity implementation at the order  $O(KM \log KM)$  has not been well studied previously except in the case of an AWGN channel [8, 9]. Assuming  $\text{E}\{\mathbf{d}\mathbf{d}^H\} = E_S \mathbf{I}_D$  (i.e., all subcarriers are subsymbols are allo-

cated with data)<sup>1</sup>, the MMSE receiver for (3.3) can be modeled as [36]

$$\mathbf{B}_{\text{MMSE}} = \mathbf{A}^H \mathbf{C}^H [\mathbf{C} \mathbf{A} \mathbf{A}^H \mathbf{C}^H + \gamma^{-1} \mathbf{I}_D]^{-1}, \quad (3.9)$$

where  $\gamma = E_S/N_0$  is the signal-to-noise ratio (SNR), and

$$\hat{\mathbf{d}} = \mathbf{B}_{\text{MMSE}} \mathbf{y}. \quad (3.10)$$

When both  $\mathbf{A}$  and  $\mathbf{C}$  are invertible, (3.9) reduces to [5]

$$\mathbf{B}_{\text{MMSE}} = [\mathbf{C} \mathbf{A} + \gamma^{-1} (\mathbf{C} \mathbf{A})^{-H}]^{-1}. \quad (3.11)$$

Either (3.9) or (3.11) involves the inversion of a matrix that is not a GFDM matrix, so Theorem 2 does not apply here to the reduction of the implementation complexity. A direct implementation requires a complexity of  $O(K^3 M^3)$  and is often not a desirable solution. Also, the frequency-domain implementation [8] is not applicable to the MMSE receiver in general since (3.9) cannot be simplified to the form in (3.8).

We propose to use the structure depicted in Fig. 3.1 in our study of a potential MMSE receiver, where coefficients  $F_k$  and entries of  $\mathbf{H}$  are to be designed. The following theorem provides the necessary and sufficient conditions on which an MMSE receiver can be implemented with such a form.

**Theorem 3** *Let  $\mathbf{A}$  be a nonsingular GFDM matrix with a  $K \times M$  phase-shifted characteristic matrix  $\bar{\mathbf{G}}$ ,  $\mathbf{C}$  be a  $D \times D$  nonsingular circulant matrix,  $\gamma$  be a positive real number,  $\mathbf{D}_C = \mathbf{W}_D \mathbf{C} \mathbf{W}_D^H$ , and  $C_l = [\mathbf{D}_C]_l, \forall 0 \leq l < D$ , where  $D = KM$ . Then, there exist  $D \times D$  nonsingular diagonal matrices  $\mathbf{D}_1, \mathbf{D}_2$  such that  $\mathbf{B}_{\text{MMSE}}$  defined in (3.11) satisfies*

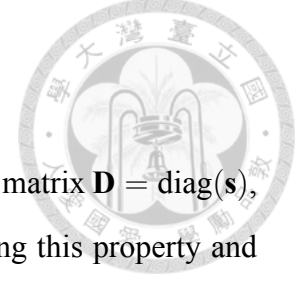
$$\mathbf{B}_{\text{MMSE}} = (\mathbf{W}_M^H \otimes \mathbf{W}_K) \mathbf{D}_2^{-1} (\mathbf{I}_M \otimes \mathbf{W}_K^H) \mathbf{\Pi}^T \mathbf{D}_1^{-1} \mathbf{W}_D \quad (3.12)$$

*if and only if  $\forall 0 \leq m < M$ , either (a)  $|[\bar{\mathbf{G}}]_{k,m}|$  is a constant in  $k$ , or (b)  $|C_{kM+m}|$  is a*

<sup>1</sup>If this is not the case, then the subsequent derived MMSE receiver is not exact, and one may want to derive a low-complexity exact MMSE receiver in the future.



constant in  $k$ , or both, where  $\mathbf{\Pi}$  is defined in (2.12).



*Proof:* Let  $\mathbf{Q} = \mathbf{I}_M \otimes \mathbf{W}_K$ . Note that for any  $D \times D$  diagonal matrix  $\mathbf{D} = \text{diag}(\mathbf{s})$ ,  $\mathbf{D}' \triangleq \mathbf{\Pi}^T \mathbf{D} \mathbf{\Pi}$  is also a diagonal matrix with  $\mathbf{D}' = \text{diag}(\mathbf{\Pi}^T \mathbf{s})$ . Using this property and (2.11)(3.2), one can show that

$$[\mathbf{CA} + \gamma^{-1}(\mathbf{CA})^{-H}]^{-1} = (\mathbf{W}_M^H \otimes \mathbf{W}_K) \mathbf{E}^{-1} \mathbf{\Pi}^T \mathbf{W}_D \quad (3.13)$$

where  $\mathbf{E}$  is defined as

$$\mathbf{E} = \mathbf{D}'_C \mathbf{Q} \bar{\mathbf{D}}_G + \gamma^{-1} \mathbf{D}'_C{}^{-H} \mathbf{Q} \bar{\mathbf{D}}_G{}^{-H}, \quad (3.14)$$

$\bar{\mathbf{D}}_G = \text{diag}(\text{vec}(\bar{\mathbf{G}}))$ ,  $\mathbf{D}'_C = \mathbf{\Pi}^T \mathbf{D}_C \mathbf{\Pi}$  is a diagonal matrix with  $\mathbf{D}'_C = \text{diag}(\mathbf{\Pi}^T \mathbf{c}_f)$ , and  $\mathbf{c}_f = [C_0 C_1 \cdots C_{D-1}]^T$ . Noting that  $\mathbf{W}_M^H \otimes \mathbf{W}_K$ ,  $\mathbf{\Pi}^T$ , and  $\mathbf{W}_D$  in (3.13) are all unitary, and that  $\mathbf{\Pi}^T \mathbf{D}_1^{-1} = \mathbf{D}_3^{-1} \mathbf{\Pi}^T$  if we define  $\mathbf{D}_3$  as  $\mathbf{D}_3 = \mathbf{\Pi}^T \mathbf{D}_1 \mathbf{\Pi}$ , we determine that (3.12) is satisfied if and only if there exist nonsingular  $D \times D$  diagonal matrices  $\mathbf{D}_3, \mathbf{D}_2$  such that  $\mathbf{E} = \mathbf{D}_3 \mathbf{Q} \mathbf{D}_2$ . Let  $\mathbf{u}_m, \tilde{\mathbf{u}}_m, \mathbf{v}_m, \tilde{\mathbf{v}}_m, \mathbf{w}_m, \mathbf{z}_m$  be  $K \times 1$  vectors  $\forall 0 \leq m < M$  such that  $\text{diag}([\mathbf{u}_0^T \cdots \mathbf{u}_{M-1}^T]^T) = \mathbf{D}'_C$ ,  $\text{diag}([\tilde{\mathbf{u}}_0^T \cdots \tilde{\mathbf{u}}_{M-1}^T]^T) = \mathbf{D}'_C{}^{-H}$ ,  $\text{diag}([\mathbf{v}_0^T \cdots \mathbf{v}_{M-1}^T]^T) = \bar{\mathbf{D}}_G$ ,  $\text{diag}([\tilde{\mathbf{v}}_0^T \cdots \tilde{\mathbf{v}}_{M-1}^T]^T) = \bar{\mathbf{D}}_G{}^{-H}$ ,

$$\text{diag}([\mathbf{w}_0^T \cdots \mathbf{w}_{M-1}^T]^T) = \mathbf{D}_3, \text{diag}([\mathbf{z}_0^T \cdots \mathbf{z}_{M-1}^T]^T) = \mathbf{D}_2. \quad (3.15)$$

Noting that  $\mathbf{Q} = \mathbf{I}_M \otimes \mathbf{W}_K = \text{blkdiag}(\{\mathbf{W}_K\}_{m=0}^{M-1})$ , we obtain that  $\mathbf{D}_3 \mathbf{Q} \mathbf{D}_2 = \text{blkdiag}(\{(\mathbf{w}_m \mathbf{z}_m^T) \circ \mathbf{W}_K\}_{m=0}^{M-1})$  and  $\mathbf{E} = \text{blkdiag}(\{\mathbf{F}_m \circ \mathbf{W}_K\}_{m=0}^{M-1})$ , where  $\forall 0 \leq m < M$ ,

$$\mathbf{F}_m = [\mathbf{u}_m \gamma^{-1} \tilde{\mathbf{u}}_m][\mathbf{v}_m \tilde{\mathbf{v}}_m]^T. \quad (3.16)$$

Since for both  $\mathbf{E}$  and  $\mathbf{Q}$ , each block diagonal submatrix is a full matrix without any zero entry,  $\mathbf{E} = \mathbf{D}_3 \mathbf{Q} \mathbf{D}_2$  is satisfied if and only if  $\mathbf{F}_m = \mathbf{w}_m \mathbf{z}_m^T$  is satisfied  $\forall 0 \leq m < M$ . For any given  $m$ , if condition (a) is satisfied:  $|[\mathbf{v}_m]_k| = |[\bar{\mathbf{G}}]_{k,m}|$  is a constant in  $k$ , then

$\tilde{\mathbf{v}}_m = |[\bar{\mathbf{G}}]_{0,m}|^{-2}\mathbf{v}_m$  and we can choose

$$\mathbf{w}_m = \mathbf{u}_m + (\gamma|[\bar{\mathbf{G}}]_{0,m}|^2)^{-1}\tilde{\mathbf{u}}_m, \quad \mathbf{z}_m = \mathbf{v}_m, \quad (3.17)$$

to make  $\mathbf{F}_m = \mathbf{w}_m\mathbf{z}_m^T$ ; if condition (b) is satisfied:  $|[\mathbf{u}_m]_k| = |C_{kM+m}|$  is a constant in  $k$ , then  $\tilde{\mathbf{u}}_m = |C_m|^{-2}\mathbf{u}_m$  and we can choose

$$\mathbf{w}_m = \mathbf{u}_m, \quad \mathbf{z}_m = \mathbf{v}_m + (\gamma|C_m|^2)^{-1}\tilde{\mathbf{v}}_m. \quad (3.18)$$

to make  $\mathbf{F}_m = \mathbf{w}_m\mathbf{z}_m^T$ . It is now clear that for any  $m$ , if at least one of (a) and (b) is satisfied, then there exist  $\mathbf{w}_m, \mathbf{z}_m$ , and consequently,  $\mathbf{D}_2, \mathbf{D}_3$ , such that  $\mathbf{E}$  in (3.14) satisfies  $\mathbf{E} = \mathbf{D}_3\mathbf{Q}\mathbf{D}_2$ . Conversely, assume that  $\mathbf{F}_m = \mathbf{w}_m\mathbf{z}_m^T$  is satisfied  $\forall 0 \leq m < M$ , but that both conditions (a) and (b) are not satisfied for some  $m$ , say,  $m_0$ . Then, both sets  $\{\mathbf{u}_{m_0}, \tilde{\mathbf{u}}_{m_0}\}$  and  $\{\mathbf{v}_{m_0}, \tilde{\mathbf{v}}_{m_0}\}$  are linearly independent. Thus,  $\text{rank}(\mathbf{F}_{m_0}) = 2$ , which can be proved by, e.g., Sylvester's law of nullity [37]. This contradicts to the assumption  $\mathbf{F}_{m_0} = \mathbf{w}_{m_0}\mathbf{z}_{m_0}^T$ . ■

Theorem 3 implies that a unitary GFDM matrix and the AWGN channel are two sufficient (but not necessary) conditions for the existence of the low-complexity MMSE receiver implementation in the form of Fig. 3.1. Specifically, assuming  $\mathbf{C}$  in Theorem 3 is the channel circulant matrix, we obtain that  $|C_{kM+m}|$  is constant in  $k$  for all  $m$  under the AWGN channel. Thus, according to (3.18), the MMSE receiver under the AWGN channel can be implemented as shown in Fig. 3.1, with  $F_l = 1, \forall 0 \leq l < D$  and  $\mathbf{H} = (\bar{\mathbf{G}} + \gamma^{-1}(\bar{\mathbf{G}}^*)^{\circ-1})^{\circ-1}$  therein. For the more practical case where  $|C_{kM+m}|$  is non-constant in  $k$  for all  $m$ , Theorem 3 implies that a sufficient condition for a low-complexity MMSE receiver implementation in the form of Fig. 3.1 is that  $|[\bar{\mathbf{G}}]_{k,m}|$  is a constant in both  $k$  and  $m$ , i.e., using a unitary GFDM matrix  $\mathbf{A}$  up to a scale factor, or equivalently, a CMCM filter, in view of Theorem 1. In this case, each  $|[\bar{\mathbf{G}}]_{k,m}|^2$  equals the energy  $\xi_G$  of  $\mathbf{A}$ , and according to (3.17), we have the Form-2 implementation of the MMSE receiver shown in Fig. 3.1, with  $F_l = 1/(C_l + (\gamma\xi_G C_l^*)^{-1}), \forall 0 \leq l < D$  and  $\mathbf{H} = \bar{\mathbf{G}}^{\circ-1}$  therein.

### 3.3 Low-Complexity Approximated MMSE Receivers

If neither conditions (a) nor (b) in Theorem 3 are satisfied for some  $m$ , then it is impossible to find  $\mathbf{D}_3, \mathbf{D}_2$  such that  $\mathbf{E} = \mathbf{D}_3 \mathbf{Q} \mathbf{D}_2$ , where  $\mathbf{E}$  is defined in (3.14) and  $\mathbf{Q} = \mathbf{I}_M \otimes \mathbf{W}_K$ . In this case, an exact MMSE receiver cannot be implemented as shown in Fig. 3.1, but we propose using an approximated MMSE receiver based on the same structure. Specifically, we minimize the Frobenius norm  $\|\mathbf{E} - \mathbf{D}_3 \mathbf{Q} \mathbf{D}_2\|_F$  by using low-rank matrix approximations. Since  $\mathbf{E} = \text{blkdiag}(\{\mathbf{F}_m \circ \mathbf{W}_K\}_{m=0}^{M-1})$ ,  $\mathbf{D}_3 \mathbf{Q} \mathbf{D}_2 = \text{blkdiag}(\{(\mathbf{w}_m \mathbf{z}_m^T) \circ \mathbf{W}_K\}_{m=0}^{M-1})$ , and  $\mathbf{W}_K$  contains constant-magnitude entries, an equivalent condition is minimizing  $\|\mathbf{F}_m - \mathbf{w}_m \mathbf{z}_m^T\|_F, \forall 0 \leq m < M$ , where  $\mathbf{w}_m, \mathbf{z}_m$ , and  $\mathbf{F}_m$  are defined in (3.15) and (3.16). By performing the singular value decomposition (SVD) of  $\mathbf{F}_m$  for each  $m$ , we obtain  $\mathbf{F}_m = \mathbf{U}_m \mathbf{\Sigma}_m \mathbf{V}_m^H$ , where  $\mathbf{U}_m$  and  $\mathbf{V}_m$  are  $D \times D$  unitary matrices, and  $\mathbf{\Sigma}_m = \text{diag}([s_m^{(1)} s_m^{(2)} 0 \cdots 0]^T)$  with  $s_m^{(1)} \geq s_m^{(2)}$ . Accordingly, we can minimize  $\|\mathbf{F}_m - \mathbf{w}_m \mathbf{z}_m^T\|_F$  by taking  $\mathbf{w}_m \mathbf{z}_m^T = s_m^{(1)} [\mathbf{U}_m]_{:,0} [\mathbf{V}_m]_{:,0}^H$  [38]. The complexity of computing the SVD of each rank-2 matrix  $\mathbf{F}_m$  is in  $O(K)$  [39], so the overall complexity of the receiver is still in  $O(KM \log KM)$ . Moreover, we will show by simulation that this approximated MMSE receiver has favorable MSE and SER performance. Note that Theorem 3 does not imply the non-existence of a low-complexity MMSE receiver in  $O(KM \log KM)$  when both conditions (a) and (b) therein are not satisfied; it just states that an MMSE receiver cannot be implemented in the form shown in Fig. 3.1. Whether an exact MMSE receiver can be implemented with low complexity remains an open question.

In summary, a low-complexity MMSE receiver implementation exists in an AWGN channel (as has been known). A less known condition for the existence of low-complexity MMSE receiver implementation is to employ a *unitary GFDM matrix*. If one chooses not to use a unitary GFDM matrix, the approximated MMSE receiver can be used for a low-complexity implementation with suboptimal performance.

#### 3.3.1 Simulation Results

The performance of the proposed low-complexity approximated MMSE (AMMSE) receiver is compared to those of the ZF and MMSE receivers through simulation. The MSE

and SER performance is evaluated through Monte-Carlo simulation with 10000 blocks for each prototype filter. We use  $(K, M) = (8, 5)$  for GFDM, and  $(K, M) = (40, 1)$  for OFDM (OFDM is a special case of GFDM using a rectangular window as the prototype transmit filter) so that GFDM and OFDM have the same block size  $D = KM$ . A Rayleigh fading channel is used. Specifically, the channel impulse response  $c[n]$  is independent circularly symmetric complex Gaussian with variance  $N_n^{(c)}$ , and the (unnormalized) power delay profile [36] is  $N_n^{(c)} = (0.64)^n$  for  $0 \leq n < D/4$  and  $N_n^{(c)} = 0$  for  $D/4 \leq n < D$ . Finally, for MMSE (and AMMSE) receivers, unbiased estimates are used for symbol detection [36].

The modulation is 16QAM, the symbol energy is  $E_S = 1$ , and the energy of the GFDM transmitter matrices is  $\xi_G = 1$ . The CP length is  $L = D/4$ . The prototype transmit filters used for GFDM include an RC filter with roll-off factor  $\alpha = 0.7$  and an RRC filter with roll-off factor  $\alpha = 1$ . To demonstrate that the AMMSE and MMSE receivers for any CMCM filter are identical, CMCM Filter 1 with the characteristic matrix  $\mathbf{G}_1$  is used in the simulation, where the phases  $\angle \mathbf{G}_1$  are arbitrarily selected and listed as follows:

$$\angle \mathbf{G}_1 = \begin{bmatrix} 0.62 & -0.40 & -1.36 & -2.16 & -1.94 \\ -1.30 & -2.65 & 2.78 & -2.95 & 2.17 \\ 1.01 & 0.07 & 2.86 & 2.92 & -0.60 \\ 1.75 & 2.09 & 1.59 & 0.48 & -1.89 \\ 1.55 & -1.83 & -0.11 & -3.01 & -0.57 \\ 0.27 & -1.21 & -2.81 & 0.37 & -2.27 \\ -1.48 & 0.46 & 2.58 & 2.72 & 0.44 \\ 1.23 & -0.31 & 1.19 & 0.06 & -0.35 \end{bmatrix}. \quad (3.19)$$

The simulation results of MSE and SER performance are shown in Figs. 3.2, 3.3, and 3.4. The SER performance is shown in two figures (Figs. 3.3 and 3.4) to make the curves clear. As indicated by Theorem 3, the AMMSE and MMSE receivers for a CMCM filter are identical. By contrast, Figs. 3.2, 3.3, and 3.4 show that the MSE and SER performance is degraded due to approximation for the RC and RRC filters, particularly the RRC filter. In this case,  $\xi_H = 1, 1.08,$  and  $1.25$  for the CMCM, RC, and RRC filters, respectively. Together with the results in Figs. 3.2, 3.3, and 3.4, this implies that higher nonuniformity of  $|\mathbf{G}_{k,l}|, \forall 0 \leq k < K, 0 \leq l < M$  engenders more errors in the approximation process. However, in Figs. 3.3 and 3.4, all AMMSE receivers show significant

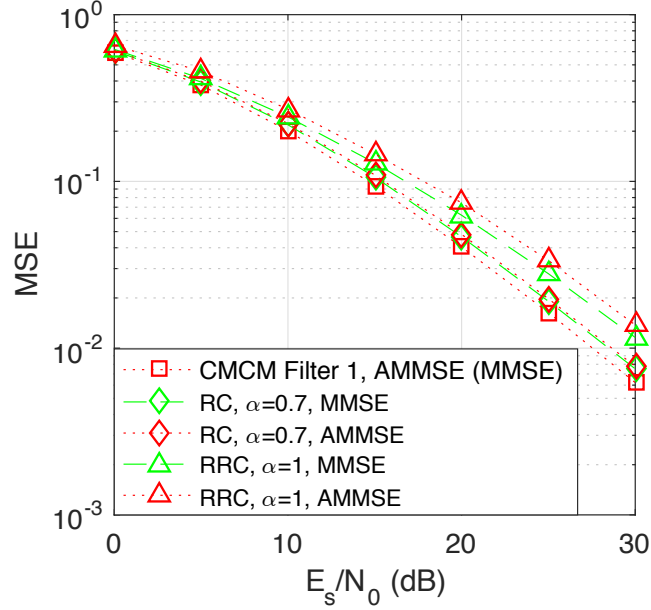


Figure 3.2: MSE for GFDM approximated MMSE (AMMSE) receiver over the Rayleigh fading channel (compared to the corresponding ZF and MMSE receivers).

performance improvements over their ZF receiver counterparts, and exhibit SERs that are the same as or only slightly higher than do the MMSE receiver counterparts. (MSEs of ZF receivers are infinite and thus not shown in Fig. 3.2.) Besides, the complexity of the MMSE receivers (directly implemented as in (3.11)) is in  $O(K^3M^3)$ , whereas that of the AMMSE receivers is in  $O(KM \log KM)$ . These show that the AMMSE receiver is a good compromise between complexity and performance.

### 3.4 Remarks on Soft-Output Demodulation

In a receiver that applies soft-output demodulation, it is essential to have the knowledge of error variances  $\sigma_{k,m}^2 \triangleq [\mathbf{R}_e]_{k+mK}, \forall 0 \leq k < K, 0 \leq m < M$ , where  $\mathbf{R}_e = E\{\mathbf{e}\mathbf{e}^H\}$  and  $\mathbf{e} = \hat{\mathbf{d}} - \mathbf{d}$ . It is worthy to note that low-complexity algorithms at the order  $O(KM \log K)$  can be found to obtain these values, using characteristic matrix techniques presented above. For the ZF receiver, using (3.4) and (3.2), we can derive  $\mathbf{R}_e = N_0(\mathbf{W}_D\mathbf{A}^{-H})^H\mathbf{D}_C^{-1}\mathbf{D}_C^{-H}(\mathbf{W}_D\mathbf{A}^{-H})$ . One may verify with some efforts, using (2.11), that  $\sigma_{k,m}^2$  is constant in  $m$  for any  $k$ , and that the vector  $\boldsymbol{\sigma} \triangleq [\sigma_{0,m}^2, \sigma_{1,m}^2, \dots, \sigma_{K-1,m}^2]^T$

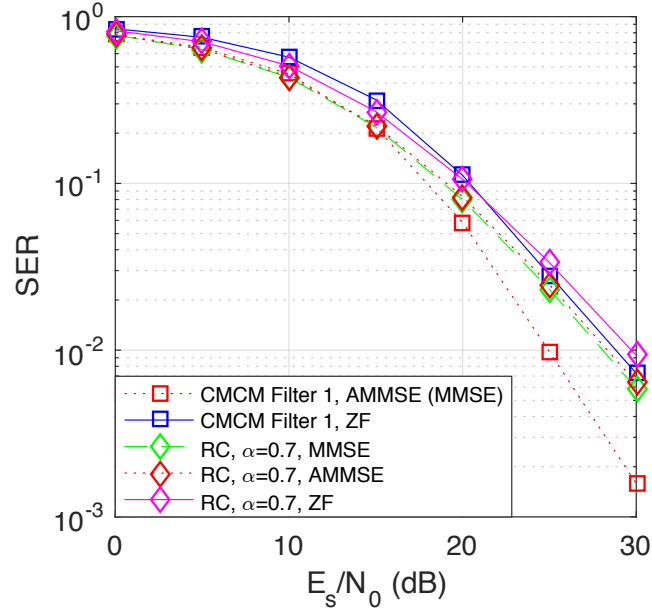


Figure 3.3: SER for GFDM approximated MMSE (AMMSE) receiver over the Rayleigh fading channel (compared to the corresponding ZF and MMSE receivers).

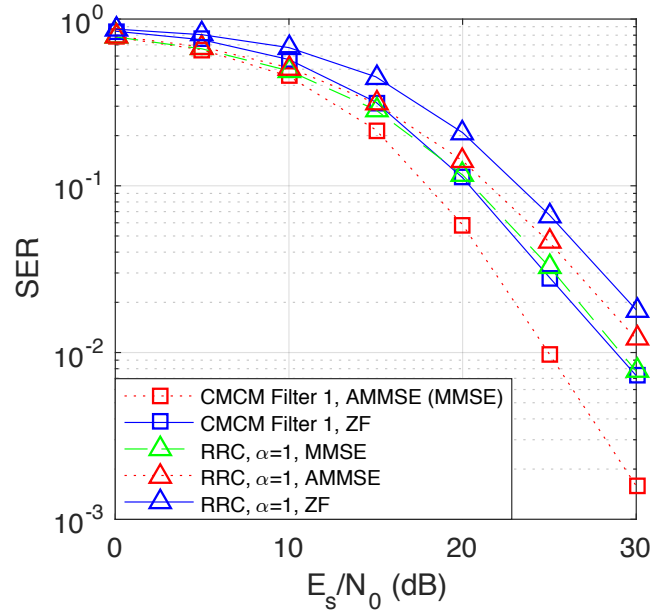


Figure 3.4: SER for GFDM approximated MMSE (AMMSE) receiver over the Rayleigh fading channel (compared to the corresponding ZF and MMSE receivers).

has the form

$$\sigma = \frac{N_0}{D} \mathbf{W}_K \sum_{l=0}^{M-1} [\text{diag}(\mathbf{t}_l) \mathbf{W}_K^H \mathbf{r}_l] \quad (3.20)$$

where

$$\mathbf{r}_l = [ |C_l|^{-2} |C_{M+l}|^{-2} \cdots |C_{(K-1)M+l}|^{-2} ]^T \quad (3.21)$$



and

$$\mathbf{t}_l^T = \sum_{p=0}^{K-1} [\bar{\mathbf{H}}]_{p,l}^* \left[ [\bar{\mathbf{H}}]_{\langle p \rangle_K, l} [\bar{\mathbf{H}}]_{\langle p+1 \rangle_K, l} \cdots [\bar{\mathbf{H}}]_{\langle p+K-1 \rangle_K, l} \right], \quad (3.22)$$

with  $\bar{\mathbf{H}} = \bar{\mathbf{G}}^{\circ-1}$ . Note that  $\mathbf{t}_l$  can be pre-computed, so the complexity for calculating (3.20) is at the order  $O(KM \log K)$ . For the MMSE receiver, assuming  $\mathbf{A}$  is unitary, we can similarly derive  $\mathbf{R}_e = E_S(\mathbf{I}_D - (\mathbf{W}_D \mathbf{A}^{-H})^H \mathbf{D}_C^H (\mathbf{D}_C \mathbf{D}_C^H + \gamma^{-1} \mathbf{I}_D)^{-1} \mathbf{D}_C (\mathbf{W}_D \mathbf{A}^{-H}))$ . Thus, we can derive that  $\sigma$  for the MMSE receiver can be expressed as in (3.20) by changing the  $k$ th entry of  $\mathbf{r}_l$  from  $|C_{kM+l}|^{-2}$  to  $|C_{kM+l}|^2 / (|C_{kM+l}|^2 + \gamma^{-1})$ , so the complexity for calculating the error variances is again at the order  $O(KM \log K)$ .





## Chapter 4

# Complexity Analysis

The computational complexity of the proposed transceiver implementations in Chapters 2 and 3 is compared to that of several GFDM and conventional OFDM transceiver implementations. As the case of AWGN channels has been well studied, we focus our complexity analysis on the case under multipath channels, which are more general and more practical. For GFDM transmitters and ZF receivers, we include the frequency-domain implementation [12] mentioned in Chapters 2 and 3, the implementation proposed in [8], which is based on performing frequency-domain convolution in time domain as element-wise vector multiplication, and the implementation in [9], which is based on exploiting the block circularity of matrices involved in modulation and demodulation. For GFDM MMSE receivers, we include the implementation in [10], which is based on calculating filter coefficients and filtering in the Zak domain, and the implementation in [11], which is based on simplifying the inversion of a band-diagonal matrix with LU decomposition. Since [11] is for a multiple-antenna system, we calculate its complexity by reducing it to a single-antenna system. It is assumed in [10, 11] that the frequency-domain prototype transmit filter  $\mathbf{g}_f$  has only  $2M$  nonzero entries, so the complexity formulae for the MMSE receivers in [10, 11] cannot be used for all general prototype filters. We also compare to direct implementations, where the matrix multiplications and inverses in (2.7), (3.4), and (3.10) are implemented directly. The comparison is based on the number of complex multiplications (CMs) required to transmit or receive  $KM$  symbols, as shown in Tables 4.1 and 4.2. For a fair comparison, the same block size  $KM$  as GFDM is used for OFDM [36].

Table 4.1: Computational complexity of GFDM transmitter and ZF receiver implementations under multipath channels

Implementation	Transmitter	ZF receiver
OFDM	$\frac{1}{2}KM \log KM$	$\frac{1}{2}KM \log KM + KM$
Direct	$K^2M^2$	$K^2M^2 + KM(\log KM + 1)$
Frequency-domain [12]	$KM(\frac{1}{2} \log KM^2 + L_T)^a$	$KM(\frac{1}{2} \log KM^2 + L_R) + KM^b$
Frequency-convolution [8]	$KM(\frac{1}{2} \log K + M)$	$KM(\frac{1}{2} \log K + M) + KM(\log KM + 1)$
Block-circularity [9]	$KM(\frac{1}{2} \log K + M)$	$KM(\frac{1}{2} \log K + M) + KM(\log KM + 1)$
Block-circularity [9], power-of-2 $M$	$KM(\frac{1}{2} \log KM^2 + 1)$	$KM(\frac{1}{2} \log KM^2 + 1) + KM(\log KM + 1)$
Zak-domain [10]	Not applicable	Not applicable
LU-decomposition [11]	Not applicable	Not applicable
Proposed Form 1	$KM(\frac{1}{2} \log KM^2 + 1)$	$KM(\frac{1}{2} \log KM^2 + 1) + KM(\log KM + 1)$
Proposed Form 2	$KM(\frac{1}{2} \log K^3M^2 + 1)$	$KM(\frac{1}{2} \log K^3M^2 + 1) + KM$

<sup>a</sup>Assumption: The frequency-domain prototype transmit filter  $\mathbf{g}_f$  has only  $L_T M$  nonzero entries.

<sup>b</sup>Assumption: The frequency-domain prototype receive filter  $\mathbf{h}_f$  has only  $L_R M$  nonzero entries.

Table 4.2: Computational complexity of GFDM MMSE receiver implementations under multipath channels

Implementation	MMSE receiver
OFDM	$KM(\frac{1}{2} \log KM + 1)$
Direct	$\frac{7}{3}K^3M^3 + 2K^2M^2$
Frequency-domain [12]	Applicable only to AWGN channels
Frequency-convolution [8]	Applicable only to AWGN channels
Block-circularity [9]	Applicable only to AWGN channels
Block-circularity [9], power-of-2 $M$	Applicable only to AWGN channels
Zak-domain [10]	$KM(\log M + 6K + 12M + 4)^a$
LU-decomposition [11]	$KM(\frac{1}{2} \log KM + 20M^2 + 22M)^a$
Proposed Form 1	$KM(\frac{1}{2} \log K^3M^4 + 4)^b$
Proposed Form 2	$KM(\frac{1}{2} \log K^3M^2 + 4)^b$

<sup>a</sup>Assumption: The frequency-domain prototype transmit filter  $\mathbf{g}_f$  has only  $2M$  nonzero entries.

<sup>b</sup>Assumption: The prototype transmit filter is a CMCM filter.

To obtain the complexity formulae, we assume that a  $p$ -point DFT [40] and the inversion of a  $p \times p$  matrix based on Gaussian elimination [41] take  $\frac{p}{2} \log p$  and  $p^3/3$  CMs, respectively, for any positive integer  $p$ , where the base of the logarithm is 2. The prototype filters for all implementations are assumed to take complex values. Since the prototype filter in [9] is assumed to be real-valued, we extend their results to the case of complex-valued filters.

As depicted in Fig. 2.2, the proposed Form-1 transmitter implementation involves four steps:  $M$  sets of  $K$ -point inverse-DFTs (IDFTs),  $K$  sets of  $M$ -point DFTs, element-wise multiplication with a  $K \times M$  matrix, and  $K$  sets of  $M$ -point IDFTs. These result in  $M\frac{K}{2} \log K + K\frac{M}{2} \log M + KM + K\frac{M}{2} \log M = KM(\frac{1}{2} \log KM^2 + 1)$  CMs. Similarly, we can derive the complexity formulae for the proposed Form-2 transmitter (2.11), Form-1 receiver (3.5), and Form-2 receiver (3.6) as described in Tables 4.1 and 4.2. If CMCM

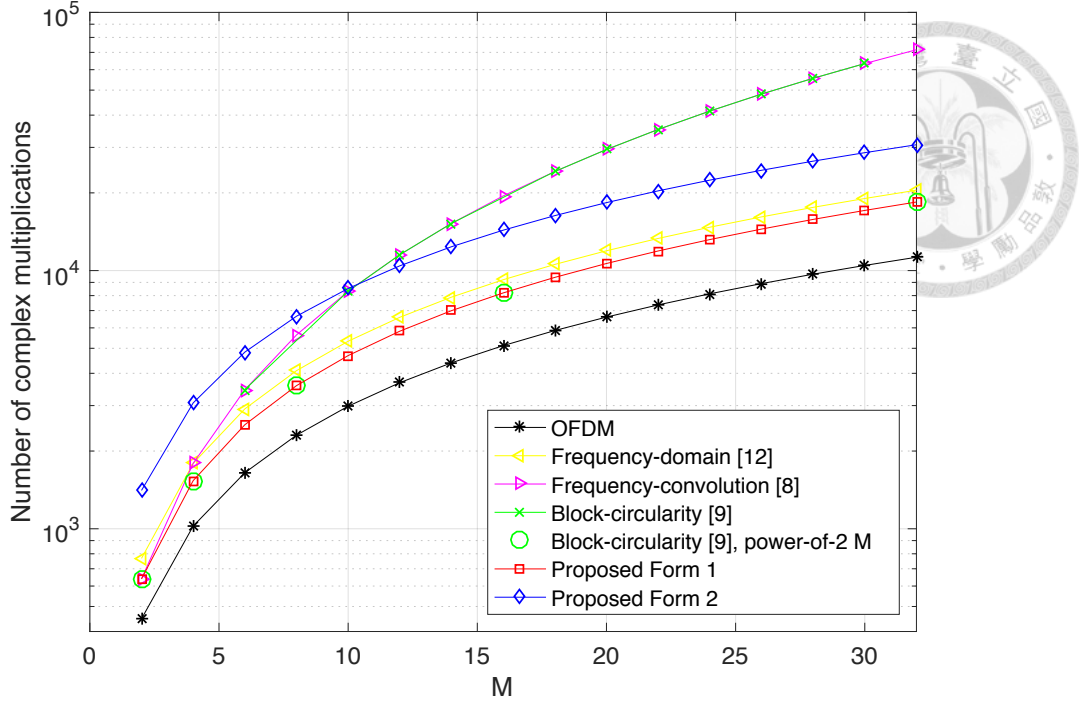


Figure 4.1: Computational complexity of GFDM transmitter implementations.  $K = 64$ .

filters are used, MMSE receivers can also be implemented based on (3.5) and (3.6) by replacing each diagonal entry  $C_l$  in the matrix  $\mathbf{D}_C$  with  $C_l + (\gamma\xi_G C_l^*)^{-1}$ , where  $\xi_G$  is the energy of the transmitter matrix, and  $\gamma = E_S/N_0$  is the SNR. In view of the number of CMs described in Tables 4.1 and 4.2, we recommend using the Form-1 implementation for transmitters and Form-2 implementation for receivers. For the frequency-domain implementation [12], the parameter  $L_T \leq K$  is the number of subcarriers spanned by the frequency-domain prototype transmit filter (i.e.,  $\mathbf{g}_f$  has only  $L_T M$  nonzero entries), and  $L_R \leq K$  is the number of subcarriers spanned by the frequency-domain prototype receive filter. It was stated in [9] that the complexity of their implementation can be reduced when  $M$  is a power of two. The reduced complexity is listed separately in Table 4.1. For a fair comparison, frequency-domain one-tap equalization  $\mathbf{W}_D^H \mathbf{D}_C^{-1} \mathbf{W}_D$ , taking  $KM(\log KM + 1)$  CMs, as in (3.5) or in (7) of [9] is used for all GFDM ZF receivers except for the proposed Form-2 receiver and the implementation in [12], in which, due to cancellation of a pair of DFT and IDFT, only  $KM$  additional CMs are needed.

The complexity formulae in Tables 4.1 and 4.2 are evaluated and plotted for  $K = 64$  subcarriers with respect to different values of number of subsymbols  $M$ . The complexity

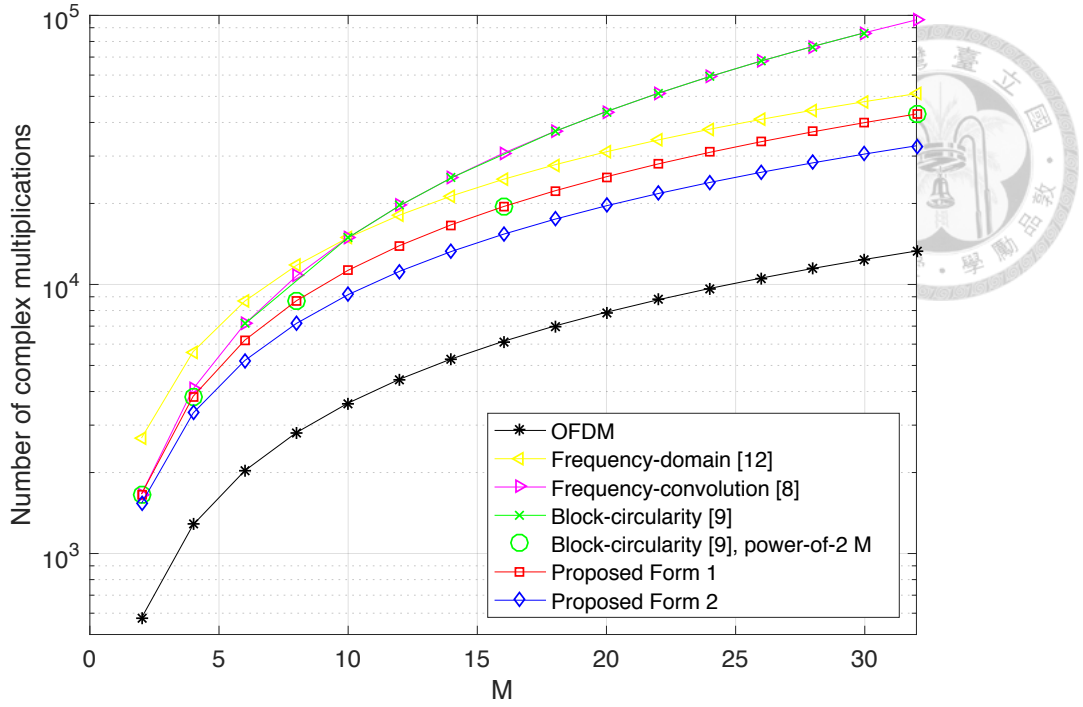


Figure 4.2: Computational complexity of GFDM ZF receiver implementations.  $K = 64$ .

of the transmitter implementations is shown in Fig. 4.1. As suggested in [12],  $L_T = 2$  is chosen for calculating the complexity of the frequency-domain implementation. According to Fig. 4.1, the number of CMs required by the proposed Form-1 transmitter is the least among all GFDM transmitters, and is only about 1.5 times as much as that required by the OFDM transmitter. The complexity of the frequency-domain implementation [12], under the assumption that  $L_T$  is as small as 2, is around 1.1 to 1.2 times the complexity of the proposed Form-1 transmitter. The complexity of the implementation in [8] and the one in [9] is even over 3 times the complexity of the proposed Form-1 transmitter when  $M$  is relatively large. (The complexity of the implementation in [12] would be higher than that of the one in [8] if  $L_T = K$  for general filters.) The reduced complexity of the implementation in [9] when  $M$  is a power of two, nevertheless, coincides that of the proposed Form-1 transmitter.

The complexity of the ZF receiver implementations is shown in Fig. 4.2. Based on the suggestion in [2],  $L_R = 16$  is chosen for the frequency-domain ZF receiver implementation [12]. According to Fig. 4.2, the number of CMs required by the proposed Form-2 ZF receiver is the least among all GFDM ZF receivers, and is only about 2.5 times as much

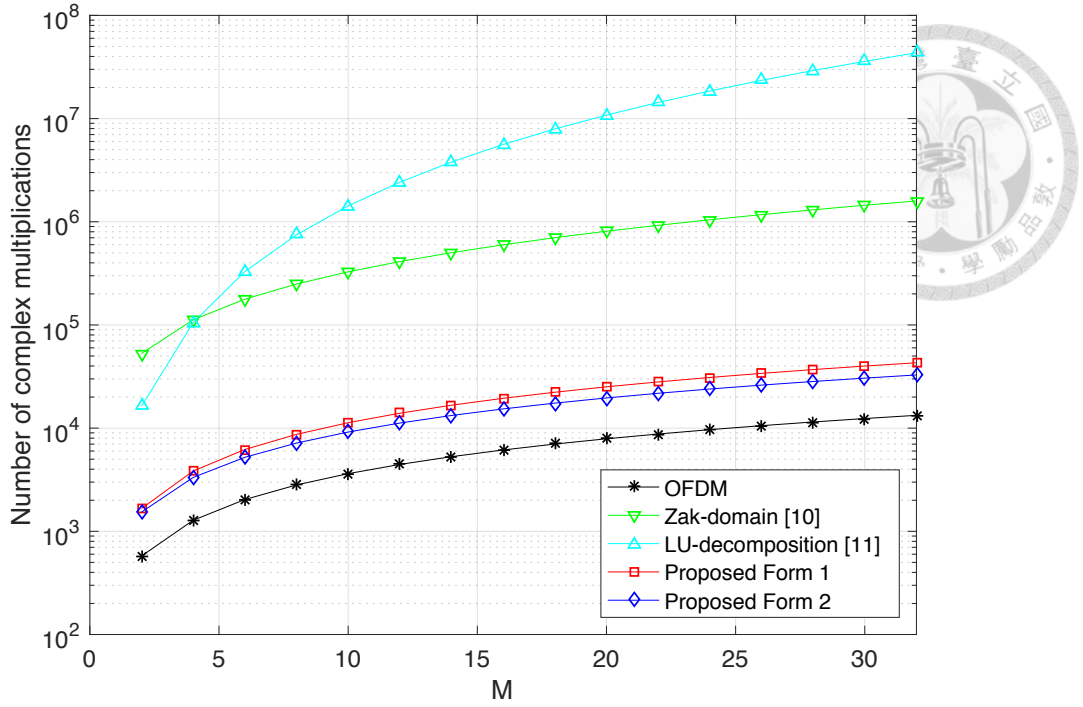


Figure 4.3: Computational complexity of GFDM MMSE receiver implementations.  $K = 64$ .

as that required by the OFDM ZF receiver. The complexity of the frequency-domain implementation [12] is around 1.6 to 1.8 times the complexity of the proposed Form-2 ZF receiver. The complexity of the implementation in [8] and the one in [9] is even nearly 3 times the complexity of the proposed Form-2 ZF receiver when  $M$  is relatively large. The reduced complexity of the implementation in [9] is still around 1.1 to 1.3 times the complexity of the proposed Form-2 ZF receiver when  $M$  is a power of two.

The complexity of the MMSE receiver implementations is shown in Fig. 4.3. We see in Fig. 4.3 that the number of CMs required by the proposed Form-2 MMSE receiver is the least among all GFDM MMSE receivers, and is only about 2.8 times as much as that required by the OFDM MMSE receiver. Compared to the implementations in [10, 11], complexity reduction of around 2 to 3 orders of magnitude can be achieved by the proposed Form-2 MMSE receiver because the complexity of the proposed implementation is linearithmic while that of the one in [10] is quadratic with the numbers of both subsymbols  $M$  and subcarriers  $K$ , and that of the one in [11] is even cubic with the number of subsymbols.

In summary, with the use of the proposed implementations, significant complexity re-

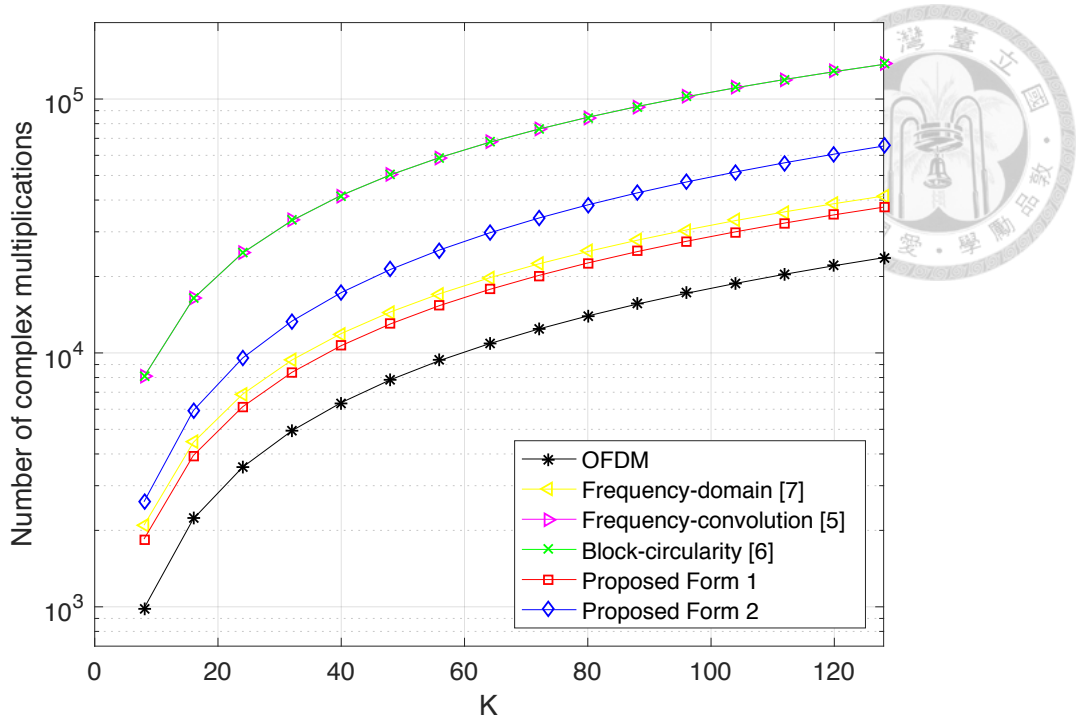


Figure 4.4: Computational complexity of GFDM transmitter implementations.  $M = 31$ .

duction can be obtained for receivers, while moderate complexity reduction is also obtained for transmitters. Note that direct implementations are not shown in Figs. 4.1, 4.2, and 4.3 because they demand extremely large numbers of CMs. For example, when  $K = 64$  and  $M = 16$ , direct implementations require about two orders of magnitude more CMs than the proposed implementations do for a transmitter or ZF receiver, and about five orders of magnitude more CMs than the proposed implementations do for an MMSE receiver.

## 4.1 Additional Complexity Comparison Results

In this section, we show complexity comparison results under the case of varying  $K$ . We will see that similar results can be obtained as under the case of varying  $M$ . Specifically, the complexity formulae in Tables 4.1 and 4.2 are evaluated and plotted for  $M = 31$  subsymbols with respect to different values of number of subcarriers  $K$ .

The complexity of the transmitter, ZF receiver, and MMSE receiver implementations is shown in Figs. 4.4, 4.5, and 4.6, respectively. The parameter settings  $L_T = 2$  and



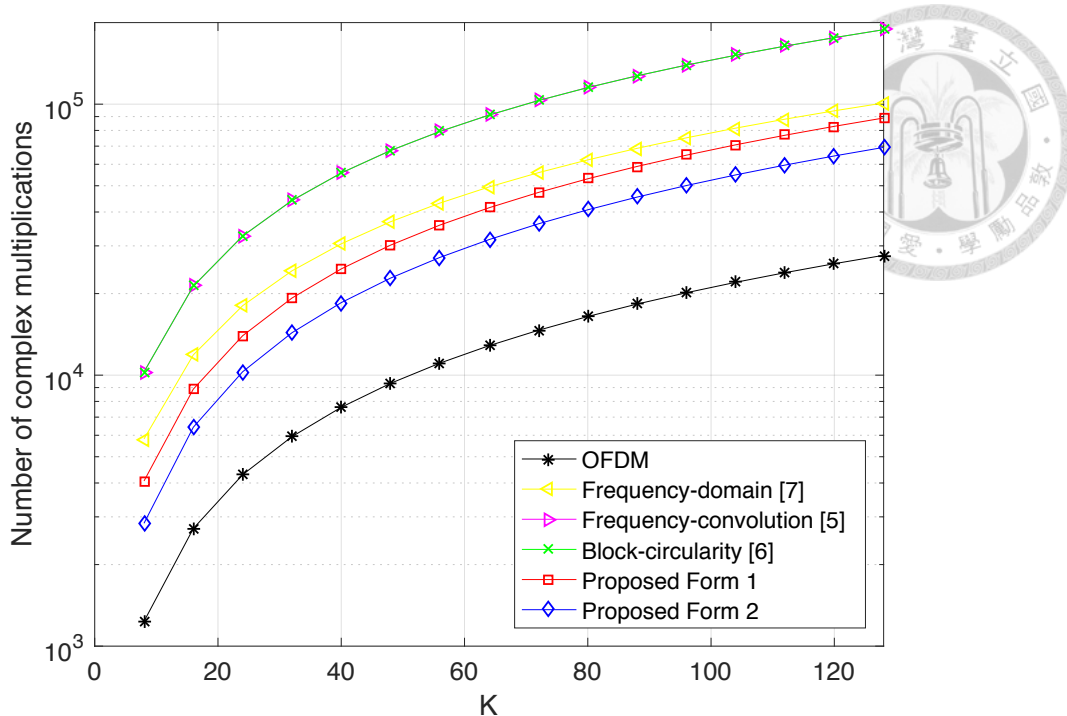


Figure 4.5: Computational complexity of GFDM ZF receiver implementations.  $M = 31$ .

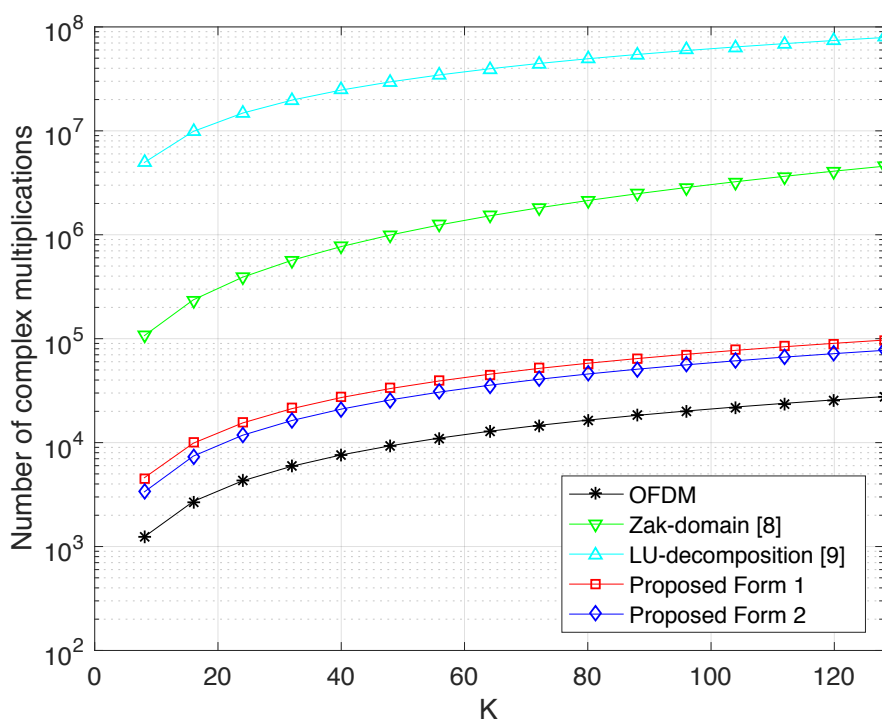


Figure 4.6: Computational complexity of GFDM MMSE receiver implementations.  $M = 31$ .

$L_R = 16$  are used again for the frequency-domain implementation [12]. According to Figs. 4.4, 4.5, and 4.6, the numbers of CMs required by the proposed Form-1 transmitter, proposed Form-2 ZF receiver, and proposed Form-2 MMSE receiver are the least among all GFDM transmitters, all GFDM ZF receivers, and all GFDM MMSE receivers, respectively. Besides, compared to the implementations in [10, 11], complexity reduction of around 2 to 3 orders of magnitude can be achieved by the proposed Form-2 MMSE receiver. These results are similar to those under the case of varying  $M$ .



## Chapter 5

# Power Spectral Density and OOB

## Leakage

In this section, which serves as an aid for simulation later, we define the OOB leakage  $O$  as a performance measure for the OOB radiation of transmit signals. To evaluate  $O$  for GFDM, we first address the power spectral density (PSD) of GFDM signals. We derive an analytical PSD expression encompassing an interpolation filter used in a D/A converter. This approach conforms to the practical realization of modern digital-signal-processing-based communication systems [36].

The GFDM digital baseband transmit signal  $x[n]$  is described as in (2.8). The analog baseband transmit signal  $x_a(t)$  is obtained by passing  $x[n]$  through a D/A converter with a sampling interval  $T_s$  and an interpolation filter  $p(t)$ , i.e.,  $x_a(t) = \sum_{n=-\infty}^{\infty} x[n]p(t - nT_s)$ . The PSD of  $x_a(t)$  is defined as  $S_a(f) = \lim_{T \rightarrow \infty} E\{\frac{1}{2T} |\int_{-T}^T x_a(t)e^{-j2\pi ft} dt|^2\}$  [42]. Let  $P(f) = \int_{-\infty}^{\infty} p(t)e^{-j2\pi ft} dt$  be the Fourier transform of  $p(t)$ , and  $G_m(e^{j\omega}) = \sum_{n=-\infty}^{\infty} g_m[n]e^{-j\omega n}$  be the discrete-time Fourier transform of  $g_m[n]$ , where  $g_m[n]$  is defined in (2.9). Assuming the data symbols are zero-mean and i.i.d. with symbol energy  $E_S$ , we can derive that

$$S_a(f) = \frac{E_S |P(f)|^2}{D'T_s} \sum_{k \in \mathcal{K}} \sum_{m \in \mathcal{M}} \left| G_m \left( e^{j2\pi(fT_s - \frac{k}{K})} \right) \right|^2. \quad (5.1)$$

With some derivations, we further obtain that

$$G_m(e^{j\omega}) = \sum_{l=0}^{D'-1} [\mathbf{g}_f^{(m)}]_l \text{sinc}_{D'}(\omega'_l) e^{-j\omega'_l \frac{D'-1}{2}}, \quad (5.2)$$



where  $\omega'_l = \omega - (2\pi l/D')$  and

$$[\mathbf{g}_f^{(m)}]_l = \frac{D'}{D} \sum_{k=0}^{D-1} \left\{ [\mathbf{g}_f]_k \text{sinc}_{D'} \left( 2\pi \left( \frac{k}{D} - \frac{l}{D'} \right) \right) e^{j\pi \left( \frac{k}{D} - \frac{l}{D'} \right) (D'-1)} e^{-j2\pi k \frac{mK+L}{D}} \right\}. \quad (5.3)$$

In (5.3),  $\mathbf{g}_f$  is the frequency-domain prototype transmit filter, defined as the  $D$ -point DFT of  $\mathbf{g}$ , i.e.,

$$\mathbf{g}_f = \sqrt{D} \mathbf{W}_D \mathbf{g}, \quad (5.4)$$

and

$$\text{sinc}_p(x) = \begin{cases} (-1)^{k(p-1)}, & x = 2\pi k, k \in \mathbb{Z} \\ \frac{\sin(px/2)}{p \sin(x/2)}, & \text{otherwise} \end{cases} \quad (5.5)$$

is the periodic sinc function for any positive integer  $p$ . Using (5.1), (5.2), (5.3), and (5.4), we can express the PSD with  $\mathbf{g}_f$ , which enables designing the PSD in terms of the frequency-domain prototype transmit filter. A special case that leads to a simple expression of  $G_m(e^{j\omega})$  is  $L = 0$ . When  $L = 0$ , (5.2) can be reduced to

$$G_m(e^{j\omega}) = \sum_{l=0}^{D-1} [\mathbf{g}_f]_l e^{-j2\pi \frac{lm}{M}} \text{sinc}_D(\omega_l) e^{-j\omega_l \frac{D-1}{2}}, \quad (5.6)$$

where  $\omega_l = \omega - (2\pi l/D)$ .

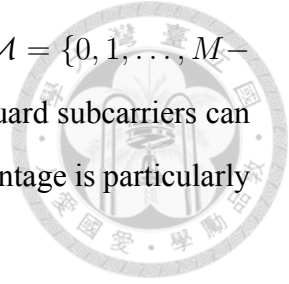
To characterize the OOB radiation, we define the OOB leakage [3] as

$$O = \frac{|\mathcal{B}_I|}{|\mathcal{B}_O|} \cdot \frac{\int_{f \in \mathcal{B}_O} S_a(f) df}{\int_{f \in \mathcal{B}_I} S_a(f) df}, \quad (5.7)$$

In (5.7),  $\mathcal{B}_I$  and  $\mathcal{B}_O$  are the set of frequencies considered in-band and out of band, respectively, and  $|\mathcal{B}_I|$  and  $|\mathcal{B}_O|$  denote the lengths of the corresponding intervals. Recall that  $\mathcal{K}$  is the set of subcarrier indices actually used. The nominal frequencies of the subcarriers in  $\mathcal{K}$  lie in  $\mathcal{B}_I$ , several guard subcarriers are used between  $\mathcal{B}_I$  and  $\mathcal{B}_O$ , and  $\mathcal{B}_O$  is reserved

for the use of other users.

Finally, note that in (2.8), the sets  $\mathcal{M}$  and  $\mathcal{K}$  are not required to be  $\mathcal{M} = \{0, 1, \dots, M-1\}$  or  $\mathcal{K} = \{0, 1, \dots, K-1\}$ . This means some guard symbols or guard subcarriers can be used. GFDM is proposed to exhibit low OOB radiation. This advantage is particularly significant if some guard symbols and guard subcarriers are used [3].







## Chapter 6

# Optimal Prototype Filters that Minimize MSE

We propose in this section to design optimal prototype filters in terms of minimizing the receiver MSE before considering the OOB radiation performance. Due to the one-to-one relation between the prototype transmit filter  $\mathbf{g}$  and the characteristic matrix  $\mathbf{G}$  in Lemma 1(a), the design of the characteristic matrix is essentially equivalent to the prototype filter design. We address the problem mainly from the perspective of the characteristic matrix, which yields many insights.

The receiver MSE is formally defined as follows. Denote the error variance on the  $k$ th subcarrier and  $m$ th subsymbol after demodulation as

$$\sigma_{k,m}^2 = \text{E} \left\{ |[\hat{\mathbf{d}} - \mathbf{d}]_{k+mK}|^2 \right\} \quad (6.1)$$

for  $k = 0, 1, \dots, K - 1$  and  $m = 0, 1, \dots, M - 1$ , where  $\hat{\mathbf{d}}$  is defined as in (3.4) or (3.10) if the ZF or MMSE receiver is used, respectively. The expectation is taken on both the noise and channel distributions. Define the receiver MSE  $\sigma^2$  as

$$\sigma^2 = \frac{1}{D} \sum_{k=0}^{K-1} \sum_{m=0}^{M-1} \sigma_{k,m}^2. \quad (6.2)$$

Our goal is to identify the optimal  $K \times M$  characteristic matrix  $\mathbf{G}$  of a  $D \times D$  GFDM matrix

$\mathbf{A}$  that minimizes the receiver MSE  $\sigma^2$  as defined in (6.2) under the following scenarios:

1. the ZF receiver over the AWGN channel;
2. the ZF receiver over (statistical) multipath channels;
3. the MMSE receiver over the AWGN channel;
4. the MMSE receiver over (statistical) multipath channels,



which we call Problems 1-4. We fix  $\xi_G$ , which equals  $\|\mathbf{g}\|^2$  by Lemma 1(d), as a normalization of the energy of the prototype filter.

## 6.1 Optimization Results for ZF Receivers

The solutions to Problems 1 and 2 are identified in the following theorem, with some additional requirements introduced for Problem 2.

**Theorem 4** (a) *Under the ZF receiver over the AWGN channel, a prototype transmit filter  $\mathbf{g}$  minimizes MSE  $\sigma^2$  if and only if it is a CMCM filter. The corresponding minimum MSE is  $\sigma_{min}^2 = N_0/\xi_G$ .*

(b) *Under the ZF receiver over any statistical channel such that the channel frequency response  $C_l$  satisfies  $E\{1/|C_l|^2\}$  being a finite constant  $\beta, \forall 0 \leq l < D$ , a prototype transmit filter  $\mathbf{g}$  minimizes MSE  $\sigma^2$  if and only if it is a CMCM filter. The corresponding minimum MSE is  $\sigma_{min}^2 = \beta N_0/\xi_G$ .*

*Proof:* (a) By (3.4) with  $\mathbf{C} = \mathbf{I}_D$  and Theorem 2(c),

$$\sigma_{k,m}^2 = E \left\{ \left| [\mathbf{A}^{-1} \mathbf{q}]_{k+mK} \right|^2 \right\} = \xi_H N_0, \quad (6.3)$$

$\forall 0 \leq k < K, 0 \leq m < M$ , where  $\xi_H$  is the energy of  $\mathbf{A}^{-H}$ . Then, the statement follows from (6.2) and the inequality

$$\xi_G \xi_H \geq 1, \quad (6.4)$$



which is shown below. By Theorem 2(b),  $\xi_H = \sum_{k=0}^{K-1} \sum_{l=0}^{M-1} (1/(D\|\mathbf{G}\|_{k,l}^2))$ . Then,  $\xi_G \xi_H \geq 1$  follows from the Cauchy-Schwarz inequality,

$$\left[ \sum_{k=0}^{K-1} \sum_{l=0}^{M-1} \|\mathbf{G}\|_{k,l}^2 \right] \left[ \sum_{k=0}^{K-1} \sum_{l=0}^{M-1} \frac{1}{\|\mathbf{G}\|_{k,l}^2} \right] \geq (KM)^2, \quad (6.5)$$



where the equality holds if and only if  $\|\mathbf{G}\|_{k,l}$  is a constant in both  $k$  and  $l$ . The expression for  $\sigma_{min}^2$  follows from (6.3) and the condition for the equality to hold for  $\xi_G \xi_H \geq 1$ .

(b) Taking the expectation of (3.20) and noting that  $E\{\mathbf{r}_l\} = \beta \mathbf{1}_K$ , we can derive that

$$\sigma_{k,m}^2 = \beta \|\bar{\mathbf{H}}\|^2 N_0 / D, \forall 0 \leq k < K, 0 \leq l < M. \quad (6.6)$$

Thus, we have  $\sigma^2 = \beta \|\bar{\mathbf{H}}\|^2 N_0 / D = \beta \xi_H N_0$ , and the result follows from  $\xi_G \xi_H \geq 1$  as proved in (a). ■

Note that in Theorem 4(b) (i.e., solution to Problem 2),  $E\{1/|C_l|^2\}$  is required to be a finite constant  $\forall 0 \leq l < D$ . Requiring them to be finite is a necessary condition for the receiver MSE  $\sigma^2$  to also be finite, and is an inherent limitation of a ZF receiver since  $\sigma^2 \propto E\{1/|C_l|^2\}, \forall 0 \leq l < D$  in this case. Besides, we require them to be a constant so that there remains some sort of symmetry as we move from the AWGN channel to statistical channels.

The following corollary considers the error variance  $\sigma_{k,m}^2$  on each subcarrier and subsymbol for the two scenarios in Theorem 4.

**Corollary 1** *For any GFDM systems,  $\sigma_{k,m}^2$  is a constant in both  $k$  and  $m$  under each of the scenarios: the ZF receiver over the AWGN channel and the ZF receiver over any statistical channel such that the channel frequency response  $C_l$  satisfies  $E\{1/|C_l|^2\}$  being a finite constant  $\beta, \forall 0 \leq l < D$ .*

*Proof:* See Appendix C. ■

The main idea of the proof is that the equal-norm property in Theorem 2(c) implies equal noise enhancement for each subcarrier and subsymbol. As mentioned in Chapter 5, some guard symbols and guard subcarriers are often used for GFDM [3]. Corollary 1

implies that we can just null the data symbols leading to the highest OOB radiation without considering the MSE performance of each subcarrier or subsymbol, as demonstrated in the simulation in Section 6.4.

After considering the statistical case for Problem 2, we now evaluate the static case. Specifically, we consider a deterministic multipath channel, or a slow fading channel such that obtaining perfect channel state information at the transmitter (CSI-T) is practical. The solution is as follows.

**Theorem 5** *Under the ZF receiver over any (static) multipath channel  $C_l$  such that  $C_l \neq 0, \forall 0 \leq l < D$ , a prototype transmit filter  $\mathbf{g}$  minimizes MSE  $\sigma^2$  if and only if  $|\mathbf{G}]_{k,l}|^2/\sqrt{\alpha_l}$  is a constant in both  $k$  and  $l$ , where  $\alpha_l = \sum_{r=0}^{K-1} 1/(|C_{l+rM}|^2)$ . The corresponding minimum MSE is  $\sigma_{min}^2 = (\sum_{l=0}^{M-1} \sqrt{\alpha_l})^2 N_0 / (KM^2 \xi_G)$ .*

*Proof:* See Appendix A. ■

The proposed filters in Theorem 5 are optimal in terms of minimizing MSE, but they require CSI-T and are less applicable than the CMCM filters derived under statistical channels in Theorem 4(b).

## 6.2 Optimization Results for MMSE Receivers

The solution to Problem 3 is given by the following theorem, whose proof is similar to that of Theorem 4(a).

**Theorem 6** *Under the MMSE receiver over the AWGN channel, a prototype transmit filter  $\mathbf{g}$  minimizes MSE  $\sigma^2$  if and only if it is a CMCM filter. The corresponding minimum MSE is  $\sigma_{min}^2 = E_S / (\gamma \xi_G + 1)$ .*

*Proof:* See Appendix B. ■

Similar to Corollary 1, the following corollary considers the error variance  $\sigma_{k,m}^2$  on each subcarrier and subsymbol for the scenario in Problem 3.

**Corollary 2** For any GFDM systems,  $\sigma_{k,m}^2$  is a constant in both  $k$  and  $m$  under the MMSE receiver over the AWGN channel.



*Proof:* See Appendix C.

Similarly, Corollary 1 imply that we can just null the data symbols leading to the highest OOB radiation without considering the MSE performance of each subcarrier or subsymbol, as demonstrated in the simulation in Section 6.4.

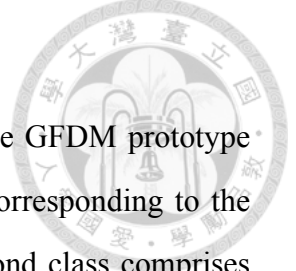
Observing that each of the solutions to Problems 1, 2, and 3 is a CMCM filter, we make the following conjecture that the solution to Problem 4, under the assumption of identically distributed  $C_l, \forall 0 \leq l < D$ , is also a CMCM filter.

*Hypothesis 1:* Under the MMSE receiver over any statistical channel such that the channel frequency response  $C_l$  are identically distributed  $\forall 0 \leq l < D$ , a prototype transmit filter  $\mathbf{g}$  minimizes MSE  $\sigma^2$  if and only if it is a CMCM filter. The corresponding minimum MSE is  $\sigma_{min}^2 = E\{E_S/(\gamma\xi_G|C_0|^2 + 1)\}$ .

In Hypothesis 1, the assumption of identically distributed  $C_l, \forall 0 \leq l < D$  is practical since many realistic channels, such as Rayleigh fading channels [42], have identically distributed  $C_l$ . Note that we do not require each  $E\{1/|C_l|^2\}$  to be finite because an MMSE receiver does not suffer from this limitation. While a mathematical proof for Hypothesis 1 is unavailable now because the inverse of  $\mathbf{C}\mathbf{A}\mathbf{A}^H\mathbf{C}^H + \gamma^{-1}\mathbf{I}_D$  in (3.9) cannot be readily simplified (one may consider properties of block circulant matrices for the simplification in the future), numerical results in Section 6.4 verify that this hypothesis tends to be correct.

The solutions to all the four problems provide criteria for the prototype transmit filter  $\mathbf{g}$  to minimize the MSE under various types of channels and receivers. Since some degrees of freedom (i.e.,  $\angle[\mathbf{G}]_{k,l}$ ) remain in all the solutions, minimizing the OOB radiation with respect to  $\mathbf{g}$  under the derived criteria would be a suitable research direction for future studies.

### 6.3 Comparison of Prototype Filter Candidates



Considering the optimization results, we find it natural to categorize GFDM prototype filters into two classes: The first class comprises CMCM filters, corresponding to the class of unitary GFDM matrices (up to a scale factor), and the second class comprises non-CMCM filters, corresponding to the class of non-unitary GFDM matrices. The first class is advantageous in minimizing the receiver MSE, whereas the second class suffers from the noise enhancement effect [5, 13, 23].

The RC, RRC, Xia [29], and Gaussian pulses [3], adopted by many previous studies, fall into the class of non-CMCM filters. GFDM systems using these filters are non-orthogonal [3]. In fact, since RC and RRC filters are even-symmetric, i.e.,  $[\mathbf{g}]_n = [\mathbf{g}]_{D-n}$  for  $n = 1, 2, \dots, D - 1$ , their GFDM matrices are singular when  $K, M$  are both even integers. This can be proved by using (2.3) to show that the corresponding characteristic matrix  $\mathbf{G}$  satisfies  $[\mathbf{G}]_{\frac{K}{2}, \frac{M}{2}} = 0$  and using Theorem 2(a) (see also [5], which also observed this point using Gabor analysis). Thus, to avoid MSE and SER performance degradation, we would not set  $D = KM$  as a power of 2 for GFDM systems using RC and RRC filters. By contrast, the simulation results in this thesis show that if the prototype transmit filter is not even-symmetric, both  $K$  and  $M$  being even does not prevent a GFDM system from exhibiting good MSE and SER performance. There is also no constraint on  $K$  and  $M$  in Theorem 1 for GFDM matrices to be unitary.

The class of CMCM prototype filters were less common in previous studies. Yet, their existence implies that noise enhancement is not always a problem of GFDM. As a simple example of CMCM filters, consider the GFDM matrix whose phase-shifted characteristic matrix  $\bar{\mathbf{G}}$  satisfies

$$[\bar{\mathbf{G}}]_{k,l} = 1, \forall 0 \leq k < K, 0 \leq l < M. \quad (6.7)$$

The corresponding frequency-domain prototype filter is  $[\mathbf{g}_f]_l = \sqrt{K} \sum_{k=0}^{M-1} \delta_{lk}$ ,  $l = 0, 1, \dots, D - 1$ . In fact, it is a frequency-shifted version of the Dirichlet pulse [3]. The Dirichlet pulse is defined by a perfect rect function in the frequency domain with the

width of  $M$  frequency bins located around the DC bin<sup>1</sup>. In other words, by defining  $\mathcal{X}_1 = \{0, 1, \dots, \lfloor \frac{M-1}{2} \rfloor\}$  and  $\mathcal{X}_2 = \{D - \lceil \frac{M-1}{2} \rceil, D - \lceil \frac{M-1}{2} \rceil + 1, \dots, D - 1\}$ , we can express the frequency-domain prototype filter as

$$[\mathbf{g}_f]_l = \sqrt{K} \sum_{k \in \mathcal{X}_1 \cup \mathcal{X}_2} \delta_{lk}, l = 0, 1, \dots, D - 1. \quad (6.8)$$

It is also a CMCM filter, and its corresponding GFDM matrix is unitary, as shown in the following corollary.

**Corollary 3** *The GFDM matrix for the Dirichlet pulse is unitary.*

*Proof:* By Lemma 1(b) and (6.8), we can derive that the phase-shifted characteristic matrix  $\bar{\mathbf{G}}$  satisfies  $\forall 0 \leq k < K$ ,

$$[\bar{\mathbf{G}}]_{k,l} = \begin{cases} 1, & 0 \leq l < \lceil M/2 \rceil \\ e^{-j2\pi k/K}, & \lceil M/2 \rceil \leq l < M \end{cases}, \quad (6.9)$$

for the Dirichlet pulse. Thus, it is a CMCM filter, and by Theorem 1, the corresponding GFDM matrix is unitary. ■

The Dirichlet pulse (6.8) instead of its frequency-shifted version (corresponding to (6.7)) will be used in the simulations because its passband is centered at the DC bin.

As another example of CMCM filters, we propose the *modified Dirichlet pulse*, defined by the frequency response

$$[\mathbf{g}_f]_l = \sqrt{K} e^{j\pi \frac{l}{D}} \sum_{k \in \mathcal{X}_1} \delta_{lk} + \sqrt{K} e^{j\pi \frac{l-D}{D}} \sum_{k \in \mathcal{X}_2} \delta_{lk}, \quad (6.10)$$

$l = 0, 1, \dots, D - 1$ . The phase-shifted characteristic matrix  $\bar{\mathbf{G}}$  for the filter satisfies

$$[\bar{\mathbf{G}}]_{k,l} = \begin{cases} e^{j\pi l/D}, & 0 \leq l < \lceil M/2 \rceil \\ e^{j\pi(-2kM+(l-M))/D}, & \lceil M/2 \rceil \leq l < M \end{cases}, \quad (6.11)$$

<sup>1</sup>Although this definition is only clear for an odd  $M$ , we give a reasonable extension for an even  $M$ .

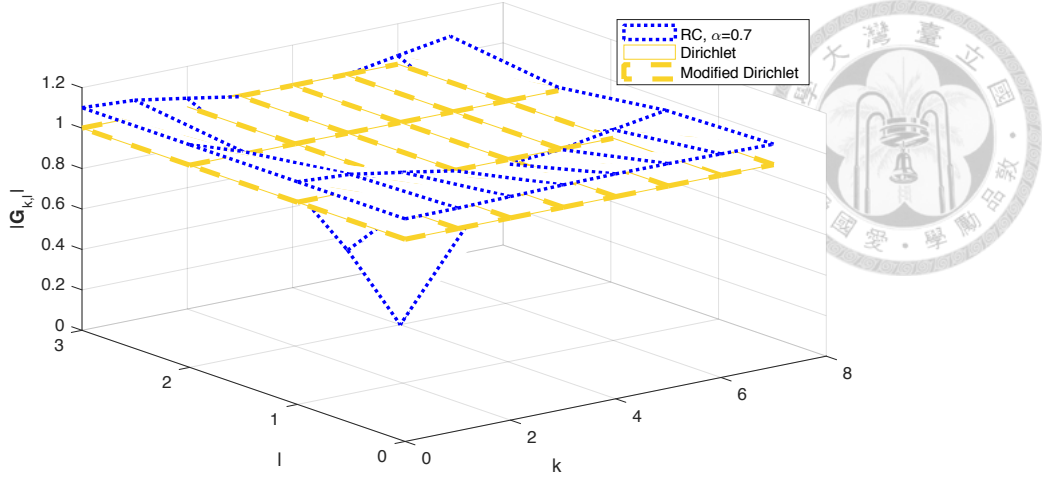


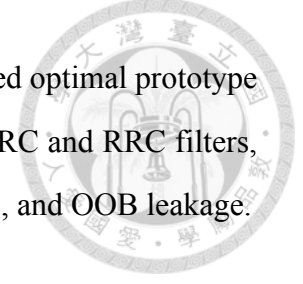
Figure 6.1: Magnitudes of entries in characteristics matrices  $\mathbf{G}$  for several GFDM prototype filters when  $K = 8, M = 4$ .

$\forall 0 \leq k < K$ , so it is a CCM filter. In Section 6.4.3, we will show by simulation that modified Dirichlet pulse exhibits lower OOB radiation than does the Dirichlet pulse. Here we briefly explain why the modified Dirichlet pulse has this advantage. Taking the absolute value of (5.6) and setting  $m = 0$  yields  $|G_0(e^{j\omega})| = |\sum_{l=0}^{D-1} [\mathbf{g}_f]_l \text{sinc}_D(\omega_l) e^{j\pi l \frac{D-1}{D}}|$ . Since  $\text{sinc}_D(x)$  alternates between positive and negative values as  $x$  crosses nonzero integer multiples of  $2\pi/D$ ,  $\text{sinc}_D(x) + e^{j\phi} \text{sinc}_D(x - 2\pi/D)$  with  $\phi = \pi$  can be viewed as the extreme case of "constructive interference" for the tails of the periodic sinc functions. Thus, as  $e^{j\pi l \frac{D-1}{D}}$  and the factor  $e^{j\pi l/D}$  introduced in (6.10) combine to form  $e^{j\pi l}$ , the modified Dirichlet pulse exhibits lower OOB radiation than does the Dirichlet pulse under the scenario that the 0th subsymbol is used as a guard symbol. In other words, we allocate as much OOB energy as possible on the discarded subsymbol.

The absolute values of the entries of characteristic matrices for the RC filter with roll-off factor  $\alpha = 0.7$ , the Dirichlet pulse, and the modified Dirichlet pulse are compared in Fig. 6.1. Note the zero for the RC filter (which makes the corresponding GFDM matrix singular). However, the other two are advantageous because they have constant magnitudes in the characteristic matrix, making both of them unitary.

## 6.4 Simulation Results

In this section, we provide numerical examples to compare the derived optimal prototype transmit filters, especially the CMCM filters, with the conventional RC and RRC filters, in terms of receiver MSE, SER, peak-to-average power ratio (PAPR), and OOB leakage.



### 6.4.1 MSE and SER Performance

The MSE and SER performance is evaluated through Monte-Carlo simulation with 10000 blocks for each prototype filter under each of the following five cases:

1. ZF-DFERF: the ZF receiver over a deep-fade-excluded Rayleigh fading channel;
2. MMSE-RF: the MMSE receiver over the Rayleigh fading channel;
3. ZF-AWGN: the ZF receiver over the AWGN channel;
4. MMSE-AWGN: the MMSE receiver over the AWGN channel;
5. ZF-MP: the ZF receiver over a (static) multipath channel.

We use  $(K, M) = (8, 4), (8, 5),$  or  $(32, 16)$  for GFDM, and  $K = 32, 40,$  or  $512, M = 1$  for OFDM (OFDM is a special case of GFDM using a rectangular window as the prototype transmit filter) so that GFDM and OFDM have the same block size  $D = KM$ . For the used Rayleigh fading channels,  $c[n]$  is independent circularly symmetric complex Gaussian with variance  $N_n^{(c)}$ , and two kinds of power delay profiles [36] are used. For cases when  $(K, M) = (8, 4)$  or  $(8, 5)$ , we use  $N_n^{(c)} = (0.64)^n$  for  $0 \leq n < D/4$  and  $N_n^{(c)} = 0$  for  $D/4 \leq n < D$ . For cases when  $(K, M) = (32, 16)$ , we use  $N_n^{(c)} = 0, -1, -2, -3, -8, -17.2, -20.8$  dB for  $n = 0, 3, 7, 9, 11, 19, 41$ , respectively, and  $N_n^{(c)} = 0$  otherwise, which is derived from the LTE Extended Pedestrian A model [43]. In Case ZF-DFERF, the channel is derived from the Rayleigh fading channel by excluding all channel realizations leading to a tap gain  $|C_l|$  smaller than -30 dB for some subcarrier  $l$  from the channel pool. This exclusion results in finite  $E\{1/|C_l|^2\}$ , and is practical since transmission is given up when deep fades occur in real communication. The (static) multipath channel (in case ZF-MP) is composed of four taps:  $-0.1518 + j0.6475, 0.2701 +$

$j0.3063, 0.5703 + j0.0767, -0.0900 + j0.2274$ . Finally, for MMSE receivers (Cases 2 and 4), unbiased estimates are used for symbol detection [36].



The modulation is 16QAM, the symbol energy is  $E_S = 1$ , and the energy of the GFDM transmitter matrices is  $\xi_G = 1$ . The CP length is  $L = D/4$ . The prototype transmit filters used for GFDM include an RC filter with roll-off factor  $\alpha = 0.7$ . To demonstrate that MSE performance is not affected by phases of entries of constant-magnitude characteristic matrices, we use CMCM filters with arbitrarily chosen phases in most of the simulation cases (except for ZF-MP). Specifically, we use CMCM Filters 1 and 2 with characteristic matrices  $\mathbf{G}_1$  and  $\mathbf{G}_2$ , respectively, with the phases  $\angle \mathbf{G}_1$  and  $\angle \mathbf{G}_2$  being arbitrarily selected and listed as follows. For systems with  $K = 8, M = 4$ ,  $\angle \mathbf{G}_1$  and  $\angle \mathbf{G}_2$  are set as

$$\angle \mathbf{G}_1 = \begin{bmatrix} 0.75 & 2.50 & -1.09 & -1.98 \\ -2.95 & 0.16 & 1.29 & 1.59 \\ -2.10 & 0.59 & 3.12 & -0.31 \\ 0.53 & 3.04 & 0.28 & -1.11 \\ 1.58 & 1.37 & -3.02 & -1.80 \\ -3.11 & 1.05 & 0.47 & -0.73 \\ 0.78 & -1.88 & 0.85 & -2.24 \\ 1.57 & -2.83 & -0.56 & 2.81 \end{bmatrix}, \quad (6.12)$$

$$\angle \mathbf{G}_2 = \begin{bmatrix} -0.31 & -3.11 & 0.82 & -1.04 \\ -1.70 & 2.53 & -0.29 & 0.71 \\ -2.49 & 2.19 & -2.69 & -1.55 \\ -1.44 & -0.77 & -2.06 & 0.19 \\ 0.23 & -1.00 & 0.31 & 0.48 \\ 0.95 & -1.50 & 2.26 & 0.09 \\ 0.21 & -1.03 & 0.76 & 0.57 \\ 2.17 & 1.79 & -2.15 & 1.88 \end{bmatrix}. \quad (6.13)$$

For systems with  $K = 8, M = 5$ ,  $\angle \mathbf{G}_1$  and  $\angle \mathbf{G}_2$  are set as

$$\angle \mathbf{G}_1 = \begin{bmatrix} 0.62 & -0.40 & -1.36 & -2.16 & -1.94 \\ -1.30 & -2.65 & 2.78 & -2.95 & 2.17 \\ 1.01 & 0.07 & 2.86 & 2.92 & -0.60 \\ 1.75 & 2.09 & 1.59 & 0.48 & -1.89 \\ 1.55 & -1.83 & -0.11 & -3.01 & -0.57 \\ 0.27 & -1.21 & -2.81 & 0.37 & -2.27 \\ -1.48 & 0.46 & 2.58 & 2.72 & 0.44 \\ 1.23 & -0.31 & 1.19 & 0.06 & -0.35 \end{bmatrix}, \quad (6.14)$$



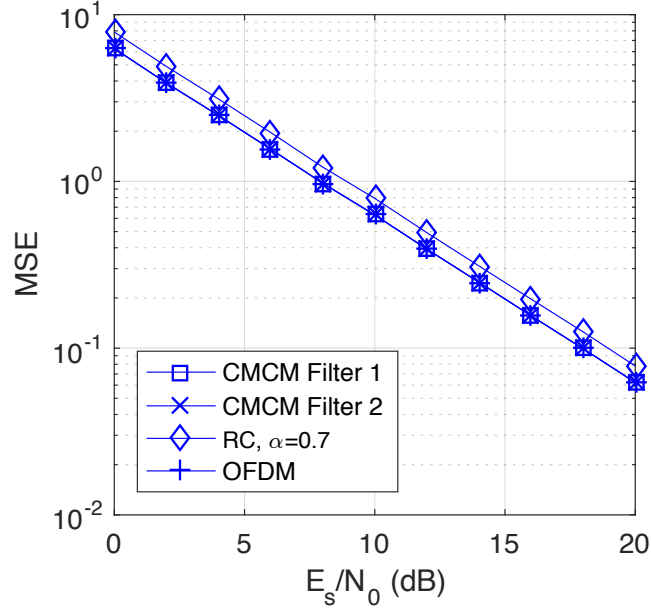


Figure 6.2: MSE for GFDM ZF receiver over a deep-fade-excluded Rayleigh fading (DFERF) channel and the corresponding OFDM receiver.  $K = 8, M = 5$ .

$$\angle \mathbf{G}_2 = \begin{bmatrix} -2.89 & -1.87 & -2.40 & -3.02 & -1.22 \\ 0.73 & 2.22 & -2.79 & 3.08 & 3.04 \\ 0.90 & -2.14 & -1.51 & -2.13 & -1.69 \\ -2.42 & -2.99 & -1.16 & -0.08 & -0.63 \\ -1.94 & -2.57 & 2.22 & 1.17 & 2.89 \\ 1.33 & 1.10 & -2.51 & -1.44 & 1.36 \\ -3.06 & -3.05 & -2.54 & -3.09 & 0.36 \\ 0.53 & 0.22 & 2.88 & -2.08 & 0.54 \end{bmatrix}. \quad (6.15)$$

For systems with  $K = 32, M = 16$ ,  $\angle \mathbf{G}_1$  and  $\angle \mathbf{G}_2$  are set in ways such that CMCM Filters 1 and 2 are the Dirichlet pulse (6.8) and modified Dirichlet pulse (6.10), respectively. For Case ZF-MP, we also use two filters proposed in Theorem 5, with the phases of the characteristic matrices  $\angle \mathbf{G}_1$  and  $\angle \mathbf{G}_2$  again arbitrarily set as in (6.12) and (6.13) for the case of  $K = 8, M = 4$ . For cases where both  $K$  and  $M$  are even, the ZF receiver for an RC filter does not exist, so we use instead the pseudo-inverse of the GFDM matrix.

Figs. 6.2, 6.3, and 6.4 show the simulation results under statistical channels. We first consider the case  $K = 8, M = 5$ . Fig. 6.2 verifies the MMSE property of CMCM filters under the ZF receiver over the deep-fade-excluded Rayleigh fading channel, as stated in Theorem 4(b). The CMCM filters are better than the RC filter, and essentially the same as OFDM in terms of MSE performance. Turning to the case  $K = 8, M = 4$ , we see similar results in Fig. 6.3. Yet, the RC filter performs even worse due to the singularity of

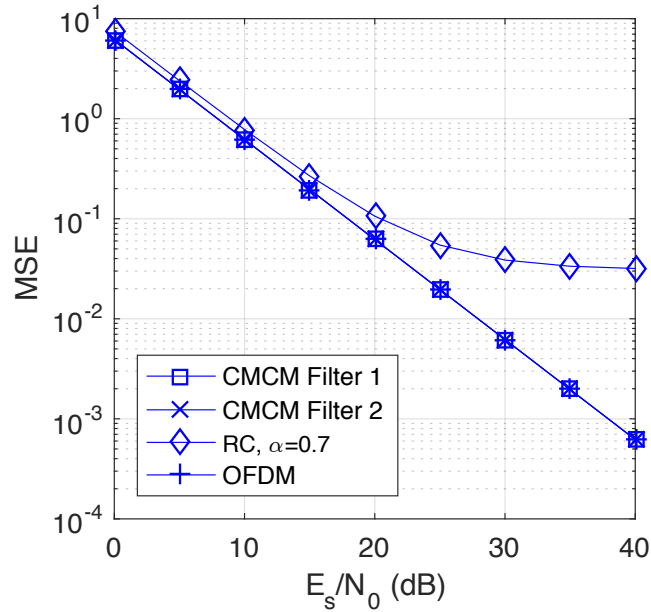


Figure 6.3: MSE for GFDM ZF receiver over a deep-fade-excluded Rayleigh fading (DFERF) channel and the corresponding OFDM receiver.  $K = 8, M = 4$ .

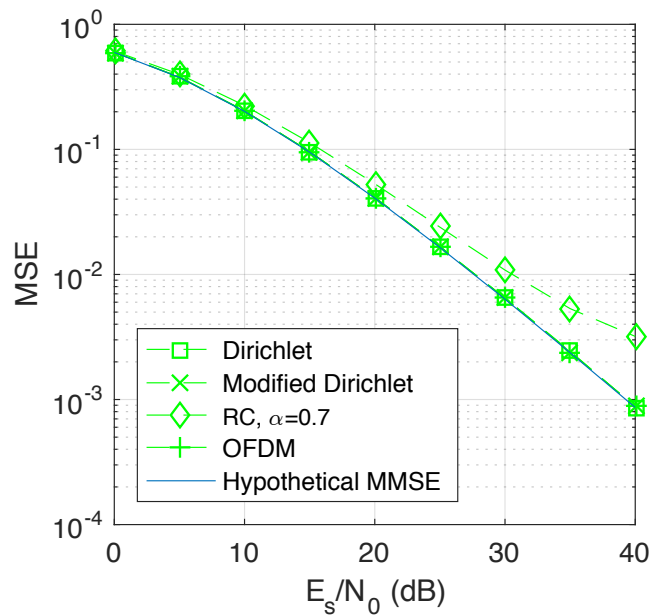


Figure 6.4: MSE for GFDM MMSE receiver over the Rayleigh fading (RF) channel and the corresponding OFDM receiver.  $K = 32, M = 16$ .

its transmitter matrix, whereas the CMCM filters do not have such degradation. Finally, similar results are again observed in Fig. 6.4 for the case of the MMSE receiver over the Rayleigh fading channel. Meanwhile, the MSEs of the CMCM filters correspond to the hypothetical minimum MSE in Hypothesis 1. These imply that Hypothesis 1 tends

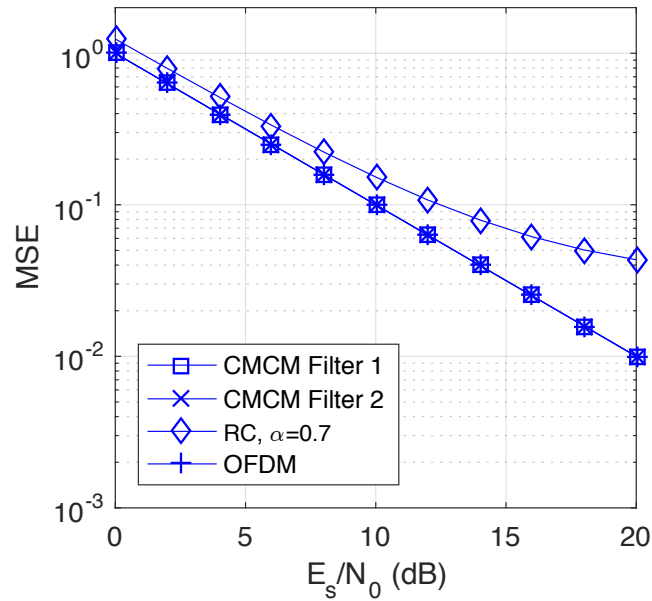


Figure 6.5: MSE for GFDM ZF receiver over the AWGN channel and the corresponding OFDM receiver.  $K = 8, M = 4$ .

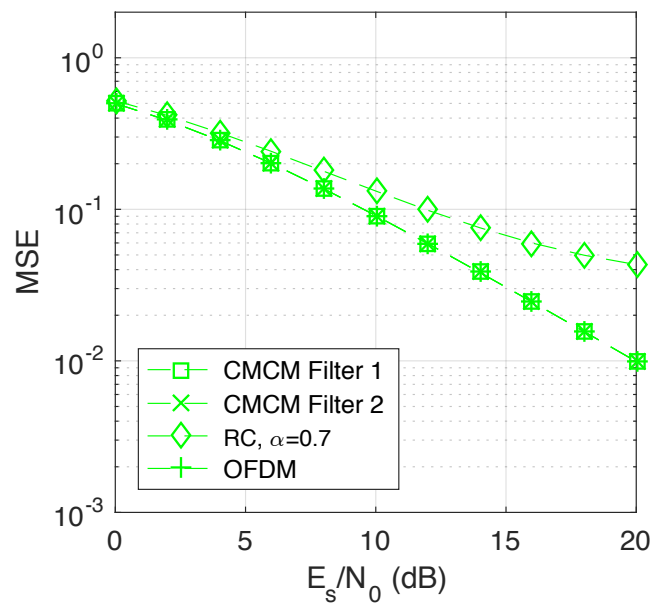


Figure 6.6: MSE for GFDM MMSE receiver over the AWGN channel and the corresponding OFDM receiver.  $K = 8, M = 4$ .

to be correct. Note that the channels used for the ZF and MMSE receivers have different statistics, so the results in Figs. 6.3, and 6.4 cannot be compared directly.

Figs. 6.5, 6.6, and 6.7 show the simulation results under static channels, including the AWGN channel. Fig. 6.5 shows that the CMCM filters are better than the RC filter, and

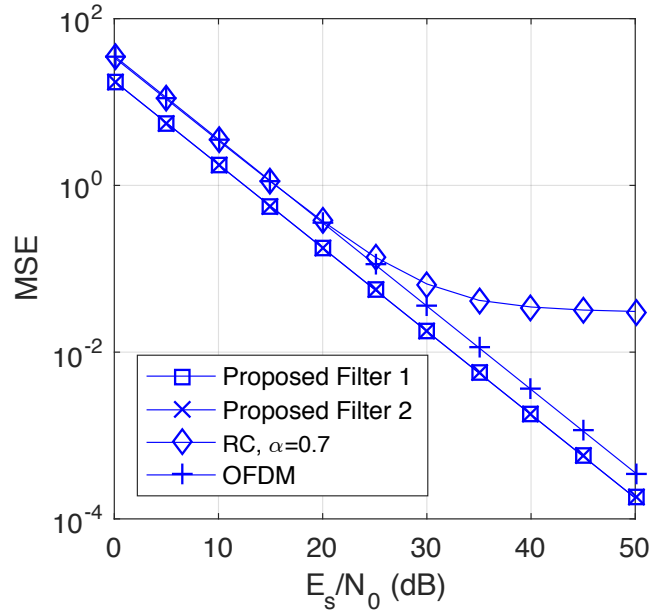


Figure 6.7: MSE for GFDM ZF receiver over a (static) multipath (MP) channel and the corresponding OFDM receivers.  $K = 8, M = 4$ .

essentially the same as OFDM in terms of MSE performance. It verifies that the CMCM filters are the prototype filters that minimize receiver MSE under the ZF receiver over the AWGN channel, as stated in Theorem 4(a). Similar results can be observed in Fig. 6.6. It verifies that the CMCM filters are the prototype filters that minimize receiver MSE under the MMSE receiver over the AWGN channel, as stated in Theorem 6. Fig. 6.7 verifies the MMSE property of the proposed filters under the ZF receiver over (static) multipath channels as stated in Theorem 5. The advantages of the proposed filters in this case come from the use of CSI-T, whereas the RC filter and the prototype filter of OFDM, i.e., the rectangular window, are predefined and are not designed according to CSI-T.

Fig. 6.8 shows the magnitude response of the prototype filters used for Case MMSE-RF, i.e., Fig. 6.4. The Dirichlet and modified Dirichlet pulses are both frequency-localized, and their spectral properties are similar to that of the RC filter. In fact, the magnitude response of the Dirichlet and modified Dirichlet pulses is a perfect rectangular window. However, we will show in the Section 6.4.3 that the RC filter exhibits lower OOB radiation. In other words, it is possible that a prototype filter with a less localized magnitude response can result in better OOB performance than that with a more localized magnitude response. This strengthens the importance of a low-complexity implementation of GFDM

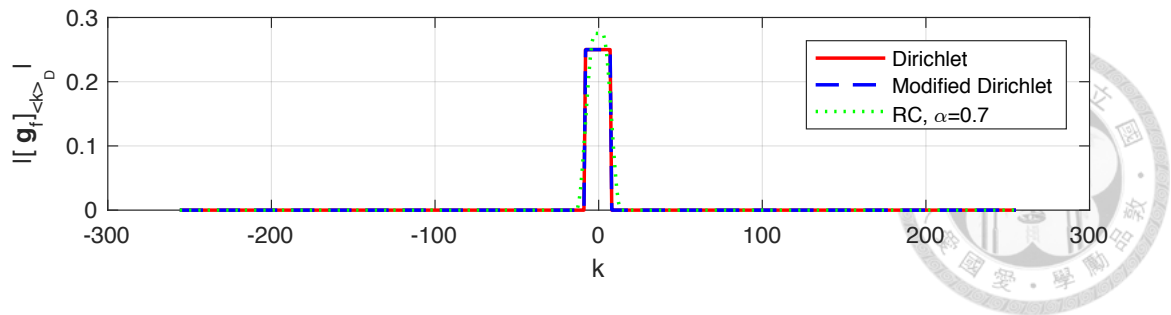


Figure 6.8: Magnitude response of the frequency-domain prototype filter  $\mathbf{g}_f$ .

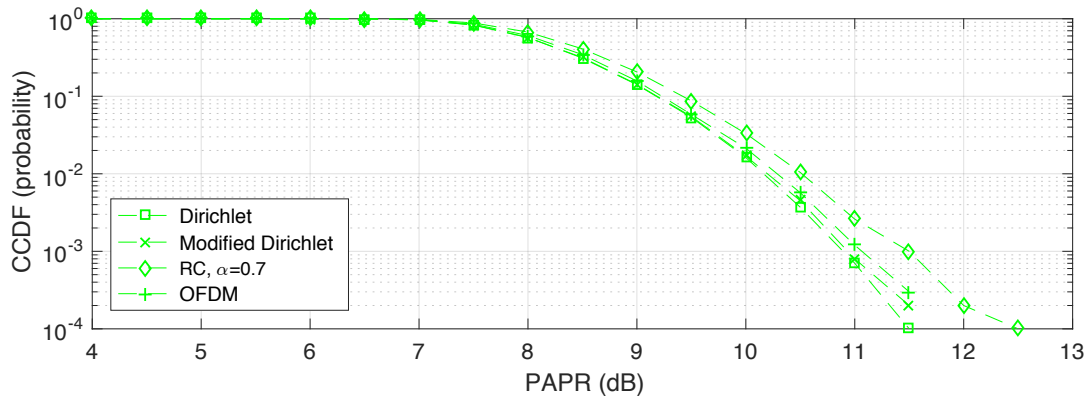


Figure 6.9: CCDF of PAPR for MMSE-RF.  $K = 32$ ,  $M = 16$ .

transceivers that is applicable to general prototype filters without any limitations on their spanned number of subcarriers.

## 6.4.2 PAPR

For Case MMSE-RF, we also evaluate the PAPR [44] of the transmit signal, which is defined as  $\max |x[n]|^2 / E\{|x[n]|^2\}$ , where  $x[n]$  is the digital baseband transmit signal (2.8). PAPR is an important issue in the multicarrier communication [45]. PAPR complementary cumulative distribution function (CCDF) curves are shown in Fig. 6.9. The Dirichlet pulse, modified Dirichlet pulse, and OFDM are shown to have similar PAPR, while the RC filter has a higher PAPR. It suggests that CMCM filters can have better PAPR performance than non-CMCM filters.

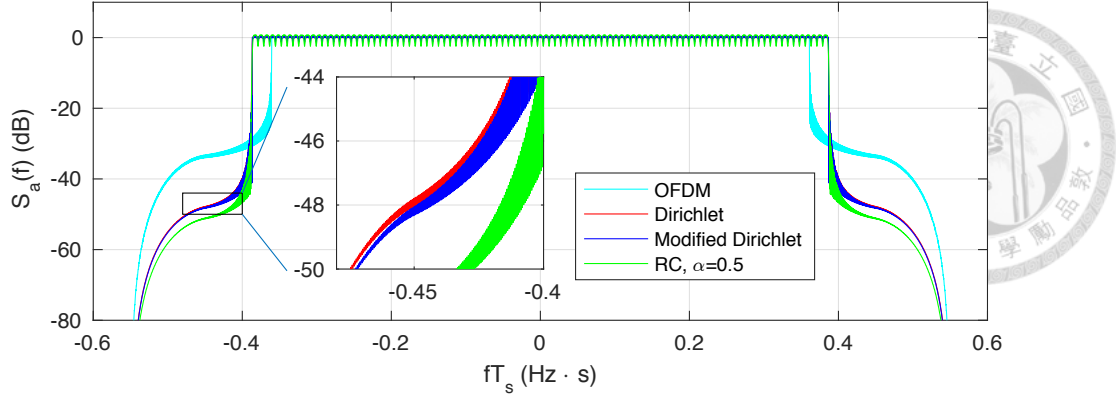


Figure 6.10: PSD for GFDM and OFDM.

### 6.4.3 OOB Leakage

The PSD of GFDM and OFDM signals is simulated according to (5.1), and the OOB leakage is evaluated according to (5.7). The average in-band PSD is normalized to 1. We basically follow the simulation parameters in [3]. An RC filter with a roll-off factor of 0.5, the Dirichlet pulse [3], and the modified Dirichlet pulse defined in (6.10) are used for GFDM. We use  $K = 128$  and  $M = 15$  for GFDM, the 0th subsymbol is used as a guard symbol, and subcarriers 50 to 78 are switched off, i.e.,  $\mathcal{K} = \{0, 1, \dots, 49\} \cup \{79, 80, \dots, 127\}$ ,  $\mathcal{M} = \{1, 2, \dots, 14\}$ . For a fair comparison,  $K = 1920$  and  $M = 1$  are used for OFDM so that the GFDM and OFDM block sizes are equal, and the number of used OFDM subcarriers is the same as the number of used resource elements in GFDM systems,  $|\mathcal{K}||\mathcal{M}|$ . Thus, the spectral efficiency of all systems with all filters are the same. The used OFDM subcarriers are contiguous, and their center is located at the DC bin. The number of GFDM guard subcarriers used between in-band  $\mathcal{B}_I$  and out-of-band  $\mathcal{B}_O$  is  $N_{gc} = 1$  or 6. The CP length is  $L = 16$ . The interpolation filter  $p(t)$  is a sample-level RC filter with roll-off factor  $\alpha = 0.1$ , and the sampling rate is  $1/T_s = 1.92$  MHz. Thus,  $\mathcal{B}_I = (-49.5, 49.5) \cdot (1/(128T_s))$  Hz and  $\mathcal{B}_O = ((-64(1 + \alpha), -49.5 - N_{gc}) \cup (49.5 + N_{gc}, 64(1 + \alpha))) \cdot (1/(128T_s))$  Hz, where  $\alpha = 0.1$  and  $N_{gc} = 1$  or 6.

We compare the OOB leakage of GFDM and OFDM systems, as presented in Table 6.1, by using the simulated PSD shown in Fig. 6.10. As shown in Table 6.1, the Dirichlet pulse, which is optimal in terms of minimizing the MSE, outperforms OFDM by at least

Table 6.1: OOB leakage in dB of the simulation in Fig. 6.10

Guard carriers	OFDM	GFDM Dirichlet	GFDM modified Dirichlet	GFDM RC
1	-35.1	-47.7	-48.0	-51.0
6	-37.1	-51.5	-51.8	-54.8

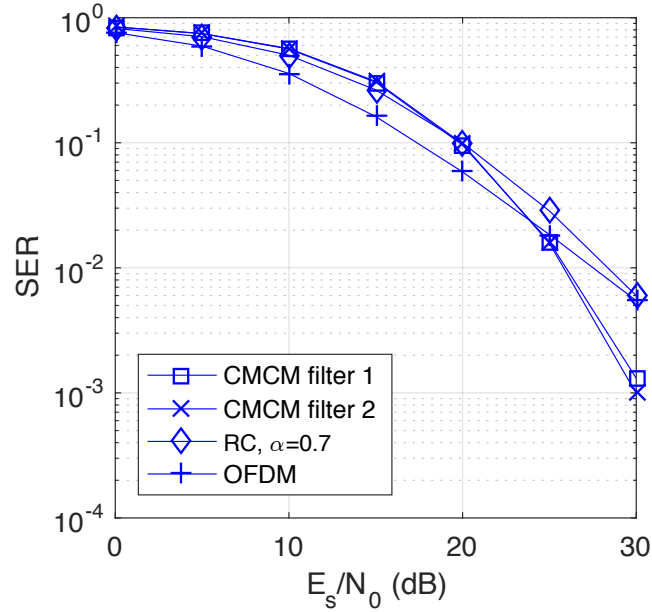
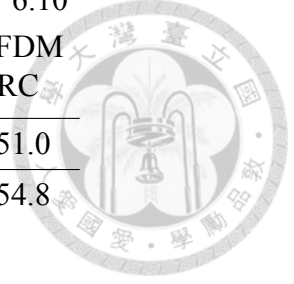


Figure 6.11: SER for GFDM ZF receiver over a deep-fade-excluded Rayleigh fading (DFERF) channel and the corresponding OFDM receiver.  $K = 8$ ,  $M = 5$ .

12 dB, and has an OOB leakage comparable to that of the RC filter. Besides, the OOB leakage of the proposed modified Dirichlet pulse in this study is even lower than that of the Dirichlet pulse; this suggests that the Dirichlet pulse known in the literature is not optimal in terms of OOB leakage among all CMCM filters, and that we may further minimize the OOB leakage in the future with respect to the prototype transmit filter under the derived MMSE criterion.

#### 6.4.4 Additional Simulation Results for SER Performance

Here, we offer additional simulation results for SER performance. The same set of parameter settings in Section 6.4.1 are used.

First, consider scenarios under statistical channels. Figs. 6.11, 6.12, and 6.13 show the SER performance of the three scenarios for Figs. 6.2, 6.3, and 6.4, respectively. According

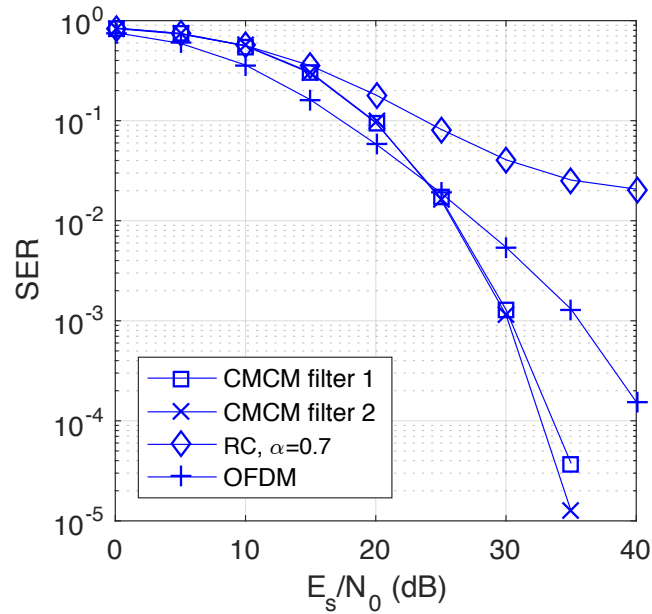


Figure 6.12: SER for GFDM ZF receiver over a deep-fade-excluded Rayleigh fading (DFERF) channel and the corresponding OFDM receiver.  $K = 8, M = 4$ .

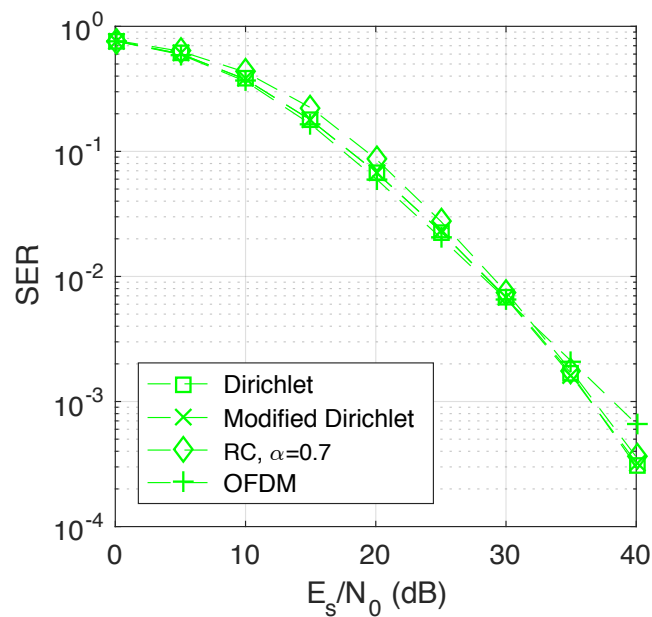


Figure 6.13: SER for GFDM MMSE receiver over the Rayleigh fading (RF) channel and the corresponding OFDM receiver.  $K = 32, M = 16$ .

to Figs. 6.11, 6.12, and 6.13, the CMCM filters are better than the RC filter in terms of SER performance. A difference between MSE and SER is that the CMCM filters have the same MSE performance as but better SER performance in the higher SNR region and worse SER performance in the lower SNR region than OFDM, which can be explained



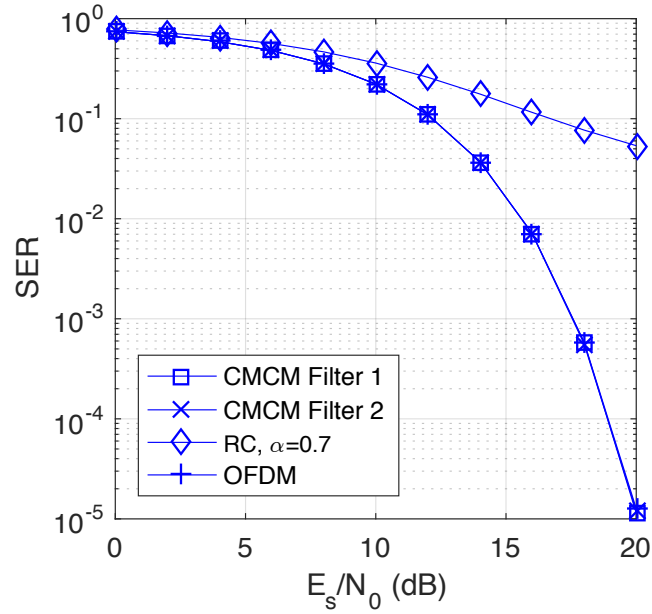


Figure 6.14: SER for GFDM ZF receiver over the AWGN channel and the corresponding OFDM receiver.  $K = 8, M = 4$ .

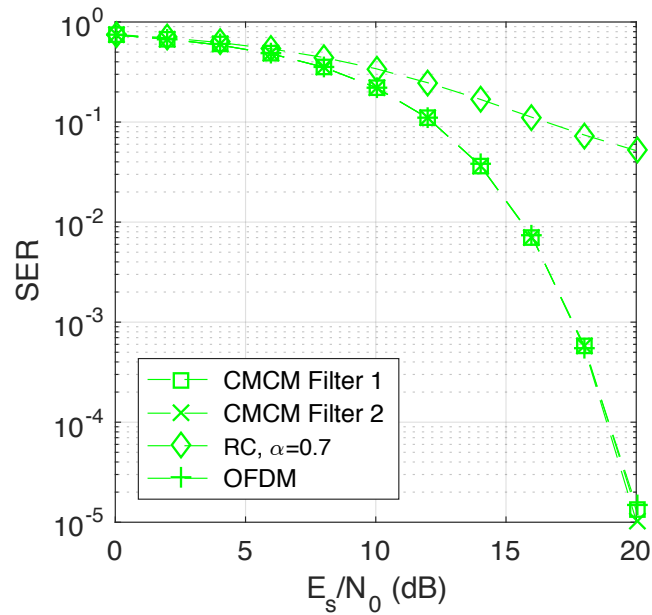


Figure 6.15: SER for GFDM MMSE receiver over the AWGN channel and the corresponding OFDM receiver.  $K = 8, M = 4$ .

by the effect of a orthogonal precoder on OFDM (due to convex and concave regions of a function composed of the Q-function) [46]. It can also be seen that for a larger block size  $KM$ , such as the case for Fig. 6.13, the SER performance degradation of RC filter compared to OFDM is less significant. This may be because a larger block size tends

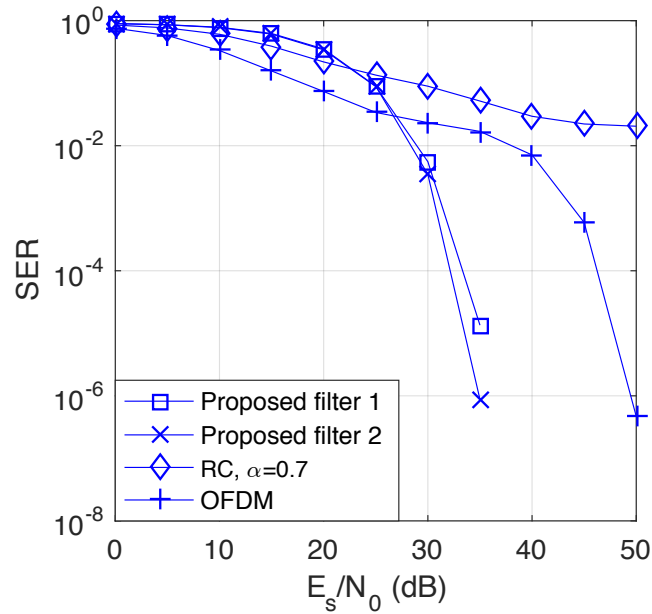


Figure 6.16: SER for GFDM ZF receiver over a (static) multipath (MP) channel and the corresponding OFDM receivers.  $K = 8, M = 4$ .

to make the vectors in the GFDM transmitter matrix of the RC filter closer to becoming perpendicular.

Then, consider scenarios under static channels. Figs. 6.14, 6.15, and 6.16 show the SER performance of the three scenarios for Figs. 6.5, 6.6, and 6.7, respectively. According to Figs. 6.14 and 6.15, the CMCM filters are better than the RC filter, and essentially the same as OFDM in terms of SER performance. Fig. 6.16 shows that the SERs of the proposed filters are much better than both the RC filter and OFDM in the higher SNR region in terms of SER performance.

Observing the subtle difference between the results of MSE and SER performance, one may want to derive optimal prototype filters that minimize SER or bit error rate in the future. This kind of design would depend on the used receivers and channels.



## Chapter 7

# Optimal Prototype Filters that Minimize MSE and OOB Radiation

In Chapter 6, optimal GFDM prototype filters in terms of minimizing MSE performance are derived without considering OOB radiation. In this chapter, we design prototype filters by considering performance and OOB radiation simultaneously.

### 7.1 Problem Formulation

We formulate a filter optimization problem to minimize OOB radiation while maintaining good in-band performance. Consider a GFDM system with the GFDM transmitter matrix  $\mathbf{A}$  and prototype filter  $\mathbf{g}$ . Let  $K, M, L, \mathcal{K}, E_S, T_s, p(t)$ , and  $\mathcal{B}_O$  be given and fixed, where  $\mathcal{B}_O$  denotes the set of frequencies considered out of band. Let  $\mathcal{M} = \{1, 2, \dots, M - 1\}$ , i.e., 1 guard subsymbol is used, which is conventional in the literature [3]. Let  $D = KM$ , and  $\eta$  be some positive real number. The problem is given by

$$\min_{\mathbf{g}} \max_{f \in \mathcal{B}_O} S_a(f) \quad (7.1a)$$

$$\text{subject to } \|\mathbf{g}\|_F^2 = 1 \quad (7.1b)$$

$$\xi_H \leq \eta, \quad (7.1c)$$

where  $S_a(f)$  is the PSD (5.1) of the GFDM analog baseband transmit signal, and  $\xi_H$  is the energy of  $\mathbf{A}^{-1}$ . According to the derived results in Chapter 6,  $\xi_H$  determines the SNR reduction of a GFDM system. For example, by Theorem 4(a), under an AWGN channel, the MSE at the ZF receiver is  $\xi_H N_0$ . The constraint (7.1c) thus pertains to maintaining a sufficiently good MSE or SER performance. The constraint (7.1b) is introduced as normalization of the prototype filter. Besides, according to (2.3), (6.4), and the definition of energy of a GFDM matrix, the constraint (7.1b) implies a natural constraint  $\xi_H \geq 1$ . Thus, the problem (7.1) is feasible only if  $\eta \geq 1$ . In particular, when  $\eta = 1$ , the feasible set is equivalent to using unitary transmitter matrices.

## 7.2 Proposed Algorithm

We intend to solve the optimization problem (7.1) by the techniques for solving convex optimization problems [47]. Since the problem (7.1) is nonconvex, some transformations on the problem is required. We introduce variables  $\mathbf{S} \in \mathbb{H}_+^D$ , defined as  $\mathbf{S} = \text{vec}(\mathbf{G})\text{vec}(\mathbf{G})^H$ , where  $\mathbf{G}$  is defined in (2.3). By the definition of the energy  $\xi_H$  and Theorem 2, we have

$$\xi_H = \frac{1}{D} \sum_{k=0}^{K-1} \sum_{l=0}^{M-1} \frac{1}{|[\mathbf{G}]_{k,l}|^2}. \quad (7.2)$$

Using (7.2), we obtain an equivalent form of the problem

$$\min_{\mathbf{s} \in \mathbb{H}_+^D} \quad \max_{f \in \mathcal{B}_o} S_a(f) \quad (7.3a)$$

$$\text{subject to} \quad \text{tr}(\mathbf{S}) = D \quad (7.3b)$$

$$\text{tr}(\mathbf{S}^{\circ-1}) \leq D\eta \quad (7.3c)$$

$$\text{rank}(\mathbf{S}) = 1. \quad (7.3d)$$

According to (5.1), (5.2), (5.3), we have

$$S_a(f) = \frac{E_S |P(f)|^2}{D' T_s} \sum_{k \in \mathcal{K}} \sum_{m \in \mathcal{M}} \left| \sum_{n=0}^{D-1} a_n(2\pi(fT_s - k/K), m) [\mathbf{g}_f]_n \right|^2, \quad (7.4)$$

where

$$a_n(\omega, m) = \frac{D'}{D} \sum_{l=0}^{D'-1} \left\{ \text{sinc}_{D'} \left( 2\pi \left( \frac{k}{D} - \frac{l}{D'} \right) \right) \cdot e^{j\pi \left( \frac{k}{D} - \frac{l}{D'} \right) (D'-1)} e^{-j2\pi k \frac{mK+L}{D}} \text{sinc}_{D'}(\omega'_l) e^{-j\omega'_l \frac{D'-1}{2}} \right\}. \quad (7.5)$$

By Lemma 1(b), we can further derive that

$$S_a(f) = \frac{E_S |P(f)|^2}{K D' T_s} \sum_{k \in \mathcal{K}} \sum_{m \in \mathcal{M}} \left| \sum_{n=0}^{D-1} b_n(f, k, m) [\text{vec}(\mathbf{G})]_n \right|^2 \quad (7.6)$$

where

$$b_n(f, k, m) = \sum_{k'=0}^{K-1} a_{k'M + \lfloor \frac{n}{K} \rfloor} (2\pi(fT_s - \frac{k}{K}), m) e^{-j2\pi \lfloor \frac{n}{K} \rfloor k'/D} e^{j-2\pi \lfloor \frac{n}{K} \rfloor k'/K}. \quad (7.7)$$

Letting  $\mathbf{b}(f, k, m)$  be a  $D \times 1$  vector with  $[\mathbf{b}(f, k, m)]_n = b_n(f, k, m)$ , we obtain

$$S_a(f) = \frac{E_S |P(f)|^2}{D' T_s} \sum_{k \in \mathcal{K}} \sum_{m \in \mathcal{M}} \mathbf{b}^H(f, k, m) \mathbf{S} \mathbf{b}(f, k, m). \quad (7.8)$$

Therefore, the objective function (7.3a) is a supremum of affine functions of  $\mathbf{S}$ , and thus convex in  $\mathbf{S}$ . We can also show that the constraints (7.3b) and (7.3c) are convex. Yet, the problem (7.3) is still nonconvex because the rank constraint (7.3d) is nonconvex.

To approach an optimization problem with a rank constraint, an iterative algorithm [48] may be used. We propose to tackle the problem (7.3) by iterating the optimal point  $\tilde{\mathbf{S}}$  of

$$\min_{\mathbf{S} \in \mathbb{H}_+^D} w |\text{tr}(\mathbf{S}\tilde{\mathbf{V}})| + \max_{f \in \mathcal{B}_O} S_a(f) \quad (7.9a)$$

$$\text{subject to } \text{tr}(\mathbf{S}) = D \quad (7.9b)$$

$$\text{tr}(\mathbf{S}^{\circ-1}) \leq D\eta \quad (7.9c)$$

with the optimal point  $\tilde{\mathbf{V}}$  of

$$\begin{aligned} \min_{\mathbf{V} \in \mathbb{H}_+^D} \quad & |\text{tr}(\tilde{\mathbf{S}}\mathbf{V})| & (7.10a) \\ \text{subject to} \quad & \mathbf{0} \preceq \mathbf{V} \preceq \mathbf{I}_D & (7.10b) \\ & \text{tr}(\mathbf{V}) = D - 1 & (7.10c) \end{aligned}$$



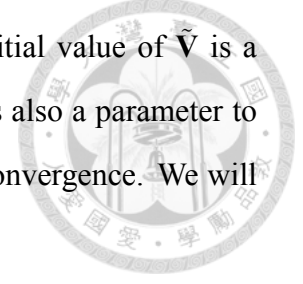
until convergence, where  $w > 0$ . The algorithm in [48] is used only for real variables. Here we extend the algorithm so that it can be used for complex variables. Specifically, the domain is changed from the set of real symmetric positive semidefinite matrices to the set of complex Hermitian positive semidefinite matrices, and we introduce the operator  $|\cdot|$  to assure that the objective functions are real-valued. According to our simulation results, the extension indeed works.

The problems (7.9) and (7.10) are convex, so the techniques for solving convex optimization problems can be applied. It is not difficult to show that all constraints of the two problems are convex. Also note that  $w > 0$  and that  $\max_{f \in \mathcal{B}_O} S_a(f)$  is convex in  $\mathbf{S}$ . Thus, to prove the convexity of the problems, we only have to show that  $|\text{tr}(\tilde{\mathbf{S}}\mathbf{V})|$  is convex in  $\mathbf{V}$ . Regard the complex variables  $\mathbf{V}$  as independent real variables, i.e., their real parts and imaginary parts. Then  $|\text{tr}(\tilde{\mathbf{S}}\mathbf{V})|$  is a norm of an affine transformation of these real variables. Since any norm is convex, and composition with an affine transformation preserves convexity, the problems are convex.

To understand the concept of the algorithm, it would be beneficial to know the solution of the problem (7.10). In fact, this problem can be solved analytically [48]. Specifically, with the ordered (in the order of non-increasing eigenvalues) eigendecomposition  $\tilde{\mathbf{S}} = \mathbf{Q}\mathbf{\Lambda}\mathbf{Q}^H$ , the optimal point is  $\tilde{\mathbf{V}} = \mathbf{U}\mathbf{U}^H$ , where  $\mathbf{U}$  is the submatrix of  $\mathbf{Q}$  obtained by removing the first column of  $\mathbf{Q}$ . In other words, the first  $D - 1$  eigenvectors of  $\tilde{\mathbf{V}}$  are the same as the last  $D - 1$  eigenvectors of  $\tilde{\mathbf{S}}$ , and all correspond to eigenvalue 1. The last eigenvalue of  $\tilde{\mathbf{V}}$  is 0. Therefore, the term  $w|\text{tr}(\tilde{\mathbf{S}}\mathbf{V})|$  introduced in the objective function (7.9a) can be considered as favoring the direction,  $\mathbf{u}\mathbf{u}^H$ , in the vector space  $\mathbb{H}_+^D$ , where  $\mathbf{u}$  is the first column of  $\mathbf{Q}$ . In this way, we expect that the algorithm can converge to a point

corresponding to a rank-1  $\mathbf{S}$ .

Our iterative algorithm starts with the problem (7.9), so the initial value of  $\tilde{\mathbf{V}}$  is a parameter that we can design. The choice of the weight  $w$ , which is also a parameter to be designed, can affect the rate of convergence and the result  $\mathbf{S}$  at convergence. We will show by simulation how  $w$  affects these in general.



## 7.3 Simulation Results

Simulation results of our iterative algorithm are shown for three cases. To solve the problem (7.9), we use CVX, a package for specifying and solving convex programs [49]. In our program, we discretize the frequency variable  $f$  by sampling at integer multiples of  $1/(16DT_s)$  Hz. The stopping criterion of the iterative algorithm is  $|s_i - s_{i-1}|/s_{i-1} < 5 \times 10^{-5}$ , where  $s_i$  is the value  $\max_{f \in \mathcal{B}_O} S_a(f)$  obtained in the  $i$ th iteration. The optimization results are compared to GFDM systems using RC filters [2] with a roll-off factor of 0.5 and Dirichlet pulses [3], and with OFDM systems in terms of PSD,  $\xi_H$ , and SER performance. Note that OFDM is a special case of GFDM using a rectangular window as the prototype filter, and always with  $M = 1$  and  $\xi_H = 1$ . For a fair comparison, the block size of OFDM systems is the same as that of GFDM systems,  $D$ , and the number of used OFDM subcarriers, denoted as  $N$ , is the same as the number of used resource elements in GFDM systems,  $|\mathcal{K}||\mathcal{M}|$ . Thus, the spectral efficiency of all systems with all filters are the same. The used OFDM subcarriers are contiguous, and their center is located at the DC bin.

### 7.3.1 Parameter Settings

The CP length is  $L = 0$ , the symbol energy is  $E_S = 1$ , and the sampling interval is  $T_s = 1 \mu\text{s}$ . We use  $\eta = 1$  in (7.9c). The interpolation filter  $p(t)$  is a sample-level RC filter [42] with a roll-off factor of 0.1. Besides, we use the  $D \times D$  zero matrix as the initial value of  $\tilde{\mathbf{V}}$ . In Table 7.1, parameter settings are shown for three simulation cases, including the weight  $w$ , the number of GFDM subcarriers  $K$  and subsymbols  $M$ , the set of used GFDM

Table 7.1: Parameter settings

Parameter	Case 1	Case 2	Case 3
$w$	0.0003	0.001	0.003
$K$	8	16	8
$M$	7	5	3
$\mathcal{K}$	$\{0, 1, 7\}$	$\{0, 1, 2, 3, 4, 12, 13, 14, 15\}$	$\{0, 1, 2, 6, 7\}$
$\mathcal{M}$	$\{1, 2, \dots, 6\}$	$\{1, 2, \dots, 4\}$	$\{1, 2\}$
$N$	18	36	10
$\mathcal{B}_O$	$(-\infty, \frac{-5}{16T_s}) \cup (\frac{5}{16T_s}, \infty)$	$(-\infty, \frac{-11}{32T_s}) \cup (\frac{11}{32T_s}, \infty)$	$(-\infty, \frac{-7}{16T_s}) \cup (\frac{7}{16T_s}, \infty)$



subcarriers  $\mathcal{K}$  and subsymbols  $\mathcal{M}$ , the number of used OFDM subcarriers  $N$ , and the set of frequencies considered out of band  $\mathcal{B}_O$ . Note that we select  $M$  as an odd number for each case because RC filters are essentially not applicable to cases where both  $K$  and  $M$  are even, as GFDM transmitter matrices under such cases are singular [5]. We set  $\mathcal{B}_O$  based on the usage of 1 guard subcarrier for GFDM. For the evaluation of SER performance, Monte-Carlo simulation with  $10^5$  blocks is run for each prototype filter. The modulation is QPSK. The ZF receiver and an AWGN channel are used.

### 7.3.2 Simulation Results for the Case of $\eta = 1$

For Case 1, the magnitude responses of the optimized filter, RC filter, and Dirichlet pulse are shown in Fig. 7.1. The optimized filter is well-localized, but its side lobes are more significant than those of the other filters. The PSD is shown in Fig. 7.2. The PSD is normalized according to the RC filter so that the maximum value of its PSD is 0 dB. Compared to the PSD of the RC filter and Dirichlet pulse, the optimized PSD is higher in the guard band, in exchange for lower OOB radiation. The higher guard-band PSD does not matter since guard band would not be used by other users. The maximum OOB PSD  $\max_{f \in \mathcal{B}_O} S_a(f)$  is presented in Table 7.2. The optimized filter outperforms the RC filter by about 7 dB, Dirichlet pulse by about 10 dB, and OFDM by about 24 dB.

The energy  $\xi_H$  is also presented in Table 7.2. Observe that  $\xi_H = 1$  for the optimized



Table 7.2: Maximum OOB PSD  $\max_{f \in \mathcal{B}_O} S_a(f)$  in dB and energy  $\xi_H$

	Case 1		Case 2		Case 3	
	OOB	$\xi_H$	OOB	$\xi_H$	OOB	$\xi_H$
OFDM	-19.76	1.000	-19.49	1.000	-15.66	1.000
Dirichlet [3]	-33.88	1.000	-33.30	1.000	-28.89	1.000
RC [2]	-37.32	1.200	-36.35	1.117	-31.30	1.063
Optimized filter	-44.11	1.000	-42.01	1.000	-41.95	1.000

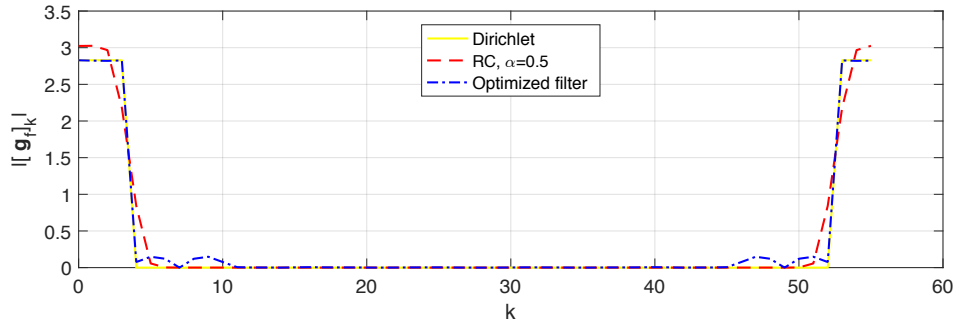


Figure 7.1: Magnitude response of the frequency-domain prototype filter  $\mathbf{g}_f$  for Case 1.

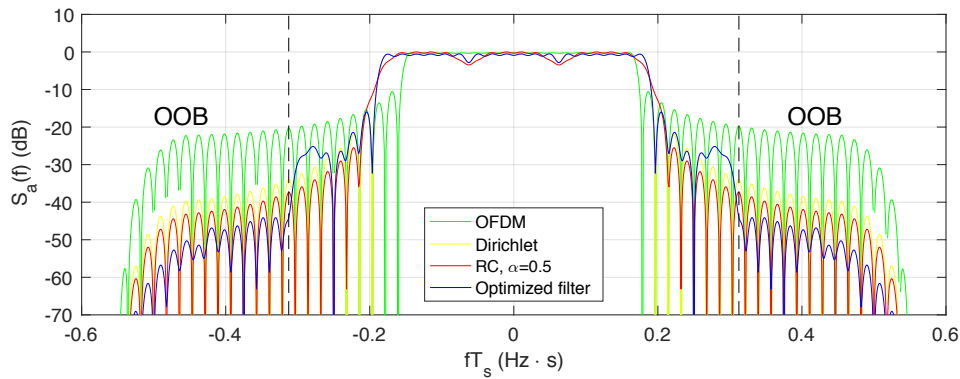


Figure 7.2: PSD for Case 1.

filter, Dirichlet pulse, and OFDM, which means unitary transmitter matrices are used. By Theorem 4, unitary transmitter matrices minimize the MSE at ZF receivers. By contrast,  $\xi_H > 1$  for the RC filter. Thus, we expect that the SER performance of the optimized filter should be the same as those of the Dirichlet pulse and OFDM, and better than that of the RC filter. This is confirmed in Fig. 7.3.

In view of these results, using RC filters can be regarded as sacrificing SER performance for lower OOB radiation, compared to Dirichlet pulses. However, this sacrifice is unnecessary because our optimized filter performs the best among the three filters and

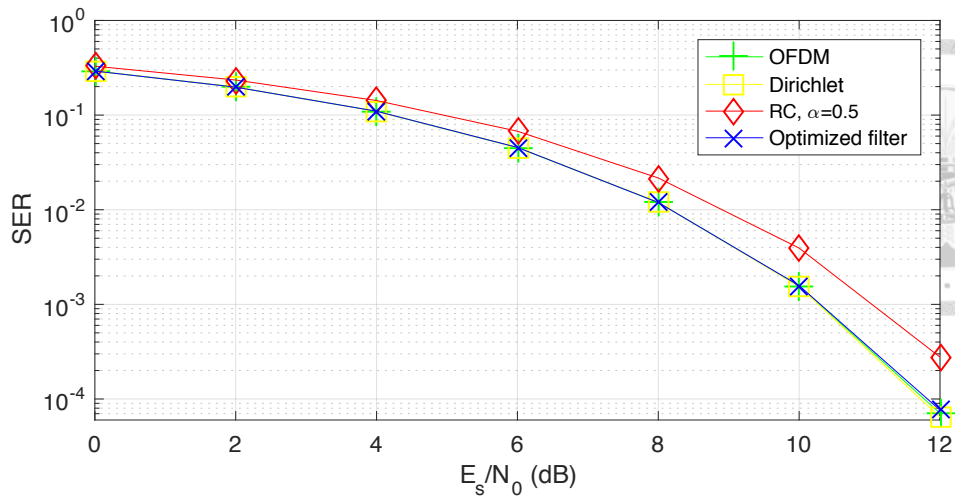


Figure 7.3: SER for Case 1.

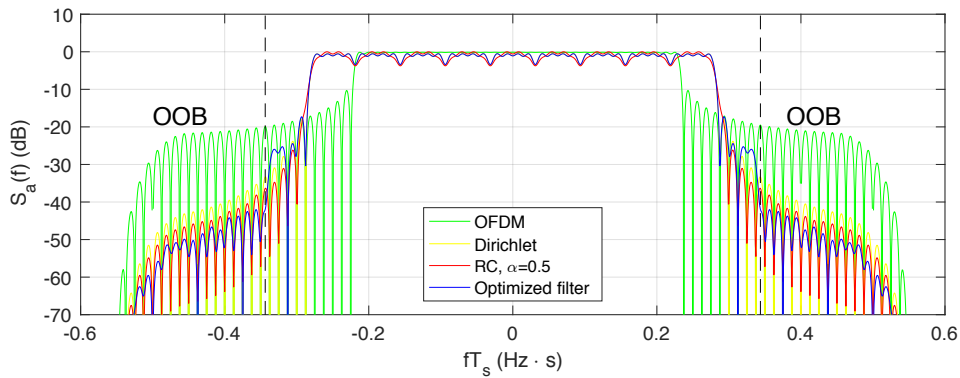


Figure 7.4: PSD for Case 2.

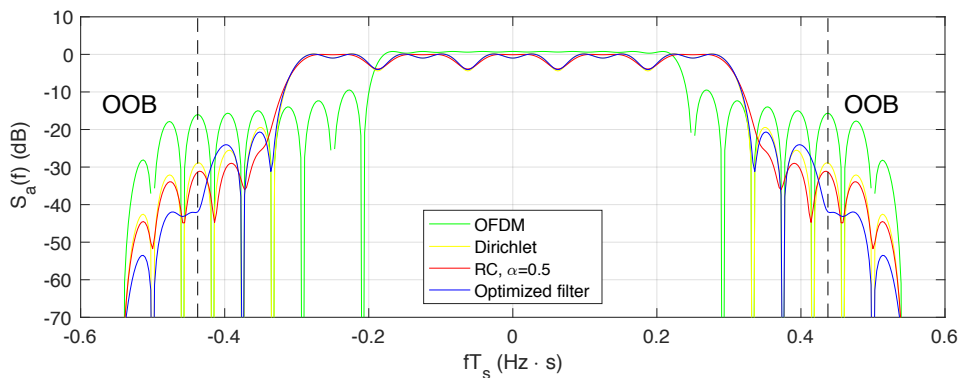


Figure 7.5: PSD for Case 3.

OFDM in terms of both OOB radiation and SER performance. Moreover, RC filters are essentially not applicable to cases where both  $K$  and  $M$  are even [5].

The PSDs for Cases 2 and 3 are shown in Figs. 7.4 and 7.5, respectively. The results of  $\max_{f \in B_O} S_a(f)$  and  $\xi_H$  are presented in Table 7.2. Trends similar to those of Case 1

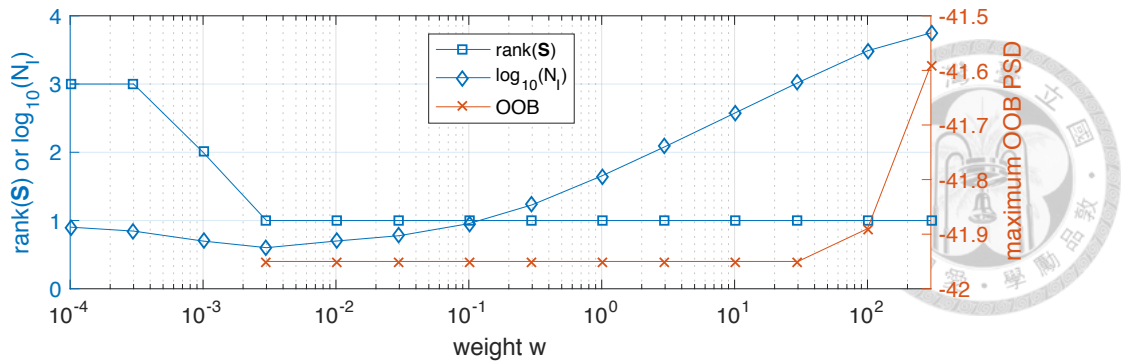


Figure 7.6: Maximum OOB PSD  $\max_{f \in \mathcal{B}_O} S_a(f)$  and rank( $\mathbf{S}$ ) obtained at convergence, and number of iterations  $N_I$  versus weight  $w$  for Case 3.

can be observed for Cases 2 and 3. That is, the optimized filter is the best in terms of both OOB radiation and  $\xi_H$ , with  $\xi_H$  characterizing MSE or SER performance. These results confirm the general effectiveness of the proposed algorithm.

### 7.3.3 Influence of the Weight $w$

To study the effects of the weight  $w$  on the obtained objective  $\max_{f \in \mathcal{B}_O} S_a(f)$  and rank( $\mathbf{S}$ ) at convergence, and the number of iterations, denoted as  $N_I$ , the proposed algorithm is implemented with different values of  $w$  for Case 3. All the other simulation parameters remain the same. As shown in Fig. 7.6, it is observed that when  $w$  is chosen within the range,  $0.003 \leq w \leq 30$ , the obtained objective is the least and the rank constraint (7.3d) is met. In fact, the obtained prototype filter  $\mathbf{g}$  at convergence is the same for all  $w$  in the range. The rank constraint is not met if  $w$  is too small, and the obtained objective gets greater if  $w$  is too large. These effects of  $w$  coincide with the empirical evidence gathered by [48]. Also, we see in Fig. 7.6 that  $N_I$  is the least when  $w = 0.003$ . As  $w$  increases above 0.003,  $N_I$  increases nearly proportionally. Thus, to minimize the obtained objective and maximize the rate of convergence, we should select  $w = 0.003$ . In fact,  $w$  in Table 7.1 has been selected in this way for each case.

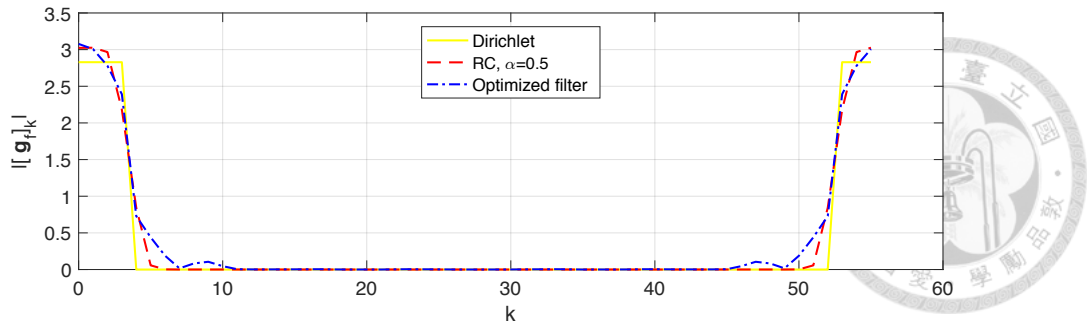


Figure 7.7: Magnitude response of the frequency-domain prototype filter  $\mathbf{g}_f$  for Case 1.  $\eta = 1.1$ .

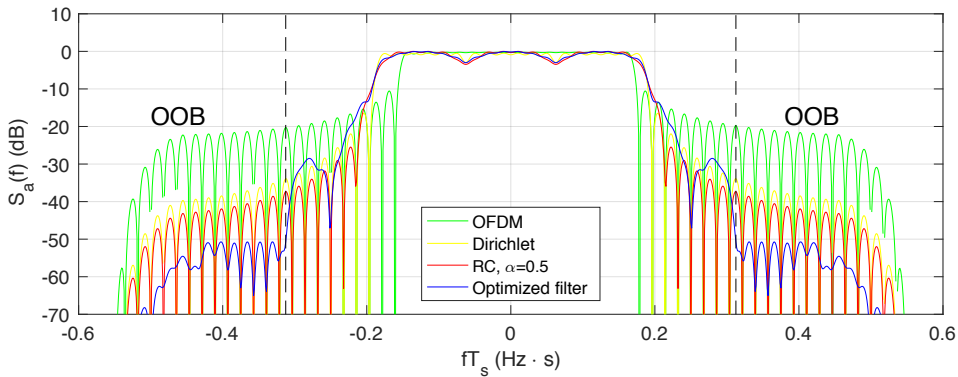


Figure 7.8: PSD for Case 1.  $\eta = 1.1$ .

### 7.3.4 Simulation Results for the Case of $\eta > 1$

The parameter  $\eta$  in our optimization problems enables us to exploit the trade-off between OOB radiation and MSE performance. To show that even lower OOB radiation can be obtained with the proposed algorithm by sacrificing a little MSE performance, we provide simulation for the case of  $\eta > 1$ . The same set of parameter settings for Case 1 in Section 7.3.1, except that the parameter  $\eta$  is set as 1.1 instead of 1.

The magnitude responses of the optimized filter obtained under  $\eta = 1.1$ , RC filter, and Dirichlet pulse are shown in Fig. 7.7. Again, the optimized filter is well-localized, but its side lobes are more significant than those of the other filters. The PSD is shown in Fig. 7.8. The PSD is normalized according to the RC filter so that the maximum value of its PSD is 0 dB. The maximum OOB PSD  $\max_{f \in B_O} S_a(f)$  is presented in Table 7.3. We also include the results of the optimized filter obtained under  $\eta = 1$  in Section 7.3.2 for comparison. The optimized filter obtained under  $\eta = 1.1$  outperforms the optimized filter obtained under  $\eta = 1$  by about 7 dB, RC filter by about 13 dB, Dirichlet pulse by about

Table 7.3: Maximum OOB PSD  $\max_{f \in \mathcal{B}_O} S_a(f)$  in dB and energy  $\xi_H$  for Case 1

	OOB	$\xi_H$
OFDM	-19.76	1.000
Dirichlet [3]	-33.88	1.000
RC [2]	-37.32	1.200
Optimized filter, $\eta = 1$	-44.11	1.000
Optimized filter, $\eta = 1.1$	-50.73	1.100



17 dB, and OFDM by about 31 dB. Meanwhile, the NEF of the optimized filter obtained under  $\eta = 1.1$  is greater than the NEF of the optimized filter obtained under  $\eta = 1$ , but less than the NEF of the RC filter. This implies that the MSE or SER performance of the optimized filter obtained under  $\eta = 1.1$  would lie between those of the optimized filter and RC filter. In other words, we can obtain even lower OOB radiation by sacrificing a little MSE or SER performance. In the future, one may exploit this trade-off between OOB radiation and performance systematically to achieve certain goals and meet certain constraints.

## 7.4 Future Work

There are many issues one can explore on the optimization problem (7.3) and the proposed iterative algorithm. First, one may want to prove whether or not the iterative algorithm indeed leads to the optimal solution of the problem (7.3). Second, one may want to prove whether or not the iterative algorithm can guarantee a rank-1  $\mathbf{S}$  at convergence for all cases of parameter settings, or one may identify particular ranges of weight  $w$  that guarantee a rank-1  $\mathbf{S}$ , guarantee a non-rank-1  $\mathbf{S}$ , and lead to indefinite results at convergence, respectively. Finally, the complexity of the iterative algorithm can be analyzed in the future. For example, one may want to derive an upper bound for the number of iterations of the algorithm if it converges. One may also develop other algorithms with less complexity to solve the optimization problem (7.3). It is worth noting that relaxing the problem (7.3) simply by ignoring the constraint (7.3d) does not lead to a desirable result. For instance, for Case 3 in Section 7.3.1, if we adopt this relaxation, we will obtain a rank-3  $\mathbf{S}$  with the

first three singular values 15.8888, 6.6526, and 1.45855.

Furthermore, many more optimization problems similar to the problem (7.1) can be formulated and solved in the future. For instance, the design of the prototype filter based on the characteristic matrix together with the design of the number and position of guard subcarriers and subsymbols for maximizing spectral efficiency under OOB-radiation and performance constraints can be studied. That is, one may want to solve the problem

$$\max_{\mathbf{g}, \mathcal{K}, \mathcal{M}} |\mathcal{K}| |\mathcal{M}| \quad (7.11a)$$

$$\text{subject to } \|\mathbf{g}\| = 1 \quad (7.11b)$$

$$\max_{f \in \mathcal{B}_O} S_a(f) \leq \rho \quad (7.11c)$$

$$\xi_H \leq \eta, \quad (7.11d)$$

where  $\eta$  and  $\rho$  are some positive real numbers. With some modifications, we believe that the proposed algorithm can be used to solve the problem (7.11). One may also consider the sum rate  $R$  as the objective function, formulating the problem

$$\max_{\mathbf{g}, \mathcal{K}, \mathcal{M}} R \quad (7.12a)$$

$$\text{subject to } \|\mathbf{g}\| = 1 \quad (7.12b)$$

$$\max_{f \in \mathcal{B}_O} S_a(f) \leq \rho. \quad (7.12c)$$

A constraint of the form  $\xi_H \leq \eta$  is not introduced in the problem (7.12) because performance is already involved in the objective function, the sum rate  $R$ . The sum rate  $R$  depends on the used type of receivers and channels, so the solution to the problem (7.12) may vary case by case.



## Chapter 8

# Multiple Access with Optimized Prototype Filters

We briefly evaluate the performance of generalized frequency division multiple access (GFDMA) [44] and compare it to that of orthogonal frequency division multiple access (OFDMA) [36]. In particular, GFDMA with the CMCM filters, which are optimal in terms of MSE performance, is shown to be promising. In our simulation, uplink transmission is considered, and the same GFDM transmitter matrix with  $K = 32$  and  $M = 15$  is used by two users. The subcarriers used by the two users are  $\mathcal{K} = \{0, 1, \dots, 14\}$  and  $\mathcal{K} = \{16, 17, \dots, 30\}$ , respectively, and the 0th subsymbol is used as a guard symbol. For a fair comparison, for OFDMA, we use  $K = 480$  and  $M = 1$ , and the subcarriers used by the two users are  $\mathcal{K} = \{0, 1, \dots, 209\}$  and  $\mathcal{K} = \{240, 241, \dots, 449\}$ , respectively, so that the spectral efficiency of GFDMA and OFDMA is the same. We evaluate the performance of one user while assuming that the other user has a normalized carrier frequency offset (CFO) [36]  $\epsilon = 0$  or  $0.2$  (normalized to the OFDM subcarrier spacing). The ZF receiver under the same deep-fade-excluded Rayleigh fading channel as mentioned in Section 6.4 is used. The modulation is 16QAM, and the CP length is  $L = D/4$ .

Fig. 8.1 shows that the MSE performance of GFDMA using the Dirichlet pulse and modified Dirichlet pulse and OFDMA are the same when  $\epsilon = 0$ . However, when  $\epsilon = 0.2$ , the Dirichlet pulse performs much better than OFDMA, and the modified Dirichlet pulse

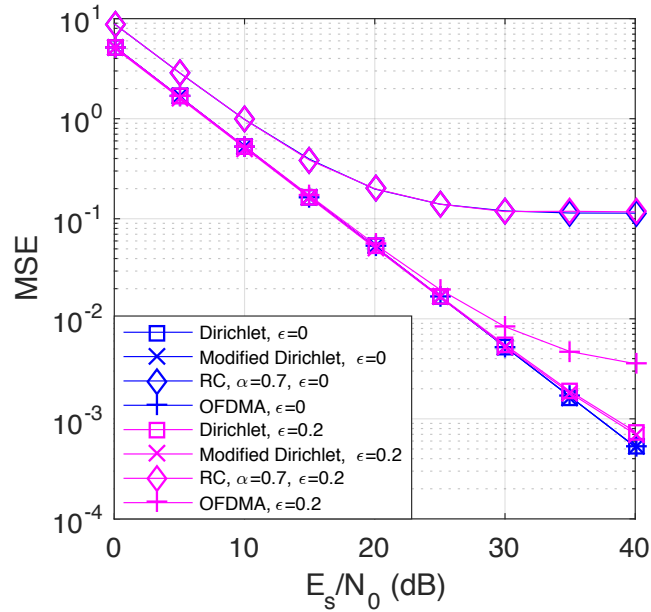


Figure 8.1: MSE for GFDMA ZF receiver over a deep-fade-excluded Rayleigh fading channel and the corresponding OFDMA receiver.  $K = 32$ ,  $M = 15$ .

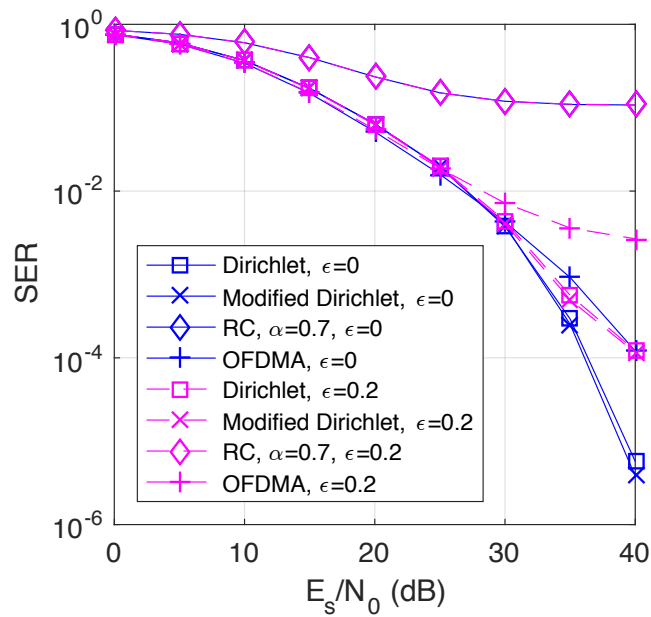


Figure 8.2: SER for GFDMA ZF receiver over a deep-fade-excluded Rayleigh fading channel and the corresponding OFDMA receiver.  $K = 32$ ,  $M = 15$ .

performs a little better than the Dirichlet pulse, which can be explained by their OOB leakage. The RC filter performs the worst when  $\epsilon = 0$  and 0.2 since its ZF prototype receiver filter is not frequency-localized and collects interference outside the desired bandwidth [2]. Similar results can be seen in Fig. 8.2 for the SER performance. Particularly,



when  $\epsilon = 0.2$ , the Dirichlet pulse performs much better than OFDMA, and the modified Dirichlet pulse performs a little better than the Dirichlet pulse, which can be explained by their OOB leakage. A difference between MSE and SER is that the Dirichlet and modified Dirichlet pulses have the same MSE performance as but better SER performance in the higher SNR region than OFDM, which can be explained by the effect of an orthogonal precoder on OFDM (due to convex and concave regions of a function composed of the Q-function) [46].

These simulation results show that GFDMA using the proposed CMCM filters is promising. According to the simulation results, we believe that GFDMA is more robust against CFO than OFDMA. In the future, one may want to explore how CFOs influence MSE and SER performance in multiple access thoroughly and systematically, such as formulating an optimization problem that involves CFOs.





## Chapter 9

### Conclusions

In this thesis, a new matrix-based characterization of generalized frequency division multiplexing (GFDM) systems is proposed. The new characterization facilitates deriving properties of GFDM (transmitter) matrices which were not easily obtained under the traditional prototype-filter point of view. The class of unitary GFDM matrices is identified through the matrix characterization, and conditions for non-singularity of GFDM matrices can be expressed clearly with the new characterization.

Moreover, low-complexity transceiver implementations are derived on the basis of the characteristic matrix. Particularly, the necessary and sufficient conditions for the existence of a form of implementation with a linearithmic complexity for an MMSE receiver are derived. Such a receiver is determined to exist if the GFDM transmitter matrix is selected to be unitary. In the case where the implementation does not exist, a low-complexity sub-optimal MMSE receiver is proposed, and its performance approximates that of an MMSE receiver, as shown by numerical results.

This study also reveals that prototype transmit filters minimizing the MSE performance under the ZF or MMSE receiver over various types of channels correspond to the class of CMCM filters, which subsequently correspond to scalar multiples of unitary GFDM matrices. The simulation verifies the MSE optimality for the CMCM filters and shows that their SER performance is superior to that of non-CMCM filters. Furthermore, joint optimization on performance and OOB radiation is considered. Specifically, a filter optimization algorithm is proposed for suppressing OOB radiation while the in-band

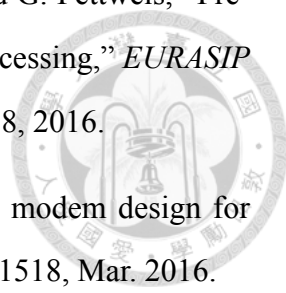
MSE and SER performance is maintained. The optimization problem is formulated in terms of the proposed characteristic matrix of the GFDM transmitter matrix. Simulation results show that under the same spectral efficiency, optimized filters perform the best in terms of both OOB radiation and SER performance, compared to RC filters, Dirichlet pulses, and OFDM. Finally, the advantage of GFDMA using CMCM filters, including the Dirichlet and modified Dirichlet pulses, over OFDMA is verified through numerical results.


In the future, the design of the prototype filter based on the characteristic matrix together with the design of the number and position of guard subcarriers and subsymbols for maximizing spectral efficiency under OOB-radiation and performance constraints can be studied. One may want to formulate optimization problems that directly involve carrier frequency offset (CFO) and SER (or bit error rate). We might also design the prototype filter based on the characteristic matrix to obtain a minimum PAPR. Moreover, issues on optimality condition, convergence condition, and complexity reduction of the proposed iterative algorithm for filter optimization are desirable for future study. Besides, a proof to Hypothesis 1, which states that CMCM filters minimize the MSE under the MMSE receiver over a statistical multipath channel, is desirable.



# Bibliography

- [1] G. Fettweis, M. Krondorf, and S. Bittner, "GFDM - generalized frequency division multiplexing," in *Veh. Technol. Conf., 2009. VTC Spring 2009. IEEE 69th*, Apr. 2009, pp. 1–4.
- [2] N. Michailow, M. Matthé, I. Gaspar, A. Caldevilla, L. Mendes, A. Festag, and G. Fettweis, "Generalized frequency division multiplexing for 5th generation cellular networks," *IEEE Trans. Commun.*, vol. 62, no. 9, pp. 3045–3061, Sep. 2014.
- [3] M. Matthé, N. Michailow, I. Gaspar, and G. Fettweis, "Influence of pulse shaping on bit error rate performance and out of band radiation of generalized frequency division multiplexing," in *Proc. IEEE ICC Workshop*, 2014, pp. 43–48.
- [4] J. Bingham, "Multicarrier modulation for data transmission: an idea whose time has come," *IEEE Commun. Mag.*, vol. 28, no. 5, pp. 5–14, May 1990.
- [5] M. Matthé, L. Mendes, and G. Fettweis, "Generalized frequency division multiplexing in a Gabor transform setting," *IEEE Commun. Lett.*, vol. 18, no. 8, pp. 1379–1382, Aug. 2014.
- [6] R. Datta, N. Michailow, M. Lentmaier, and G. Fettweis, "GFDM interference cancellation for flexible cognitive radio PHY design," in *Veh. Technol. Conf. (VTC Fall), 2012 IEEE*, Sep. 2012, pp. 1–5.
- [7] R. Datta, G. Fettweis, Z. Kollár, and P. Horváth, "FBMC and GFDM interference cancellation schemes for flexible digital radio PHY design," in *Digital System Design (DSD), 2011 14th Euromicro Conf. on*, Aug. 2011, pp. 335–339.

- 
- [8] M. Matthé, L. Mendes, I. Gaspar, N. Michailow, D. Zhang, and G. Fettweis, “Pre-coded GFDM transceiver with low complexity time domain processing,” *EURASIP J. on Wireless Commun. and Networking*, vol. 2016, no. 1, p. 138, 2016.
- [9] A. Farhang, N. Marchetti, and L. E. Doyle, “Low-complexity modem design for GFDM,” *IEEE Trans. Signal Process.*, vol. 64, no. 6, pp. 1507–1518, Mar. 2016.
- [10] M. Matthé, I. Gaspar, D. Zhang, and G. Fettweis, “Reduced complexity calculation of LMMSE filter coefficients for GFDM,” in *Veh. Technol. Conf. (VTC Fall), 2015 IEEE 82nd*, Sept 2015, pp. 1–2.
- [11] M. Matthé, D. Zhang, and G. Fettweis, “Iterative detection using MMSE-PIC demapping for MIMO-GFDM systems,” in *Eur. Wireless 2016; 22th Eur. Wireless Conf.*, May 2016, pp. 1–7.
- [12] N. Michailow, I. Gaspar, S. Krone, M. Lentmaier, and G. Fettweis, “Generalized frequency division multiplexing: Analysis of an alternative multi-carrier technique for next generation cellular systems,” in *2012 Int. Syst. on Wireless Commun. Syst. (ISWCS)*, Aug 2012, pp. 171–175.
- [13] N. Michailow, S. Krone, M. Lentmaier, and G. Fettweis, “Bit error rate performance of generalized frequency division multiplexing,” in *Veh. Technol. Conf. (VTC Fall), 2012 IEEE*, Sep. 2012, pp. 1–5.
- [14] S. K. Bandari, A. Drosopoulos, and V. V. Mani, “Exact SER expressions of GFDM in Nakagami-m and Rician fading channels,” in *Eur. Wireless 2015; 21th Eur. Wireless Conf.; Proc. of*, May 2015, pp. 1–6.
- [15] B. M. Alves, L. L. Mendes, D. A. Guimaraes, and I. S. Gaspar, “Performance of GFDM over frequency-selective channels,” in *Proc. Int. Workshop on Telecommun.*, 2013.
- [16] S. Tiwari, S. S. Das, and K. K. Bandyopadhyay, “Precoded generalised frequency division multiplexing system to combat inter-carrier interference: performance analysis,” *IET Commun.*, vol. 9, no. 15, pp. 1829–1841, 2015.

- 
- [17] A. RezazadehReyhani, A. Farhang, and B. Farhang-Boroujeny, “Circularly pulse-shaped waveforms for 5G: Options and comparisons,” in *2015 IEEE Global Commun. Conf. (GLOBECOM)*, Dec. 2015, pp. 1–7.
- [18] M. Matthé, L. L. Mendes, and G. Fettweis, “Asynchronous multi-user uplink transmission with generalized frequency division multiplexing,” in *2015 IEEE Int. Conf. on Commun. Workshop (ICCW)*, Jun. 2015, pp. 2269–2275.
- [19] M. Matthé, I. Gaspar, D. Zhang, and G. Fettweis, “Near-ML detection for MIMO-GFDM,” in *Veh. Technol. Conf. (VTC Fall), 2015 IEEE 82nd*, Sep. 2015, pp. 1–2.
- [20] M. Matthé, L. L. Mendes, N. Michailow, D. Zhang, and G. Fettweis, “Widely linear estimation for space-time-coded GFDM in low-latency applications,” *IEEE Trans. Commun.*, vol. 63, no. 11, pp. 4501–4509, Nov. 2015.
- [21] Z. Sharifian, M. J. Omid, A. Farhang, and H. Saeedi-Sourck, “Polynomial-based compressing and iterative expanding for PAPR reduction in GFDM,” in *2015 23rd Iranian Conf. on Elect. Eng.*, May 2015, pp. 518–523.
- [22] S. Li, Y. Zhao, L. He, Z. Wu, and Y. Li, “Design and performance analysis of a GFDM-DCSK communication system,” in *2016 13th IEEE Annu. Consumer Commun. Networking Conf. (CCNC)*, Jan. 2016, pp. 802–803.
- [23] S. Han, Y. Sung, and Y. H. Lee, “Filter design for generalized frequency-division multiplexing,” *IEEE Trans. Signal Process.*, submitted for publication. [Online]. Available: <https://arxiv.org/abs/1607.04004v2>
- [24] I. Gaspar and G. Fettweis, “An embedded midamble synchronization approach for generalized frequency division multiplexing,” in *2015 IEEE Global Commun. Conf. (GLOBECOM)*, Dec. 2015, pp. 1–5.
- [25] L. Chang, G. Y. Li, J. Li, and R. Li, “Blind parameter estimation of GFDM signals over frequency-selective fading channels,” *IEEE Trans. Commun.*, vol. 64, no. 3, pp. 1120–1131, Mar. 2016.

- [26] P. S. Wang and D. W. Lin, "Maximum-likelihood blind synchronization for GFDM systems," *IEEE Signal Process. Lett.*, vol. 23, no. 6, pp. 790–794, Jun. 2016.
- [27] I. Gaspar, L. Mendes, M. Matthé, N. Michailow, A. Festag, and G. Fettweis, "LTE-compatible 5G PHY based on generalized frequency division multiplexing," in *2014 11th Int. Symp. on Wireless Commun. Syst. (ISWCS)*, Aug. 2014, pp. 209–213.
- [28] I. Gaspar, A. Festag, and G. Fettweis, "Synchronization using a pseudo-circular preamble for generalized frequency division multiplexing in vehicular communication," in *Veh. Technol. Conf. (VTC Fall), 2015 IEEE 82nd*, Sep. 2015, pp. 1–5.
- [29] X.-G. Xia, "A family of pulse-shaping filters with ISI-free matched and unmatched filter properties," *IEEE Trans. Commun.*, vol. 45, no. 10, pp. 1157–1158, Oct. 1997.
- [30] P.-C. Chen, B. Su, and Y. Huang, "Matrix characterization for GFDM systems: Low-complexity MMSE receivers and optimal prototype filters," *IEEE Trans. Signal Process.*, to appear. [Online]. Available: <http://arxiv.org/abs/1611.04429v4>
- [31] P.-C. Chen and B. Su, "Filter optimization of out-of-band radiation with performance constraints for GFDM systems," *accepted to the 18th IEEE Int. Workshop on Signal Process. Advances in Wireless Commun. (SPAWC)*, 2017.
- [32] H. Bolcskei and F. Hlawatsch, "Discrete Zak transforms, polyphase transforms, and applications," *IEEE Trans. Signal Process.*, vol. 45, no. 4, pp. 851–866, Apr. 1997.
- [33] A. J. Laub, *Matrix Analysis for Scientists and Engineers*. SIAM: Society for Industrial and Applied Mathematics, 2004.
- [34] D. W. Lin and P. S. Wang, "On the configuration-dependent singularity of GFDM pulse-shaping filter banks," *IEEE Commun. Lett.*, vol. 20, no. 10, pp. 1975–1978, Oct. 2016.
- [35] M. Zibulski and Y. Y. Zeevi, "Oversampling in the Gabor scheme," *IEEE Trans. Signal Process.*, vol. 41, no. 8, pp. 2679–2687, Aug. 1993.



- [36] Y.-P. Lin, S.-M. Phoong, and P. P. Vaidyanathan, *Filter Bank Transceivers for OFDM and DMT Systems*. New York, NY, USA: Cambridge University Press, 2010.
- [37] G. Matsaglia and G. P. H. Styan, "Equalities and inequalities for ranks of matrices," *Linear and multilinear Algebra*, vol. 2, no. 3, pp. 269–292, 1974.
- [38] C. Eckart and G. Young, "The approximation of one matrix by another of lower rank," *Psychometrika*, vol. 1, no. 3, pp. 211–218, 1936.
- [39] M. Brand, "Fast low-rank modifications of the thin singular value decomposition," *Linear Algebra and Its Appl.*, vol. 415, no. 1, pp. 20–30, May 2006.
- [40] P. Duhamel and M. Vetterli, "Fast Fourier transforms: A tutorial review and a state of the art," *Signal Process.*, vol. 19, no. 4, pp. 259–299, 1990.
- [41] G. Strang, *Introduction to linear algebra*, 4th ed. Wellesley Cambridge Press, 2009.
- [42] S. Haykin, *Communication Systems*, 4th ed. Wiley Publishing, 2001.
- [43] S. Sesia, M. Baker, and I. Toufik, *LTE-the UMTS long term evolution: from theory to practice*. John Wiley & Sons, 2011.
- [44] Z. Sharifian, M. J. Omidi, H. Saeedi-Sourck, and A. Farhang, "Linear precoding for PAPR reduction of GFDMA," *IEEE Wireless Commun. Lett.*, vol. 5, no. 5, pp. 520–523, Oct. 2016.
- [45] S. H. Han and J. H. Lee, "An overview of peak-to-average power ratio reduction techniques for multicarrier transmission," *IEEE Wireless Commun.*, vol. 12, no. 2, pp. 56–65, Apr. 2005.
- [46] Y.-P. Lin and S.-M. Phoong, "BER minimized OFDM systems with channel independent precoders," *IEEE Trans. Signal Process.*, vol. 51, no. 9, pp. 2369–2380, Sep. 2003.
- [47] S. Boyd and L. Vandenberghe, *Convex optimization*. Cambridge University Press, 2009.

[48] J. Dattorro, *Convex optimization & Euclidean distance geometry*. Meboo Publishing, 2016.

[49] M. Grant and S. Boyd, "CVX: Matlab software for disciplined convex programming, version 2.1," <http://cvxr.com/cvx>, Mar. 2014.





# Appendix A

## Proof of Theorem 5

Using (3.20) and noting that  $\sigma^2 = \mathbf{1}_K^T \boldsymbol{\sigma} / K$ , we obtain

$$\sigma^2 = \frac{N_0}{KD} \sum_{k=0}^{K-1} \sum_{l=0}^{M-1} \left( \sum_{r=0}^{K-1} \frac{1}{|C_{l+rM}|^2} \right) \frac{1}{|[\mathbf{G}]_{k,l}|^2}. \quad (\text{A.1})$$

Let  $\alpha_l = \sum_{r=0}^{K-1} 1/(|C_{l+rM}|^2)$ . According to the Cauchy-Schwarz inequality, we have

$$\left[ \sum_{k,l} |[\mathbf{G}]_{k,l}|^2 \right] \left[ \sum_{k,l} \frac{\alpha_l}{|[\mathbf{G}]_{k,l}|^2} \right] \geq \left[ \sum_{k=0}^{K-1} \sum_{l=0}^{M-1} \sqrt{\alpha_l} \right]^2, \quad (\text{A.2})$$

where the equality holds if and only if  $|[\mathbf{G}]_{k,l}|^2 / \sqrt{\alpha_l}$  is a constant in both  $k$  and  $l$ . Using (A.1) and (A.2), we obtain

$$\sigma^2 \geq \frac{N_0}{KM^2 \xi_G} \left( \sum_{l=0}^{M-1} \sqrt{\alpha_l} \right)^2. \quad (\text{A.3})$$





## Appendix B

### Proof of Theorem 6

Let  $\mathbf{e} = \hat{\mathbf{d}} - \mathbf{d}$  be the error vector. By direct computation, we obtain that the autocorrelation matrix  $\mathbf{R}_e = E\{\mathbf{e}\mathbf{e}^H\}$  is

$$\mathbf{R}_e = E_S(\mathbf{I}_D - \mathbf{A}^H(\mathbf{A}\mathbf{A}^H + \gamma^{-1}\mathbf{I}_D)^{-1}\mathbf{A}). \quad (\text{B.1})$$

Plugging (2.5) into (B.1) yields  $\mathbf{R}_e = (\mathbf{W}_M^H \otimes \mathbf{W}_K) \mathbf{D}_e (\mathbf{W}_M \otimes \mathbf{W}_K^H)$ , where  $\mathbf{D}_e$  is a  $D \times D$  diagonal matrix with  $[\mathbf{D}_e]_{k'+lK, k'+lK} = N_0 / (||[\mathbf{G}]_{k',l}^2 + \gamma^{-1})$ ,  $\forall 0 \leq k' < K, 0 \leq l < M$ . Since the magnitude of each entry of  $(\mathbf{W}_M^H \otimes \mathbf{W}_K)$  is  $1/\sqrt{D}$ , we obtain  $\forall 0 \leq k < K, 0 \leq m < M$ ,

$$\sigma_{k,m}^2 = [\mathbf{R}_e]_{k+mK, k+mK} = \sum_{k'=0}^{K-1} \sum_{l=0}^{M-1} \frac{N_0/D}{||[\mathbf{G}]_{k',l}^2 + 1/\gamma}. \quad (\text{B.2})$$

According to the Cauchy-Schwarz inequality, we have

$$\left[ \sum_{k',l} \frac{1}{||[\mathbf{G}]_{k',l}^2 + \frac{1}{\gamma}} \right] \left[ \sum_{k',l} \left( ||[\mathbf{G}]_{k',l}^2 + \frac{1}{\gamma} \right) \right] \geq D^2, \quad (\text{B.3})$$

where the equality holds if and only if  $||[\mathbf{G}]_{k',l}$  is a constant in both  $k'$  and  $l$ . Thus,

$$\sigma_{k,m}^2 \geq \frac{E_S}{\gamma \xi_G + 1}, \forall 0 \leq k < K, 0 \leq m < M, \quad (\text{B.4})$$

and the result follows from (6.2).





## Appendix C

### Proof of Corollaries 1 and 2

According to (6.3), we have  $\sigma_{k,m}^2 = \xi_H N_0, \forall 0 \leq k < K, 0 \leq m < M$  under the ZF receiver over the AWGN channel. Thus,  $\sigma_{k,m}^2$  is a constant in both  $k$  and  $m$  under this scenario. The statement for the other two scenarios can be proved in a similar way by noting (6.6) and (B.2), respectively.